

3 1176 00121 0005

CONFIDENTIAL

Copy
RM E57J17

5

c2

NACA RM E57J17



RESEARCH MEMORANDUM

EXPERIMENTAL INVESTIGATION OF THE EFFECT OF
CIRCUMFERENTIAL INLET FLOW DISTORTION ON
THE PERFORMANCE OF A FIVE-STAGE AXIAL-

FLOW RESEARCH COMPRESSOR WITH
TRANSONIC ROTORS IN ALL STAGES

By William H. Robbins and Frederick Glaser

Lewis Flight Propulsion Laboratory
Cleveland, Ohio

By Authority of TPA # 27 Date 7-28-60
ga

UNCLASSIFIED INFORMATION CHANGED

LIBRARY COPY

MAR 6 1958

LANGLEY AERONAUTICAL LABORATORY
LIBRARY, NACA
LANGLEY FIELD, VIRGINIA

CLASSIFIED DOCUMENT

This material contains information affecting the National Defense of the United States within the meaning of the espionage laws, Title 18, U.S.C., Secs. 793 and 794, the transmission or revelation of which in any manner to an unauthorized person is prohibited by law.

**NATIONAL ADVISORY COMMITTEE
FOR AERONAUTICS**

WASHINGTON

March 5, 1958

CONFIDENTIAL

UNCLASSIFIED



UNCLASSIFIED

NATIONAL ADVISORY COMMITTEE FOR AERONAUTICS

RESEARCH MEMORANDUM

EXPERIMENTAL INVESTIGATION OF THE EFFECT OF CIRCUMFERENTIAL
INLET FLOW DISTORTION ON THE PERFORMANCE OF A FIVE-
STAGE AXIAL-FLOW RESEARCH COMPRESSOR WITH
TRANSONIC ROTORS IN ALL STAGES

By William H. Robbins and Frederick Glaser

SUMMARY

The performance of a five-stage transonic research compressor was investigated with distorted inlet flow. Both over-all performance and individual blade-row performance results over a range of compressor speeds and equivalent weight flows were obtained with three circumferential inlet flow-distortion patterns covering annular extents of 60°, 120°, and 180°.

The inlet flow distortions were characterized by large gradients in static pressure and flow angularity as well as in total-pressure and velocity distortions. The magnitude of the total-pressure distortion increased with compressor speed. In contrast, the velocity distortion remained relatively constant over the entire speed range. The effects of distorted inlet flow on the over-all compressor performance were small. The pressure ratio and efficiency levels were approximately the same as those obtained without distortion; however, a 3-percent loss in equivalent weight flow was incurred at 90 and 100 percent of design speed.

The results of surveys of the individual blade rows indicated that the magnitude of both the total-pressure distortion and the velocity distortion was reduced through the compressor. However, the variation of velocity distortion was not directly reflected by the total-pressure distortion. The stator-blade rows showed little or no ability to reduce the distortion. The rate of distortion removal was greater near the tip section of the blade than at the hub.

Distorted inlet flow had very little effect on the stall-limit line at 70 and 80 percent of design speed. At higher values of compressor speed, the stall-limit line was not determined.



UNCLASSIFIED

4710

CB-1

INTRODUCTION

Turbojet-engine installations in present day aircraft are usually associated with flow distortions at the compressor inlet. Distortion of compressor inlet flow is defined, in general, as a deviation from uniform inlet flow conditions of constant total pressure, constant total temperature, and zero rotational velocity. Inlet flow distortions have caused several aircraft and engine operating problems including poor acceleration rate, altitude ceiling limitations, limited maneuverability, and thrust loss which is primarily due to adverse compressor performance. Therefore, the NACA is conducting a program on distortion covering a wide scope with an aim toward a better understanding of the engine aerodynamic effects of distortions.

Numerous compressor and engine distortion investigations have been conducted at the Lewis laboratory. This program was designed to explore both the distortion effects on over-all performance and also the internal aerodynamics of distortions. Several engines were investigated with various types of inlet distortions and are reported in references 1 to 7. The results of these investigations indicate that the effects of inlet flow distortions on compressor performance were reflected primarily in a shift of the stall-limit line toward the operating line. The extent of the shift varied with the compressor configuration and the type of distortion. Changes in the steady-state-speed curves were also manifested, but these changes in general were small. The compressors of these engines all operated at subsonic-inlet relative Mach numbers in conjunction with inlet guide vanes.

Research on distortion-reducing devices is also included in the program. Distortion reduction using screens has been investigated in references 8 and 9. This solution to the problem does not appear to be satisfactory in that large total-pressure losses are usually incurred at the current inlet-Mach-number levels of modern engines. Freely rotating fans (windmills) have also been investigated both theoretically and experimentally. The results of these investigations have been reported in references 10 to 12. Some success in reducing distortion with windmills has been realized. In general, the pressure loss is relatively low, and exit total-pressure distortion is approximately 50 percent of the inlet value. However, in reducing the total-pressure distortion, a temperature distortion and a rotational component of velocity are introduced in the flow. Windmills have the added disadvantage of increased powerplant weight.

The compressor investigated and reported herein differed from those of the previous investigations in that the design-inlet relative Mach number was transonic, and the compressor operated without inlet guide vanes. The purposes of the present investigation are as follows: (1) to determine initially the effects of distortion on over-all compressor

performance; and (2) to trace the distortion flow patterns through several blade rows from the inlet to the discharge of the compressor in order to isolate the regions of the compressor most sensitive to distortion. The compressor was operated as a component of a conventional turbojet engine in a sea-level static test stand.

Three circumferential distortion patterns were investigated corresponding to distortion extents of 60°, 120°, and 180°. For each distortion extent the compressor was operated at corrected tip speeds that were 70, 80, 90, and 100 percent of design speed. Data were obtained along an operating line corresponding to open exhaust nozzle. An attempt was also made to establish the stall-limit line; however, this was done only at 70 and 80 percent of design speed. At higher speeds, limiting turbine-inlet temperature was encountered before surge. This was investigated at the NACA Lewis laboratory. The design, over-all performance, and blade-element performance of the compressor are reported in references 13 to 16.

SYMBOLS

The following symbols are used in this report:

| | |
|----------|--|
| A_F | compressor frontal area, sq ft |
| H | total enthalpy, Btu/lb |
| i | incidence angle, angle between inlet relative-air-velocity vector and tangent to blade mean camber line at leading edge, deg |
| P | absolute total pressure, lb/sq ft |
| p | static pressure, lb/sq ft |
| T | absolute total temperature, °R |
| U | blade speed, ft/sec |
| V | absolute air velocity, ft/sec |
| V' | velocity of air relative to blade row, ft/sec |
| W | airflow rate, lb/sec |
| β | absolute airflow angle measured from axial direction, deg |
| β' | airflow angle relative to blade row measured from axial direction, deg |
| η | adiabatic temperature-rise efficiency |

- 8 ratio of inlet total pressure to NACA standard sea-level pressure,
 $P_2/2116$
- θ ratio of inlet total temperature to NACA standard sea-level temperature,
 $T_2/518.7$
- φ flow coefficient, V_z/U_t
- ψ pressure coefficient, $\frac{(\Delta H)_{id}}{U_t^2}$

Subscripts:

- H high-pressure region
- id ideal conditions
- L low-pressure region
- t compressor tip
- z axial direction
- O bellmouth inlet
- 1 compressor flow-measuring station
- 2,4 stations ahead of rotors 1 and 2
- 3,5 stations ahead of stators 1 and 2
- 6 station at second-stator discharge
- 7 station at fifth-stator discharge

APPARATUS AND PROCEDURE

Test Facility

The compressor test facility utilized in this investigation was similar to the one described in reference 16. In brief, the compressor operated as a component of an existing turbojet engine in a sea-level static test stand. A bellmouth that conformed to ASME specifications was installed at the engine inlet. Directly behind the bellmouth, a distortion-screen assembly was installed to provide a convenient method for creating inlet-flow distortions. At the exit, the engine was supplied

with a variable-area exhaust nozzle in order to allow the compressor to operate over a range of airflows at given values of rotative speed.

Distortion Screen Assembly

4710 A sketch of the passage contour with the distortion screen installed is shown in figure 1. The distortion screen was placed approximately 1 foot ahead of the first rotor-blade row. The distortion-screen assembly consisted of a 1/2-inch mesh screen, covering the entire annulus, which served as a support for a finer mesh (24 mesh, 0.012-in. wire) distortion screen. Preliminary performance data indicated that the steady-state performance was not affected by the support screen. The distortion-screen circumferential segments used in this investigation extended 60°, 120°, and 180°.

The distortion screen was mounted on rollers which permitted rotation about the compressor axis. Mounting the distortion screen in this manner, provided a convenient way of utilizing instrumentation at one circumferential position to determine the distorted-flow patterns around the complete circumference of the compressor.

Instrumentation

Instrumentation was provided at seven axial stations. Measurements at stations 0 and 1 were utilized for computing the airflow rate. Temperature and pressure readings were taken at station 0 (fig. 1) and were considered inlet stagnation conditions. At station 1, static pressure was obtained from a five-tube radial static-pressure rake and static-pressure wall orifices equally spaced around the circumference. Airflow through the compressor, for over-all performance, was then calculated from the inlet stagnation conditions, wall boundary-layer blockage factor, arithmetical average of the static-pressure rake (at station 1) for 30 circumferential positions of the distortion screen, and the continuity equation. A discussion of boundary-layer blockage allowance is given in reference 15. For these tests, the boundary-layer blockage allowance used was 0.98 and was constant over the entire weight-flow range tested.

Station 2 instrumentation (rotor inlet) consisted of four static-pressure orifices equally spaced at the outer wall and a combination self-balancing temperature-pressure-angle survey probe (fig. 2). Similar instrumentation existed at stations 3, 4, 5, 6, and 7.

Measurements were made at five radial positions corresponding to 10, 30, 50, 70, and 90 percent of the passage depth from the casing, and at 30 circumferential positions (12° intervals) on the distortion screen. Static pressure was measured at the five radial positions by using one

calibrated balancing tube of the combination survey probe. An included angle of 60° between the balancing tubes of the combination probe was reasonably satisfactory for measuring static pressure. The temperatures and static pressures were calibrated and corrected for Mach-number effects. Shown in figure 3 is a comparison of circumferential variation of static pressure as measured by both the combination probe (with the calibration applied) at 10 percent of the passage depth and the static-pressure wall orifices, and this comparison was typical of the variations that existed for the distortion investigation. Although the curves vary in absolute magnitude, they follow the same trends.

Procedure

Three circumferential distortion patterns were investigated corresponding to distortion extents of 60° , 120° , and 180° . For each distortion extent the compressor was operated at corrected tip speeds of 70, 80, 90, and 100 percent of design speed. At 70 percent of design speed the compressor was limited to one operating point corresponding to an open exhaust nozzle. A slight closure of the exhaust nozzle resulted in compressor rotating stall. Open exhaust-nozzle (maximum weight flow) and closed exhaust-nozzle (minimum weight flow) data were obtained at 80 and 90 percent of design speed. The closed-nozzle data were near the stall-limit line of the compressor at 80 percent of design speed; at 90 percent of design speed, the minimum weight flow was limited by turbine-inlet temperature. At design speed, data were obtained at open nozzle. Closed-nozzle data could not be obtained because of limiting turbine-inlet temperature.

In addition, exploratory stall studies were made with a hot wire anemometer over the complete range of operating conditions. Failure of the first-stage rotor blades prevented completion of the intended research program on this compressor.

RESULTS AND DISCUSSION

The results of this investigation are presented in curve form in figures 4 to 17. Initially, the compressor-inlet conditions are indicated (fig. 4). Following these plots the over-all performance map is presented (fig. 5). Circumferential variations of the flow through the first two stages and at the compressor discharge are then given (figs. 7 to 10), and finally complete velocity diagrams (figs. 11 to 14) in the distorted- and undistorted-flow regions are shown with the rate of decay of the axial velocity and total-pressure distortions (figs. 15 and 17) through the compressor. Analysis of data is limited primarily because of the absence of a firm compressor theoretical analysis that can be applied to the case

of nonuniform circumferential inlet flow. Insofar as possible, however, qualitative explanations of the curves are presented.

Two parameters have been used to rate the magnitude of the distortion throughout this report. The first method, rating distortion on a total-pressure basis, is a very common technique used almost exclusively in previously established distortion literature because it can be related directly to engine thrust. The other method based on axial velocity is especially useful and probably more significant from a blade-row or blade-element point of view because compressor internal-flow changes are more directly reflected. Axial velocity is also a common parameter to both rotating and stationary blade rows. The distortion parameters at the inlet to each blade row (axial stations 2, 3, 4, 5, 6, and 7) were defined as follows:

(1) Total-pressure-distortion parameter, $\frac{P_H - P_L}{P_H}$

(2) Velocity-distortion parameter, $\frac{V_{z,H} - V_{z,L}}{V_{z,H}} = \frac{\phi_H - \phi_L}{\phi_H}$

Compressor-Inlet Conditions and Over-all Performance

The variation of inlet flow distortion with equivalent weight flow is indicated in figure 4 where the total-pressure-distortion and velocity-distortion parameters are plotted against equivalent weight flow for three distortion extents. Values of the distortion parameter at the various speeds are identified by appropriate symbols and represent radially averaged values from hub to tip. The values of total-pressure distortion increased with equivalent weight flow (and speed) from a value of approximately 0.05 at the lowest flow investigated to a maximum value of 0.185 at the highest flow investigated for the 180° extent. Values of the total-pressure distortion parameter for the 120° extent and 60° extent were somewhat lower over the entire flow range.

Values of the inlet velocity distortion are shown in the upper portion of figure 4, and although some scatter of data exists, in general, the values of velocity distortion seem to remain relatively constant with equivalent weight flow (and compressor speed), suggesting that strong static-pressure gradients were present in the inlet flow. The existence of static-pressure gradients will be discussed more fully in a later section.

The over-all performance map is shown in figure 5 where total-pressure ratio and adiabatic efficiency are plotted against equivalent weight flow at the compressor inlet. The solid lines represent the uniform inlet flow-performance map reported in reference 16. The data points

at 70-percent speed were taken at a flow just slightly higher than that at which rotating stall occurred. The minimum-flow points at 80-percent design speed are data points near the stall-limit line (surge points). The minimum-flow data points at 90-percent speed and those at design speed are not surge points but represent values of pressure ratio and weight flow where the limiting turbine-inlet temperature was reached. The uniform-inlet minimum-flow data points at 90- and 100-percent speed do not represent the stall-limit line either. In general, the effects of distortion are small. At 70 and 80 percent of design speed, the pressure-ratio level has remained about the same as the uniform inlet-flow values, and some increase in efficiency has been observed. The indicated increase in efficiency is probably due to inaccuracies in the temperature measurements.

At 70-percent design speed with distorted inlet flow, rotating stall was incurred at somewhat higher values of the weight flow (approximately 3 percent) than the stall values of the uniform flow; at 80-percent speed, no significant change in the stall-limit line was observed. In this speed range associated with low values of distortion, the stall-limit line was not expected to change radically. However, at supersonic flight Mach numbers where the equivalent speed is low and the inlet-flow distortion is high, serious compressor operating problems may exist because of the reduced stall-free operating range

Some penalty in equivalent weight flow at the compressor face (approximately 3 percent) was observed at 90 and 100 percent of design speed. The decrease in flow was not attributed to increased boundary-layer buildup at the compressor face because of longer inlet ducting with the distortion-screen assembly installed upstream of the compressor, because preliminary tests with the backing screen (1/2-inch mesh covering the complete annulus) indicated no decrease in equivalent flow.

A typical distorted flow model and compressor characteristic curves are shown in figure 6. Two axial stations are considered; station 1 is at the compressor inlet, and station 2 is downstream of the compressor. At the downstream station, it is assumed that the total pressure is constant. The compressor characteristic and uniform inlet flow operating point are indicated in figure 6(b). For the case of distorted inlet flow, the axial velocity will be low at station 1_L , and therefore ϕ will decrease and ψ will increase (fig. 6(b)). Conversely, at station 1_H ϕ will increase and ψ will decrease, and the average flow coefficient will depend on the shape of the compressor characteristic, the stage and engine matching requirements, and the compressor operating point. In this particular case a net flow loss at the compressor face (station 1) was observed.

Since the compressor with distorted flow tended to operate at somewhat higher values of pressure coefficient and lower values of flow

coefficient, the stall-free operating range of the compressor will be somewhat less than that for undistorted operation. For example, the data taken at 70 percent of design speed indicated that the rotating-stall region of the compressor map increased with distorted inlet flow.

Individual Blade-Row Performance

In order to gain a better insight into the internal-compressor flow patterns, the individual blade-row performance of the first two stages of the compressor is presented. Circumferential variations of the measured-flow parameters are indicated, with velocity diagrams of the high- and low-pressure flow regions. The distortion parameters discussed previously are used as the basis for the analysis.

Circumferential flow patterns. - The circumferential distortion-flow patterns at six axial stations (2 to 6, fig. 1) are shown in figures 7 to 10 where total pressure, static pressure, absolute flow angle, total temperature, and absolute velocity are plotted against circumferential position. The circumferential survey points were equally spaced covering the complete annulus (360°). Three radial positions are presented corresponding to 10, 50, and 90 percent of the passage depth. One data point at each of four compressor speeds for the 120° extent is shown. The data for this distortion extent were presented because it was the most consistent and reliable. These plots indicate that the circumferential extent of distorted flow remains relatively constant through the compressor; at the compressor discharge (station 7) the total-pressure distortion has been greatly reduced. The difference in total pressure in the high- and low-pressure regions appears to increase slightly through the first two stages; the static-pressure variation followed a similar pattern. The static-pressure gradient at the inlet is not surprising in view of the variation of the flow angle, which indicates large streamline curvatures at the compressor inlet. The data suggest that the inlet flow picture is very similar to that shown in figure 6(a). A velocity distortion also existed at the compressor inlet. In contrast to the total- and static-pressure gradients that persisted throughout the first two stages, the velocity distortion and the gradients of the flow angle seem to dissipate quite markedly.

At the compressor discharge, however, a significant velocity distortion exists, which is surprising in view of the velocity distortion decay that occurred in the inlet stages. An examination of the total- and static-pressure variations at the compressor discharge (station 7) indicated that (in contrast to the pressure variations at the other axial stations) the region of high total pressure was associated with the region of low static pressure (figs. 7, 8, 9, and 10(p) to (r)), resulting in a sizeable velocity distortion. As a consequence, the circumferential variations of static pressure were viewed with suspicion. Although the

data for the 60° and 180° extents were not presented, similar trends were exhibited. The distorted flow region, of course, spiraled through the compressor. The circumferential location of this region was predicted accurately at any axial station from the absolute mean flow angle and velocity. This rotation amounted to approximately 20° in each of the first two compressor stages.

Velocity diagrams. - In order to reduce the data somewhat for analysis, the circumferential-flow-variation plots (figs. 7 to 10) were used as a basis for dividing the compressor into two regions. The high-pressure region was taken as the undistorted region, and the low-pressure region was considered the region of distorted flow. The values of the flow parameters were arithmetically averaged in each region, and complete velocity diagrams were then computed. The velocity diagrams are shown in figures 11 to 14 for the data of figures 7 to 10. The high-pressure regions are shown as solid lines, the low-pressure regions are indicated by the dotted lines. At the compressor inlet, the distorted flow diagrams are characterized by a somewhat lower axial velocity and a higher angle of incidence on the first rotor. As the flow passes through the rotor, the axial velocity change is greater in the distorted region. Since the relative outlet flow angle is nearly equal for both regions, the effect is in the direction of decreasing the velocity distortion. The velocity diagrams indicate that this effect is more predominant at the tip and mean radius than at the hub. The velocity distortions are also greatly diminished at the exit to the second stage. In many cases the second-stage distorted and undistorted diagrams are coincident.

Flow variations through the compressor. - The distortion patterns through the compressor in terms of the total-pressure-distortion parameter $\frac{P_H - P_L}{P_H}$ and the velocity-distortion parameter $\frac{V_{z,H} - V_{z,L}}{V_{z,H}}$ are

presented in figure 15 for the three distortion extents. One point at each compressor speed is shown for the 180° and 120° extents. The distortion data at 70 percent of design speed for the 60° distortion extent were not presented because the magnitude and extent of the distortion were so small that it was extremely difficult to isolate the high- and low-pressure flow regions on the circumferential plots. The data are plotted against station number in the compressor (fig. 1) and represent radially averaged values of the distortion parameters. Both the total-pressure distortion and velocity distortion decrease through the first two rotor blade rows. In contrast, through the stator blades the distortion either remains constant or increases slightly. This suggests that energy addition is required to remove a significant amount of distortion and also indicates that inlet guide vanes probably are not effective for distortion removal. The rate of decay of the velocity distortions through the first two stages appears to be greater than the rate of decay of the total-pressure distortions. This is desirable because it is felt

that total-pressure distortion as such is not detrimental to compressor performance. Velocity-diagram distortions, however, create serious compressor operating problems because of mismatching of the stages. Figure 15 also confirms previous suspicions that the inlet stages are probably the most critical from a distortion standpoint in that a greater stall-free angle-of-attack range is required to accommodate a distorted inlet flow.

The velocity diagram plots, for example, (figs. 11 to 14) indicate that the inlet stage operates over a greater incidence-angle range than the second stage. In many cases the second-stage high- and low-pressure velocity diagrams are coincident; however, the inlet-stage diagrams in all cases show that the stage must operate over an angle-of-attack range.

At the compressor discharge (station 7) the total-pressure distortion has almost completely dissipated. In contrast, a significant velocity distortion is indicated which again illustrates that the velocity distortion is not reflected by the total-pressure distortion.

Radial gradients of inlet flow. - In figure 16 radial variations of the total-pressure distortion parameter, the velocity distortion parameter, and change in angle of incidence are shown at the compressor face (station 2) for the three distortion extents. Again one data point at each compressor speed is presented except for the 60° extent where the 70-percent design-speed data is not shown. As expected, the total-pressure distortion remained relatively constant from hub to tip, and the distortion level increased with speed.

The velocity distortion curves do not exhibit the same trend. The velocity distortion increases from 70 percent to 90 percent of design speed; however, there is a reduction in velocity distortion as the speed is increased from 90 percent to 100 percent. The velocity distortions are somewhat higher at the mean radius than at the hub and tip. The incidence-angle curves indicate the same general trends as the velocity-distortion plots. The smallest change in incidence angle occurred near the tip of the blade; this was fortunate in that the tip region has the smallest stall-free incidence-angle range. In addition, the velocity-distortion parameter and change in incidence angle (which are most significant from the standpoint of compressor operation) are not truly reflected by the total-pressure distortion parameter. In view of these results, the velocity-diagram studies, rather than analysis of total-pressure variations, present a good approach to the solution of the distortion problem.

Radial variations of flow through the compressor. - In figure 17 the values of the total-pressure-distortion parameter and velocity-distortion parameter for three radial positions are plotted against compressor station number (fig. 1) for the first two stages and at the

4710

CP-2 back

compressor discharge. The data for three distortion extents is shown. The data points on these curves represent average values of the distortion parameter for the four compressor speeds investigated. The plots were presented on an average basis because the scatter of data was reduced somewhat. Near the tip of the blade, the total-pressure distortion is reduced considerably through the first rotor-blade row and remains relatively constant to the outlet of the second stage. At the compressor discharge the total-pressure distortion is virtually eliminated. The velocity distortion was also diminished very rapidly in one blade row; in fact, values of the velocity distortion are negative in some cases at stations 3 to 6. At the discharge the velocity distortion has increased to a positive value.

The trends at the hub are quite different. Both the total-pressure distortion and velocity distortion increase through the first stage, and a marked drop through the second stage is indicated. As stated previously, it is suspected that variations of energy addition in the compressor-blade rows exert considerable influence on the distortion patterns through the compressor. In general, the rate of change of energy addition with flow coefficient at the hub is much smaller than that at the tip. This fact is manifested by observing a typical compressor characteristic as shown in figure 18(a), where pressure coefficient is plotted against flow coefficient for typical hub and tip sections. Near the tip section of the blade, the performance curve is characterized by a steep slope.

For simplicity, it is assumed that undistorted operation of the compressor occurs at point A with radially constant axial velocity; the distorted operating point is at B. At points A and B the first-stage velocity profiles (from energy addition considerations) will resemble those shown in figure 18(b). For the compressor operation at point A, the axial velocity will remain constant at all stations. Operation at point B (distorted flow) will be somewhat different. At station 2 the axial velocity (B_2) is decreased and remains constant radially (assuming no whirl at the inlet). By moving to station 3 (after the rotor), axial velocity will be higher at the tip than at the hub because of increased energy addition at the tip section. Through the stators (B_4) the same trend will persist since the same energy gradient exists over a smaller passage height.

The velocity profiles through stage 2 are shown in figure 18(c). Increased axial velocity at the tip at the exit to stage 1 will result in less energy addition at the tip than hub and the profiles will tend to again approach the condition of constant axial velocity. A plot of the velocity profiles through two compressor stages in terms of the distortion parameters at the hub and tip is shown in figure 18(d). The trend of the curves are the same as those of figure 17. It is realized that

this simplified picture of the distorted flow will be complicated by gradients of entropy, streamline curvature, and tangential velocity gradients. In view of the experimental data, however, it is felt that the analytic approach has some significance.

Exploratory stall studies. - In addition to the steady-state data obtained, surveys were taken after the first rotor-blade row with a hot-wire anemometer. The purpose of this investigation was to determine stall regions during compressor operation with inlet flow distortions. Surveys were taken over the complete range of performance with the three distortion screens discussed previously. In addition, the flow was observed with one-sixth of the annulus completely blocked by a steel plate. For the distortions investigated it was impossible to stall the distorted portion of the annulus while the other portion operated without stall.

SUMMARY OF RESULTS

The performance of a five-stage transonic research compressor was investigated with distorted inlet flow. Both over-all performance and individual blade-row performance results were obtained for three circumferential inlet flow distortion patterns

| | | Distortion | |
|---|------|------------|---|
| | | Extent | Magnitude |
| 1 | 180° | | $\left(\frac{\Delta P}{P_H}\right)_{max} = 0.185$ |
| 2 | 120° | | $\left(\frac{\Delta P}{P_H}\right)_{max} = 0.142$ |
| 3 | 60° | | $\left(\frac{\Delta P}{P_H}\right)_{max} = 0.125$ |

The following results were obtained in this investigation:

1. The effects of distorted inlet flow on the over-all performance map were small. The values of pressure ratio and efficiency were approximately the same as those indicated on the steady-state performance map; however, a 3-percent loss in equivalent weight flow was indicated at 90 and 100 percent of design speed. In addition, a slightly larger region of rotating stall existed at 70 percent of design speed.

2. The inlet total-pressure distortion increased as compressor speed increased. In contrast, the inlet-velocity distortion remained relatively constant over the compressor-speed range.

3. The inlet flow patterns were characterized by large gradients of static pressure and flow angularity as well as total-pressure and velocity distortions. However, the data indicated that while the total- and static-pressure gradients were not greatly affected as the flow passed through the first two stages, the velocity distortions and angularity were greatly reduced. A significant velocity distortion existed at the compressor discharge; in contrast, the total-pressure distortion was virtually eliminated.

4. The stator-blade rows showed little or no ability to reduce distortions.

5. The tip section of the compressor seemed to have greater distortion-removal ability than the hub section.

6. It was not possible to stall the distorted region of the compressor while the undistorted region operated without stall.

Lewis Flight Propulsion Laboratory
National Advisory Committee for Aeronautics
Cleveland, Ohio, October 23, 1957

REFERENCES

1. Conrad, E. William, and Sobolewski, Adam E.: Investigation of Effects of Inlet-Air Velocity Distortion on Performance of Turbojet Engine. NACA RM E50G11, 1950.
2. Wallner, Lewis E., Conrad, E. William, and Prince, William R.: Effect of Uneven Air-Flow Distribution to the Twin Inlets of an Axial-Flow Turbojet Engine. NACA RM E52K06, 1953.
3. Walker, Curtis L., Sivo, Joseph N., and Jansen, Emmert T.: Effect of Unequal Air-Flow Distribution from Twin Inlet Ducts on Performance of an Axial-Flow Turbojet Engine. NACA RM E54E13, 1954.
4. Harry, David P., III, and Lubick, Robert J.: Inlet-Air Distortion Effects on Stall, Surge, and Acceleration Margin of a Turbojet Engine Equipped with Variable Compressor Inlet Guide Vanes. NACA RM E54K26, 1955.

- 4710
5. Huntley, S. C., Sivo, Joseph N., and Walker, Curtis L.: Effect of Circumferential Total-Pressure Gradients Typical of Single-Inlet Duct Installations on Performance of an Axial-Flow Turbojet Engine. NACA RM E54K26a, 1955.
 6. Conrad, E. William, Hanson, Morgan P., and McAulay, John E.: Effect of Inlet-Air-Flow Distortion on Steady-State Altitude Performance of an Axial-Flow Turbojet Engine. NACA RM E55A04, 1955.
 7. Fenn, David B., and Sivo, Joseph N.: Effect of Inlet Flow Distortion on Compressor Stall and Acceleration Characteristics of a J-65-B-3 Turbojet Engine. NACA RM E55F20, 1955.
 8. Piercy, Thomas G.: Factors Affecting Flow Distortions Produced by Supersonic Inlets. NACA RM E55L19, 1956.
 9. Sterbentz, William H.: Factors Controlling Air-Inlet Flow Distortions. NACA RM E56A30, 1956.
 10. Collar, A. R.: The Use of a Freely Rotating Windmill to Improve the Flow in a Wind Tunnel. R. & M. No. 1866, British ARC, Nov. 1938.
 11. Johnston, I. H.: The Use of Freely Rotating Blade Rows to Improve Velocity Distribution in an Annulus. Memo. No. M.109, British NGTE, Feb. 1951.
 12. English, Robert E., and Yohner, Peggy L.: Theoretical Analysis of One-Stage Windmills for Reducing Flow Distortion. NACA RM E57D05, 1957.
 13. Sandercock, Donald M., Kovach, Karl, and Lieblein, Seymour: Experimental Investigation of a Five-Stage Axial-Flow Research Compressor with Transonic Rotors in All Stages. I - Compressor Design. NACA RM E54F24, 1954.
 14. Kovach, Karl, and Sandercock, Donald M.: Experimental Investigation of a Five-Stage Axial-Flow Research Compressor with Transonic Rotors in All Stages. II - Compressor Over-All Performance. NACA RM E54G01, 1954.
 15. Sandercock, Donald M., and Kovach, Karl: Experimental Investigation of a Five-Stage Axial-Flow Research Compressor with Transonic Rotors in All Stages. III - Interstage Data and Individual Stage Performance Characteristics. NACA RM E56G24, 1956.
 16. Sandercock, Donald M.: Experimental Investigation of a Five-Stage Axial-Flow Research Compressor with Transonic Rotors in All Stages. IV - Blade-Element Performance. NACA RM E57B12, 1957.

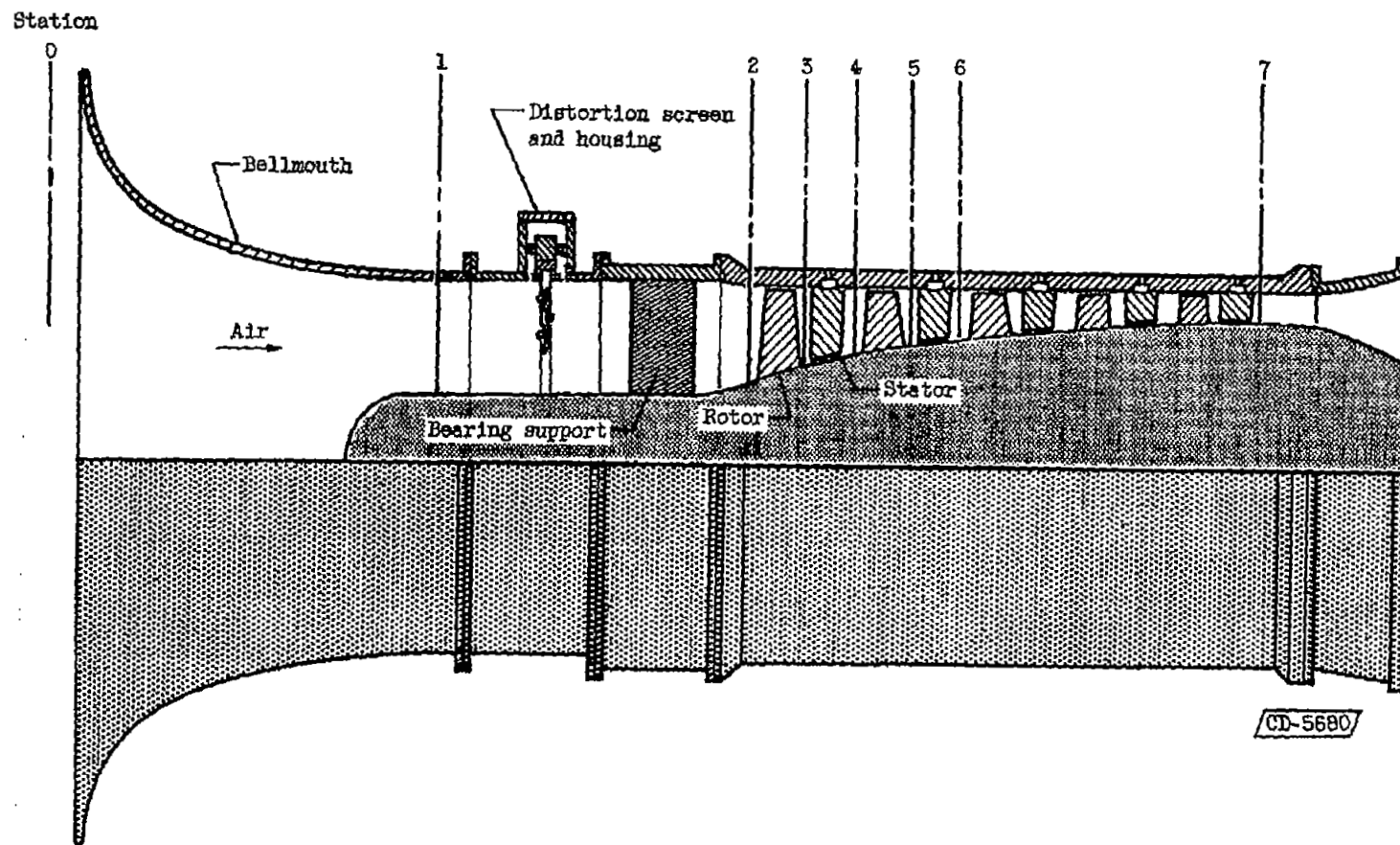


Figure 1. - Schematic diagram of compressor installation.

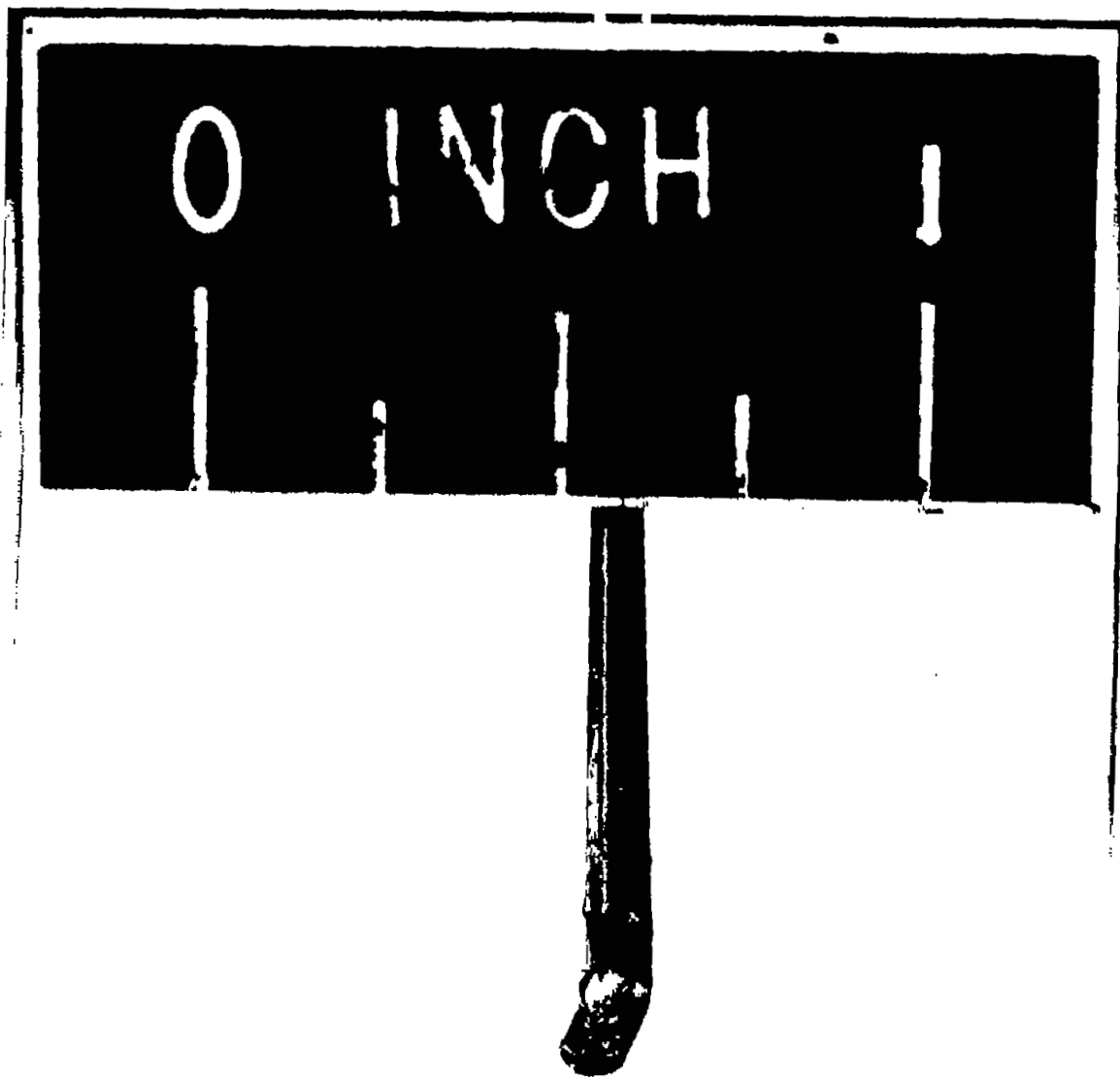


Figure 2. - Photograph of combination probe.

C-44952

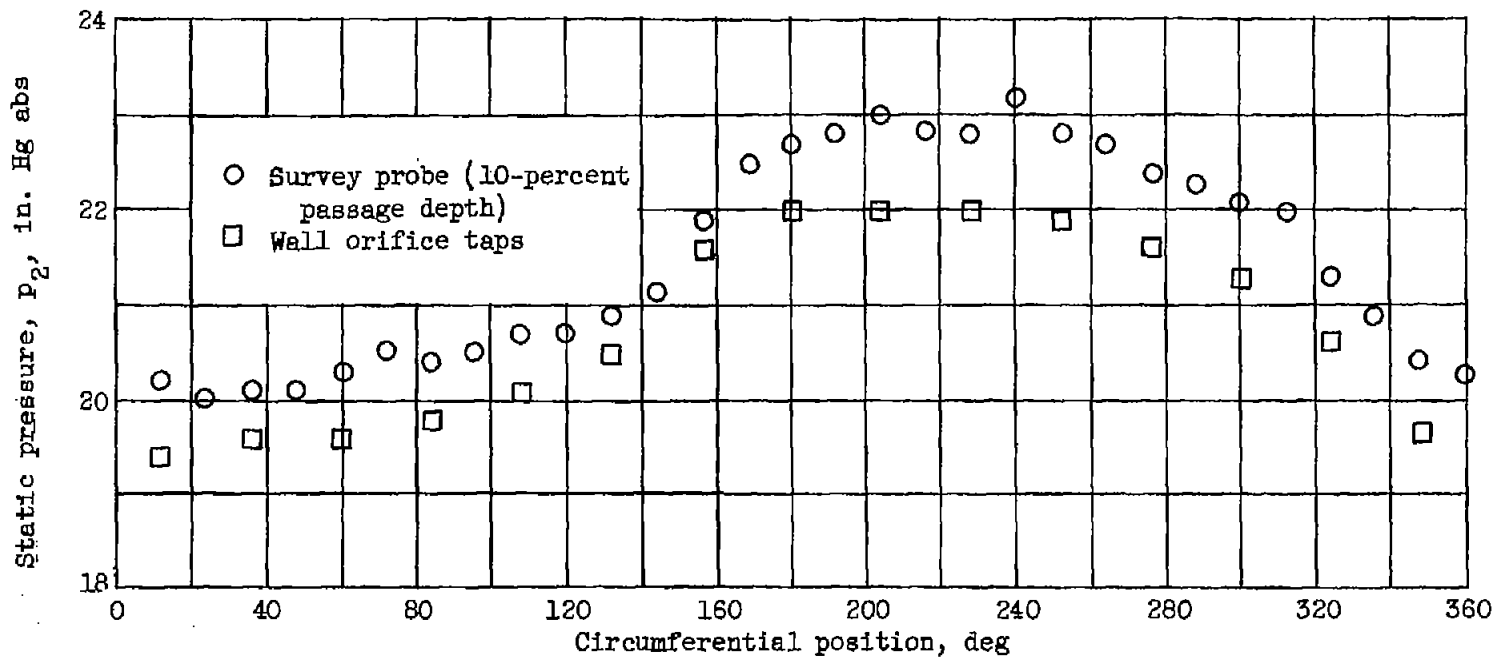


Figure 3. - Circumferential variation of static pressure at compressor inlet (face) as measured by combination probe at 90-percent design speed and 180° screen extent.

4710

CB-3 back

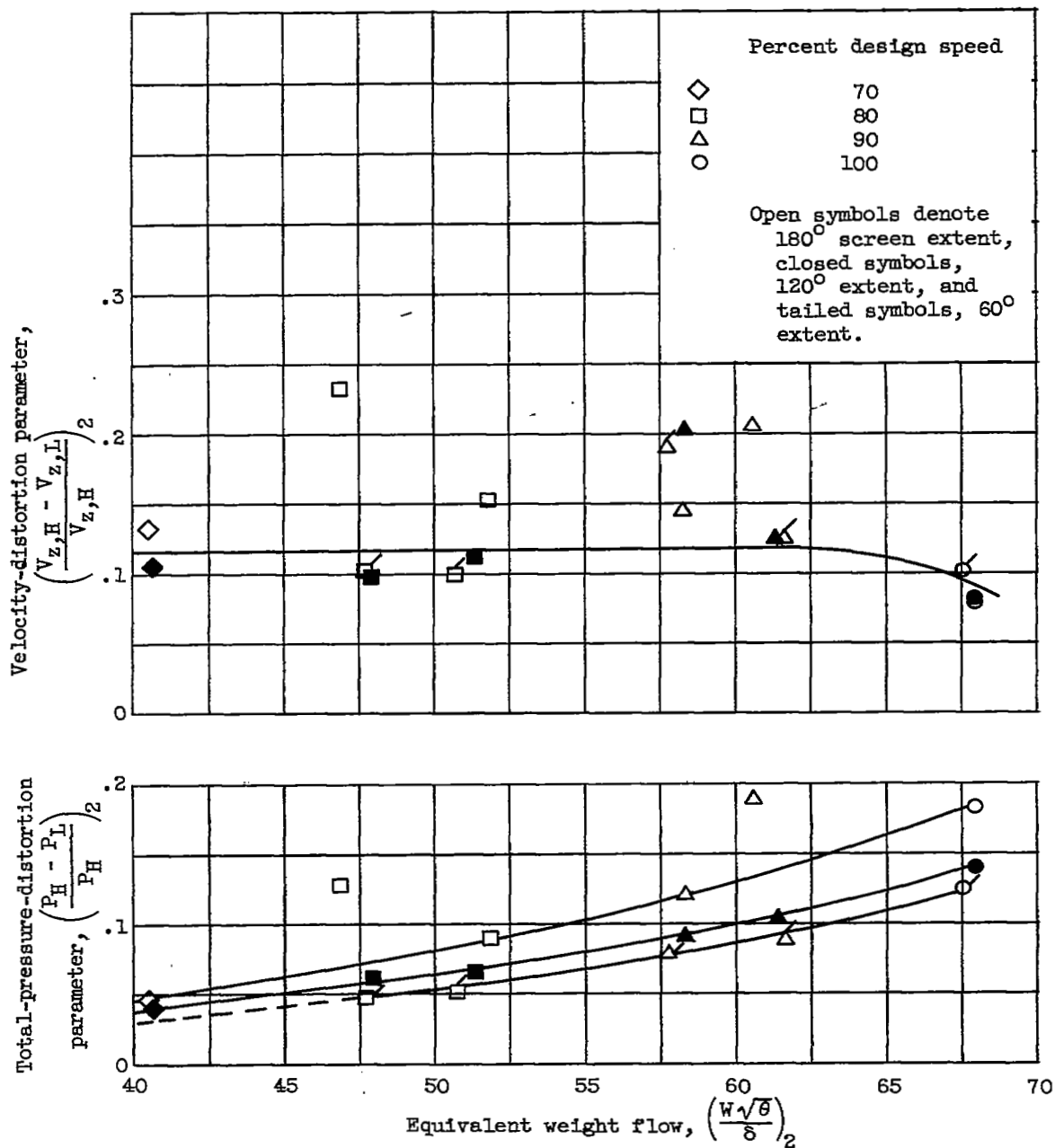


Figure 4. - Variation of compressor-inlet total pressure and velocity distortion with equivalent weight flow.

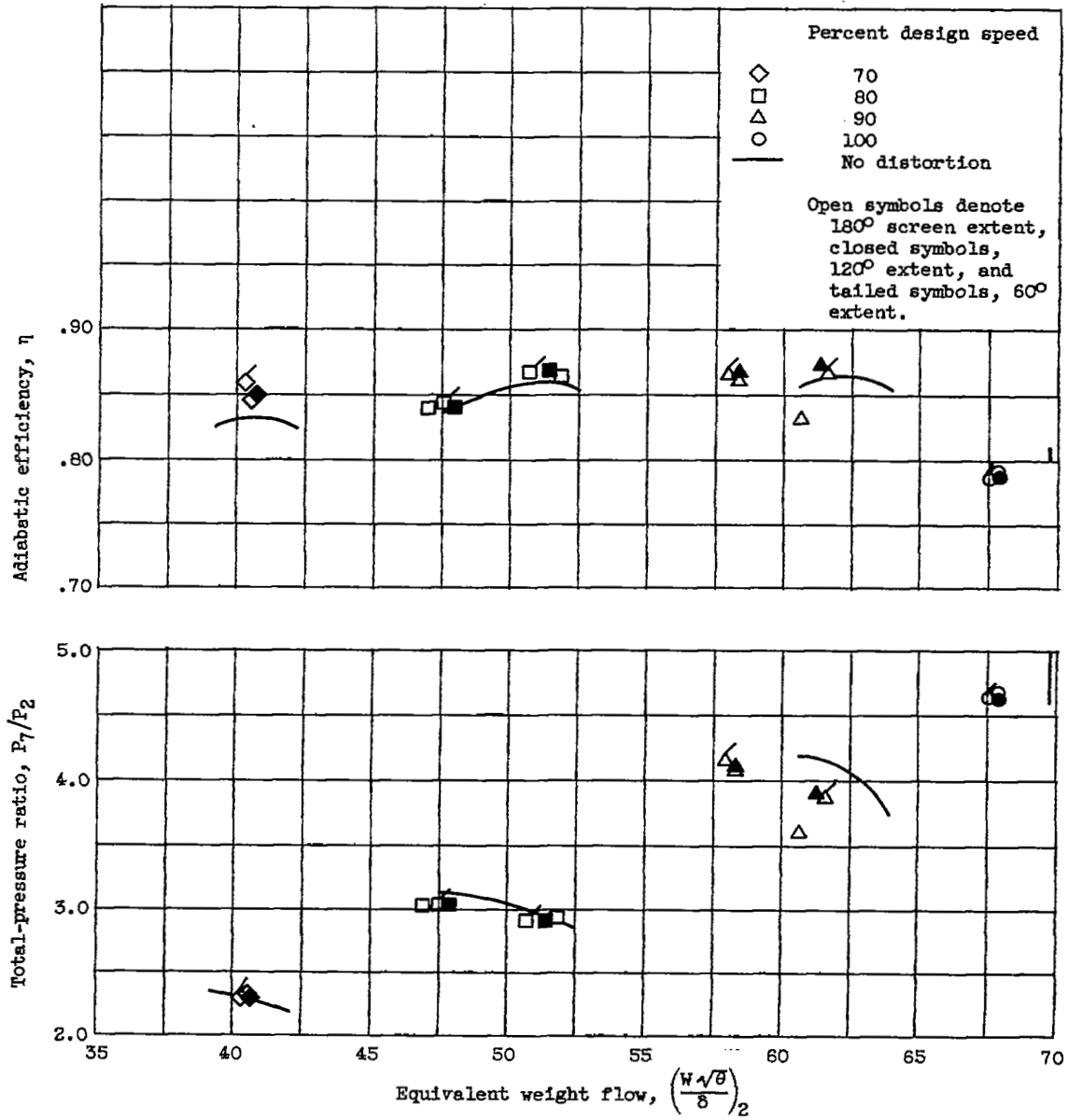
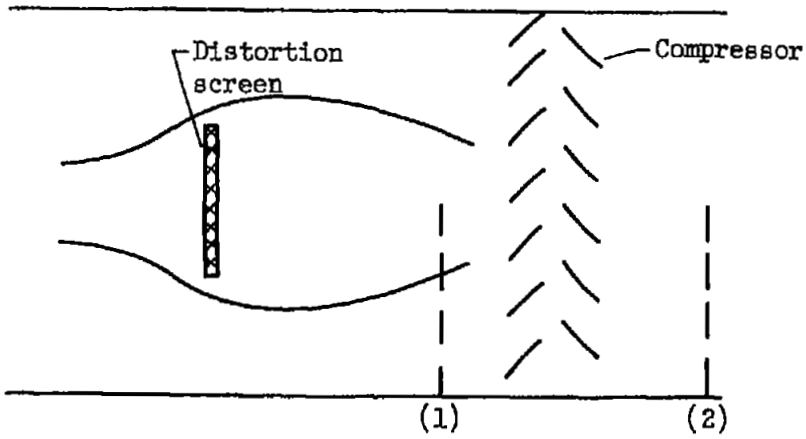
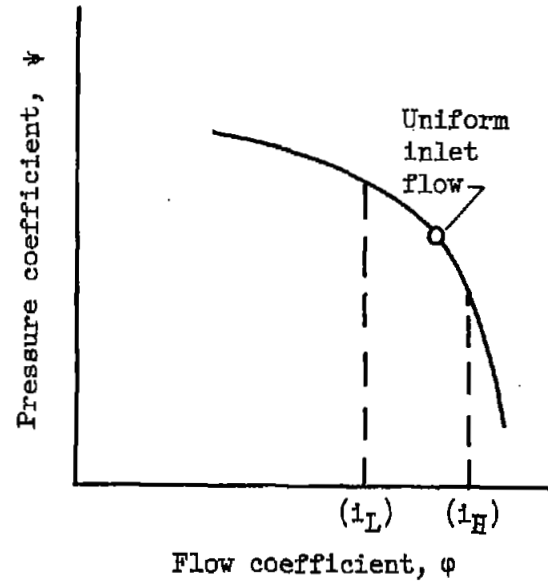


Figure 5. - Over-all performance map based on equivalent weight flow at compressor face.

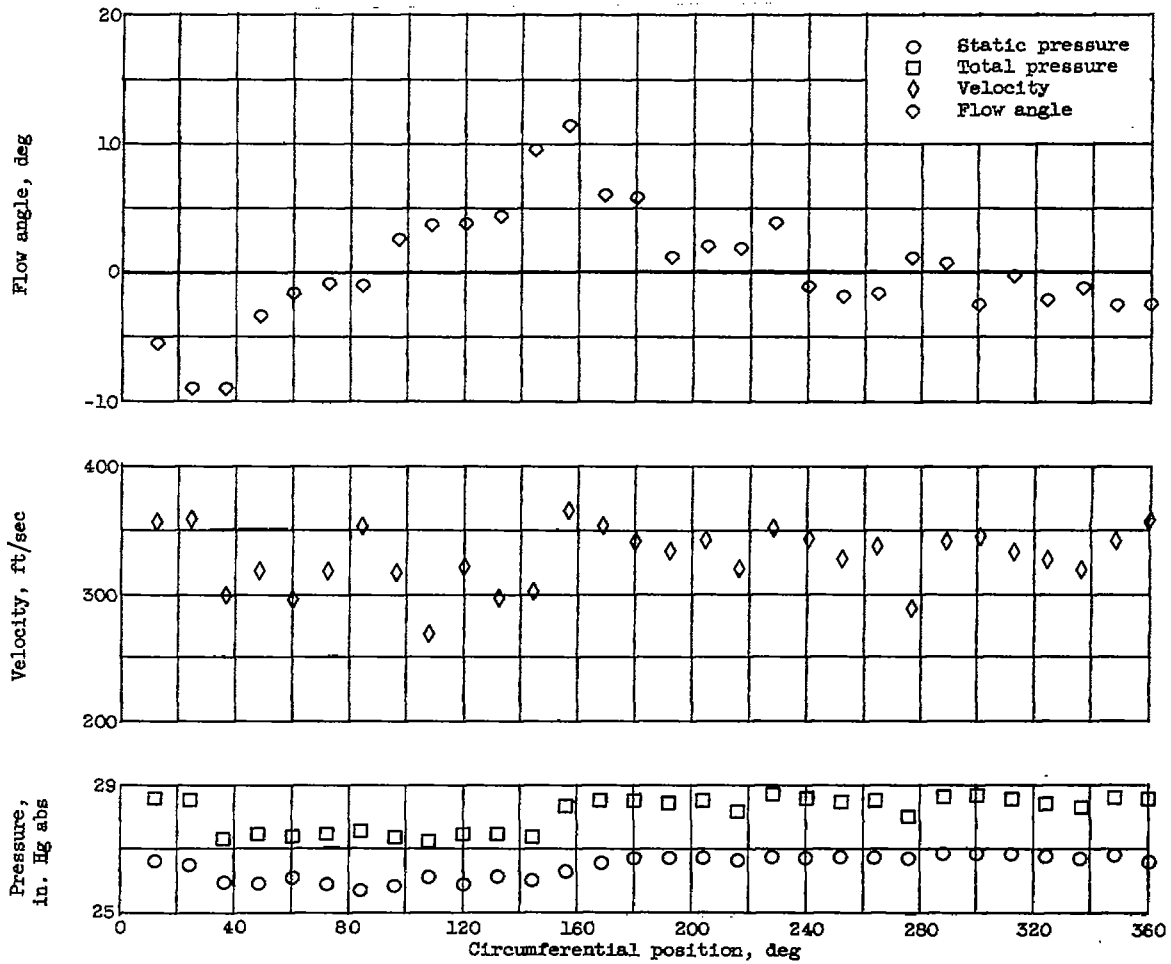


(a) Flow model.



(b) Operating points.

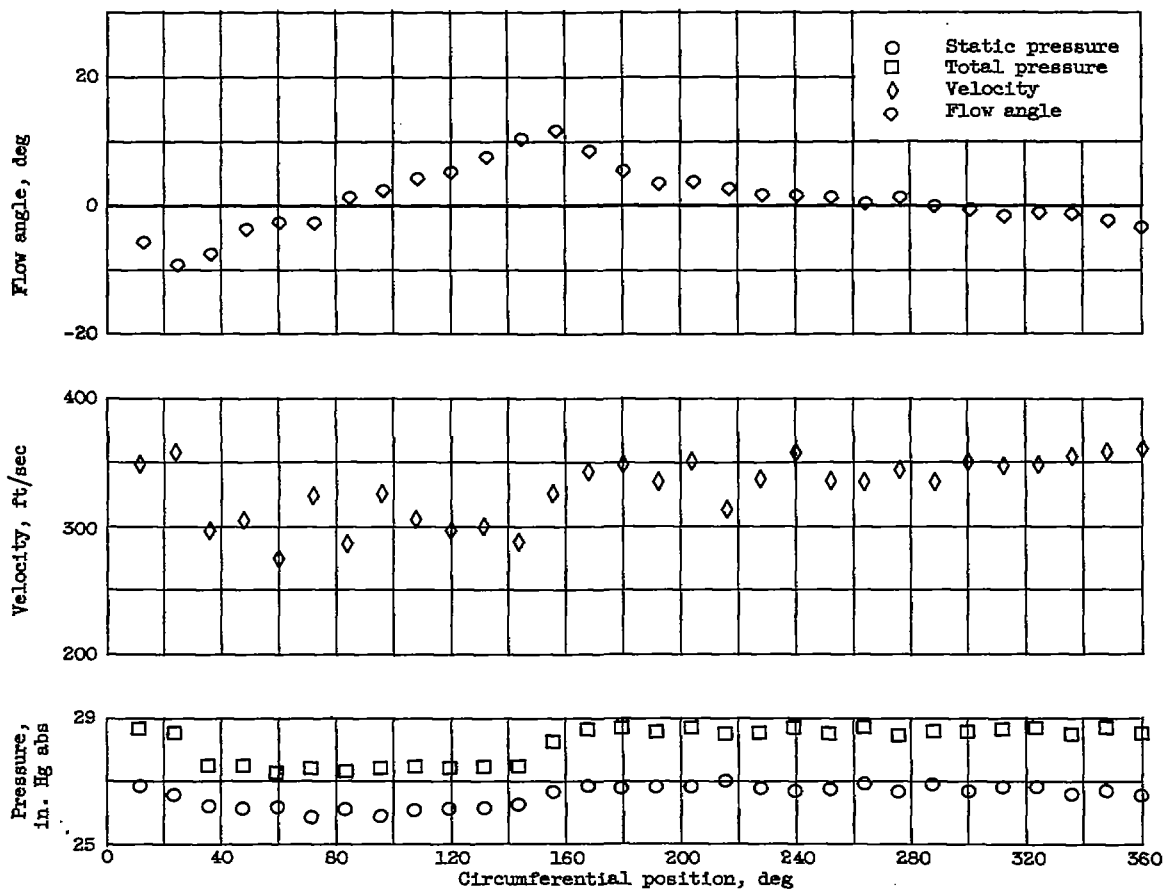
Figure 6. - Compressor operation with inlet flow distortion.



(a) 10-Percent passage depth (tip); station 2; absolute total temperature, 535° R.

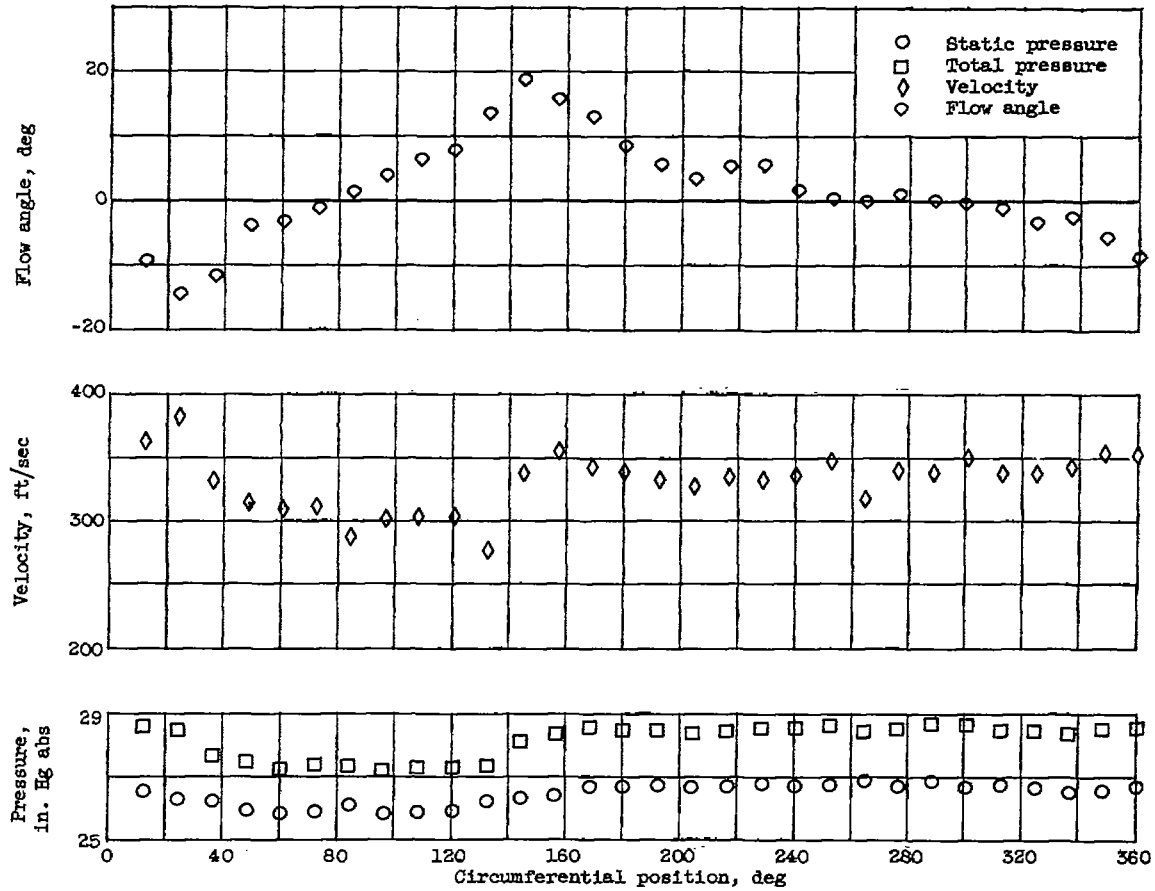
Figure 7. - Variation of distorted-flow patterns with circumferential position. 70-Percent speed.

4710



(b) 50-Percent passage depth (mean); station 2; absolute total temperature, 538° R.

Figure 7. - Continued. Variation of distorted-flow patterns with circumferential position. 70-Percent speed.

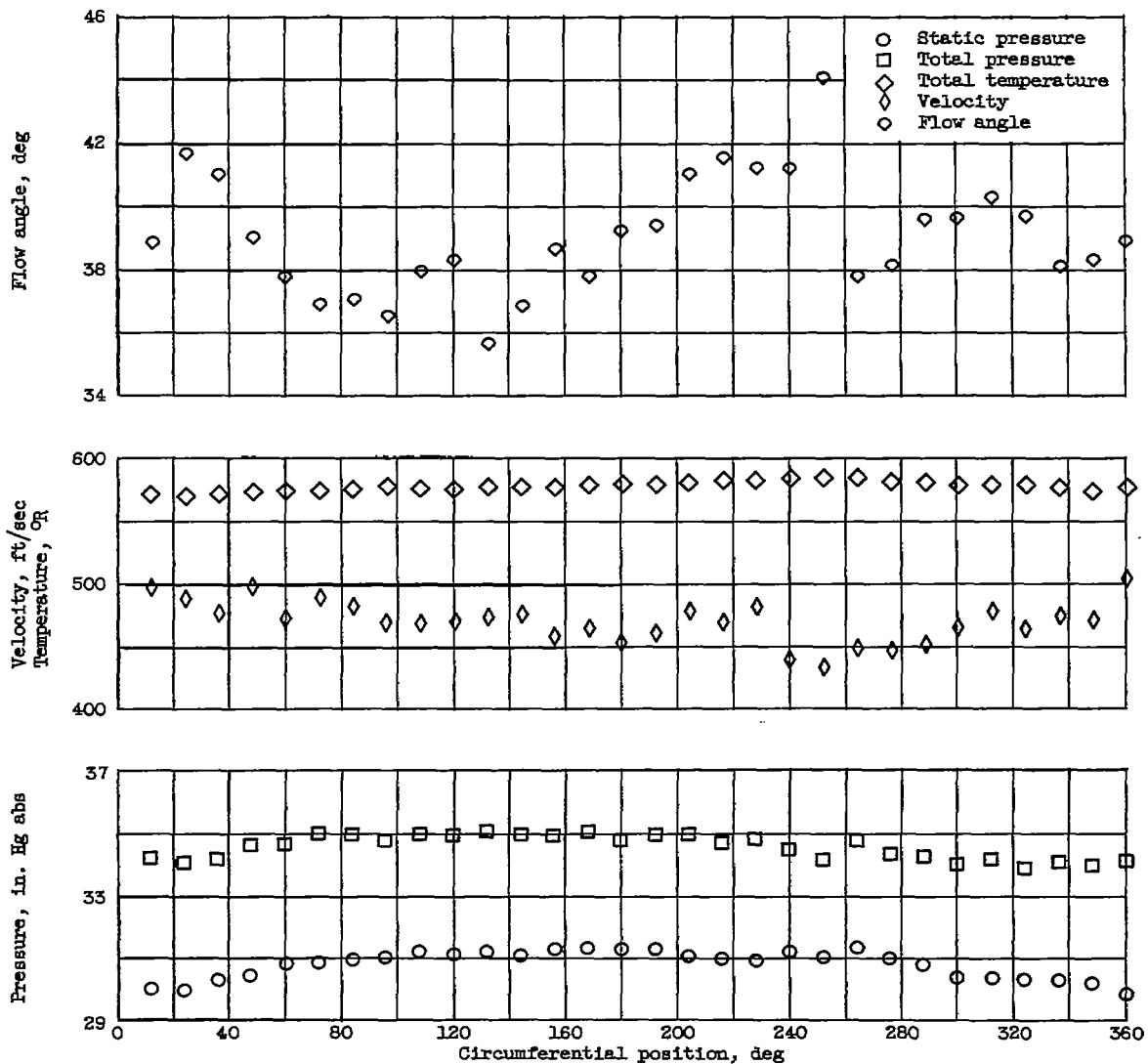


(c) 90-Percent passage depth (hub); station 2; absolute total temperature, 540° R.

Figure 7. - Continued. Variation of distorted-flow patterns with circumferential position. 70-Percent speed.

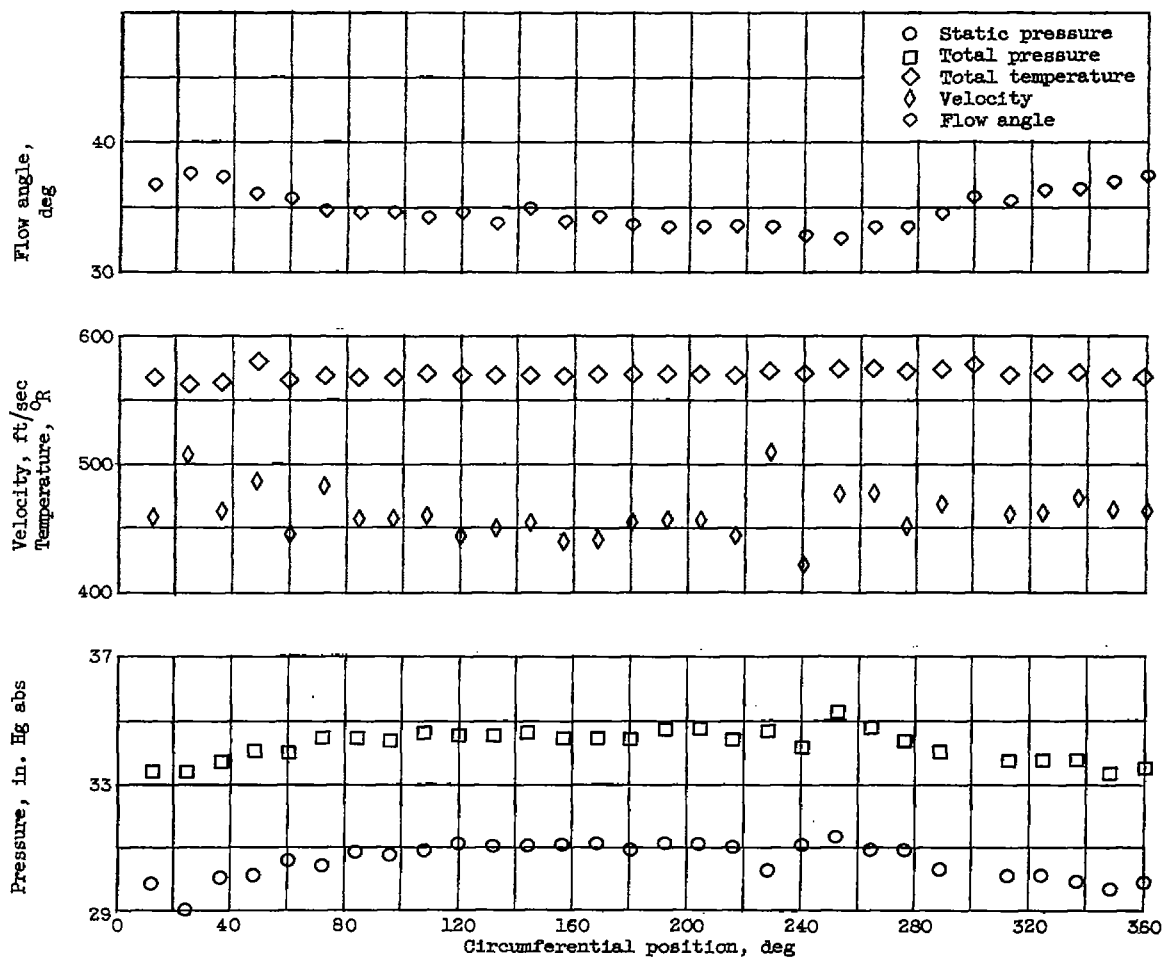
4710

CB-4



(d) 10-Percent passage depth (tip); station 3.

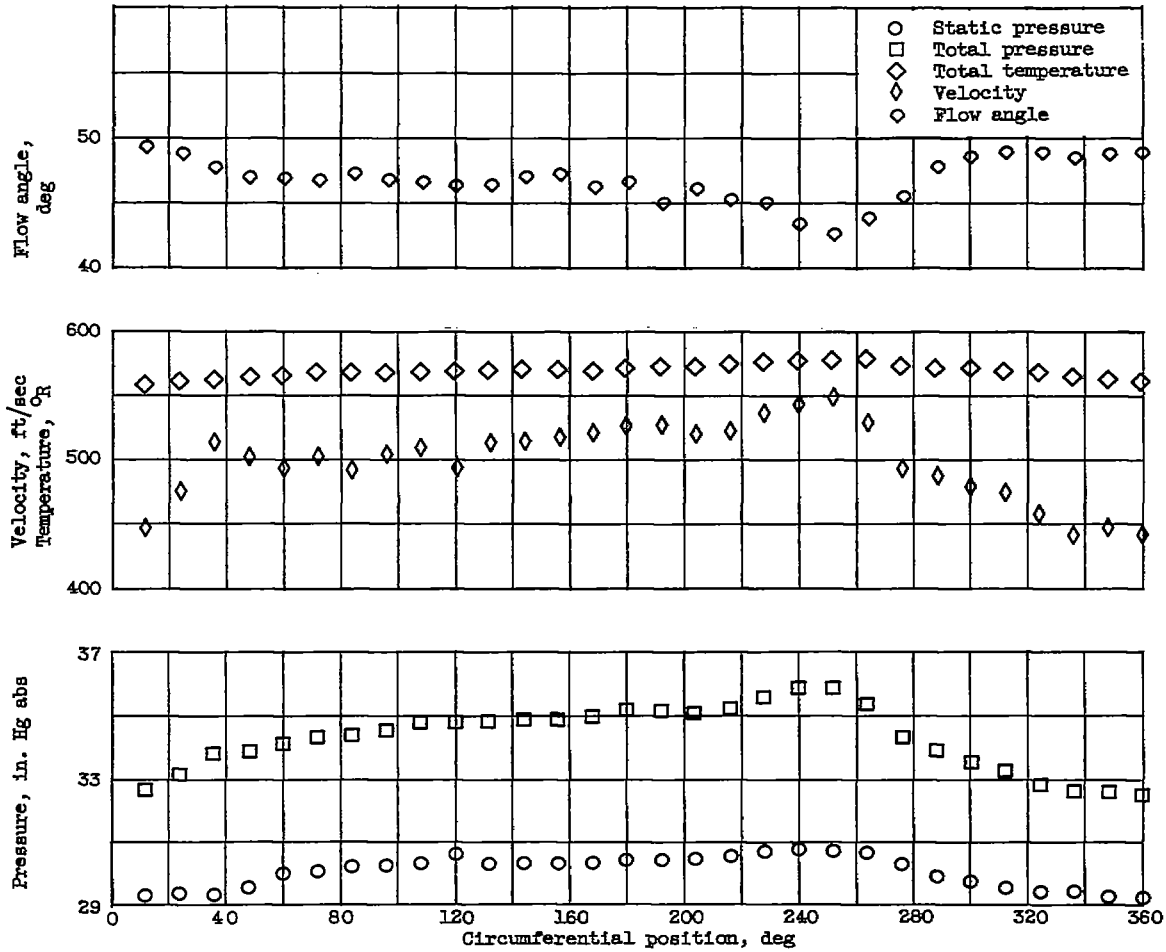
Figure 7. - Continued. Variation of distorted-flow patterns with circumferential position. 70-Percent speed.



(e) 50-Percent passage depth (mean); station 3.

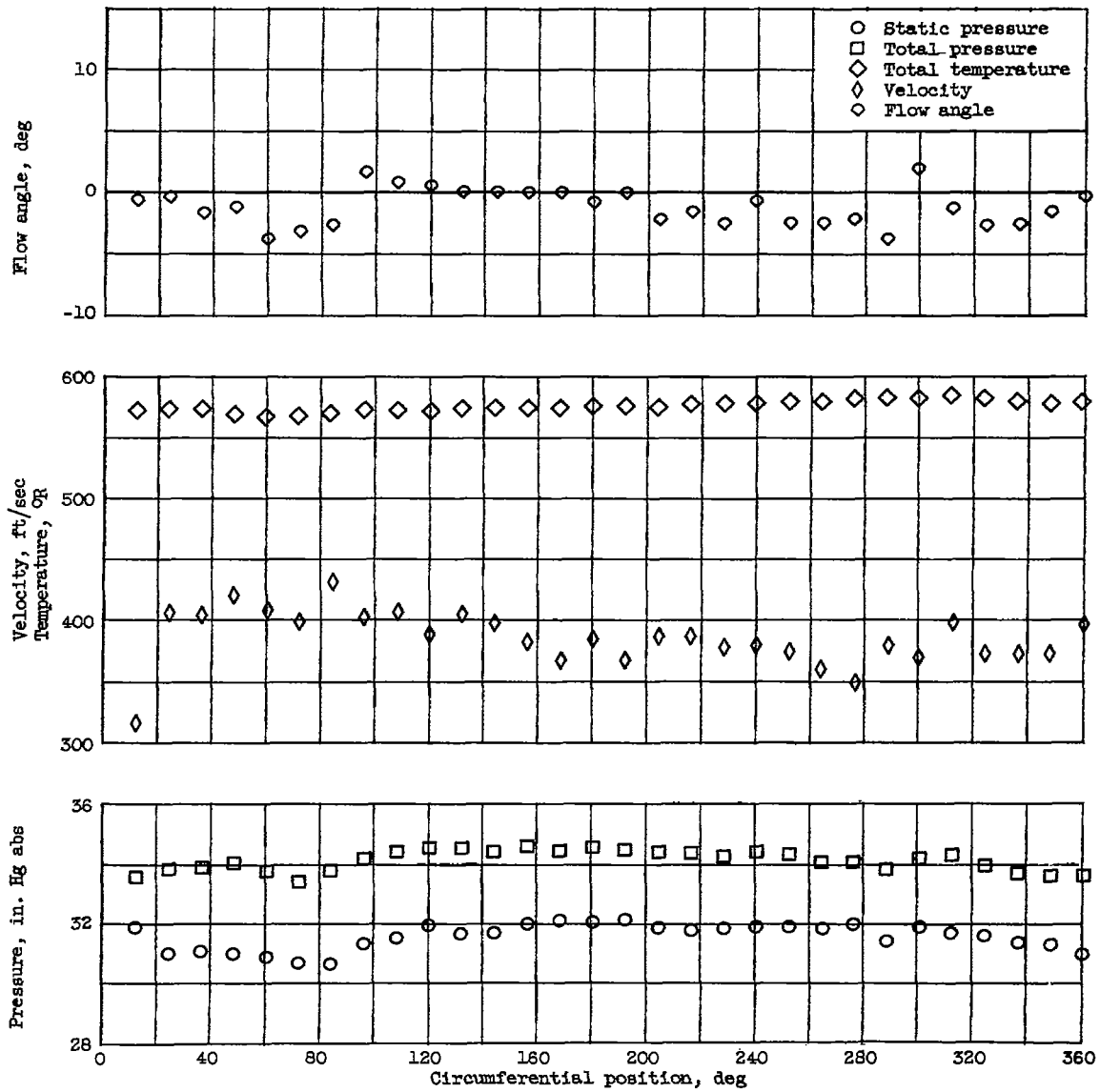
Figure 7. - Continued. Variation of distorted-flow patterns with circumferential position. 70-Percent speed.

4710 CB-4 back



(f) 90-Percent passage depth (hub); station 3.

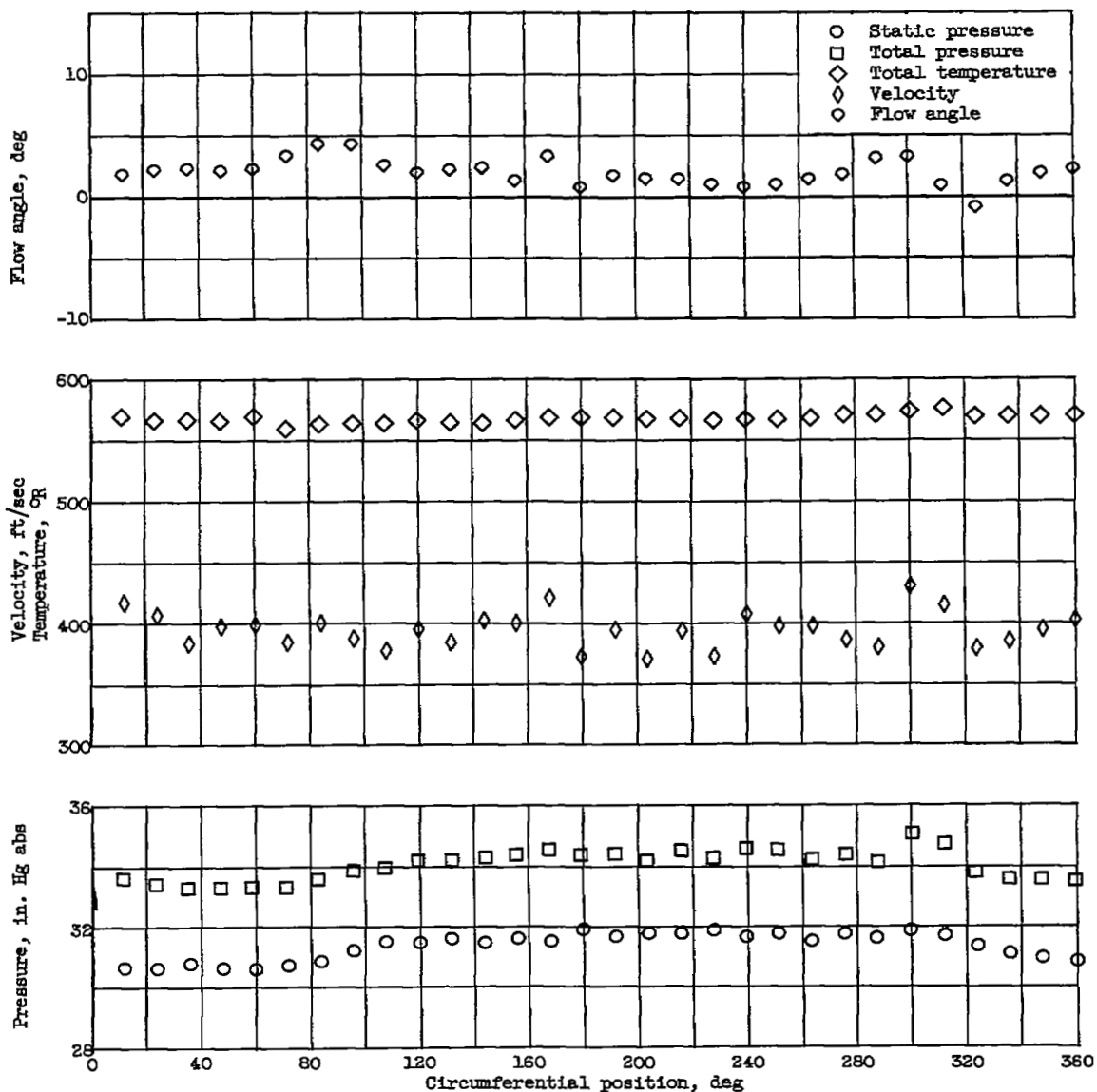
Figure 7. - Continued. Variation of distorted-flow patterns with circumferential position. 70-Percent speed.



(g) 10-Percent passage depth (tip); station 4.

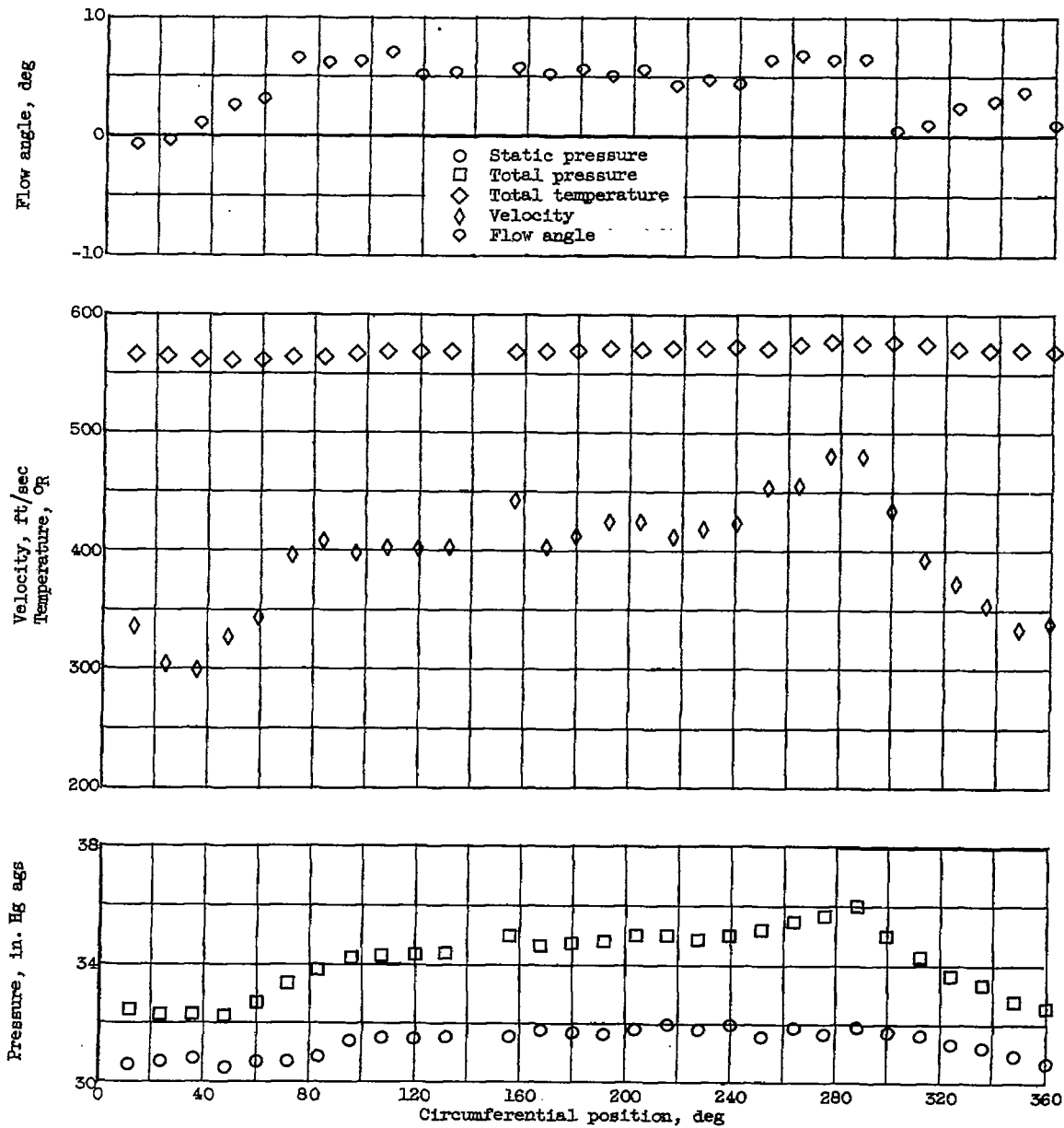
Figure 7. - Continued. Variation of distorted-flow patterns with circumferential position. 70-Percent speed.

4710



(h) 50-Percent passage depth (mean); station 4.

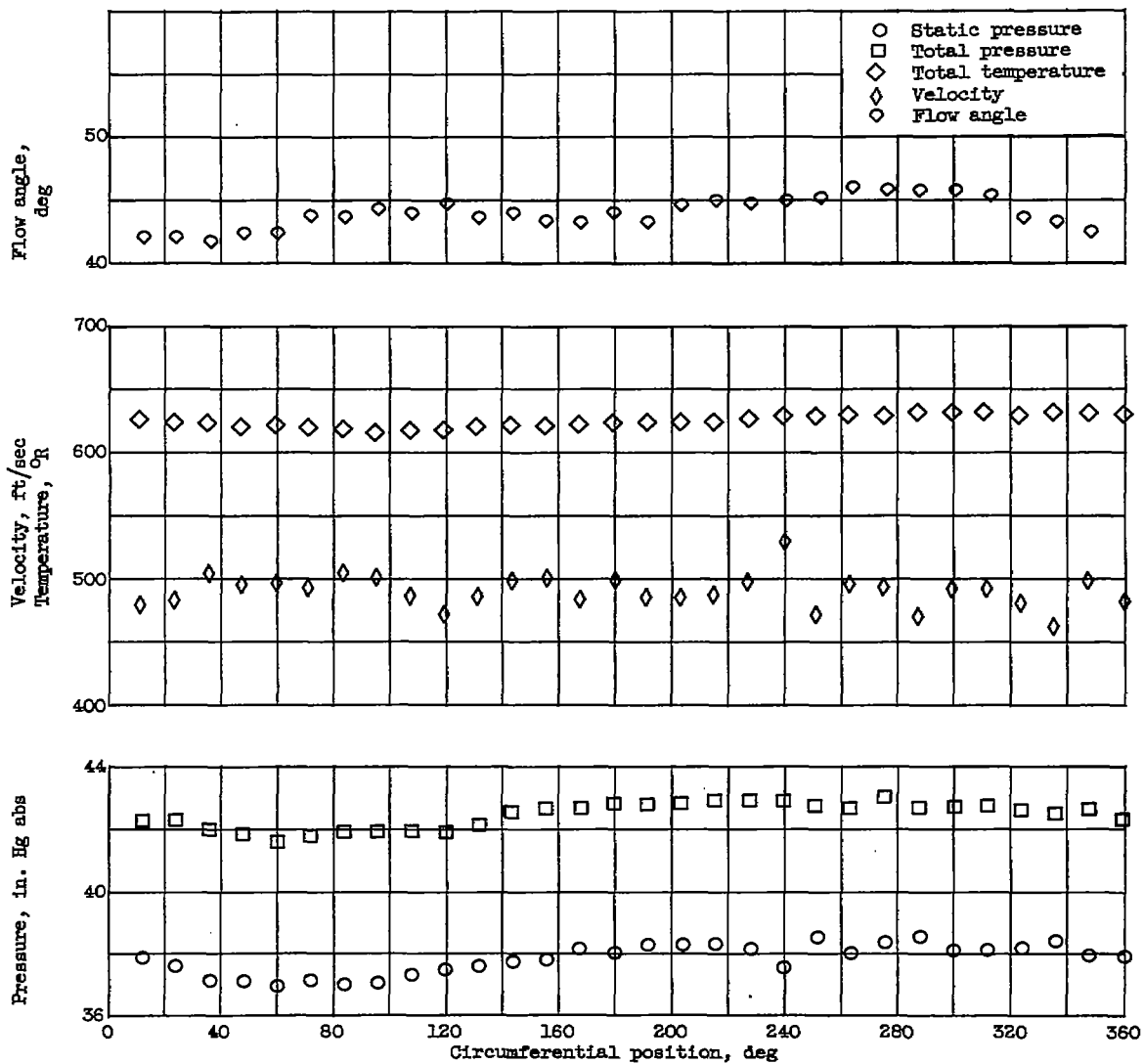
Figure 7. - Continued. Variation of distorted-flow patterns with circumferential position. 70-Percent speed.



(i) 90-Percent passage depth (hub); station 4.

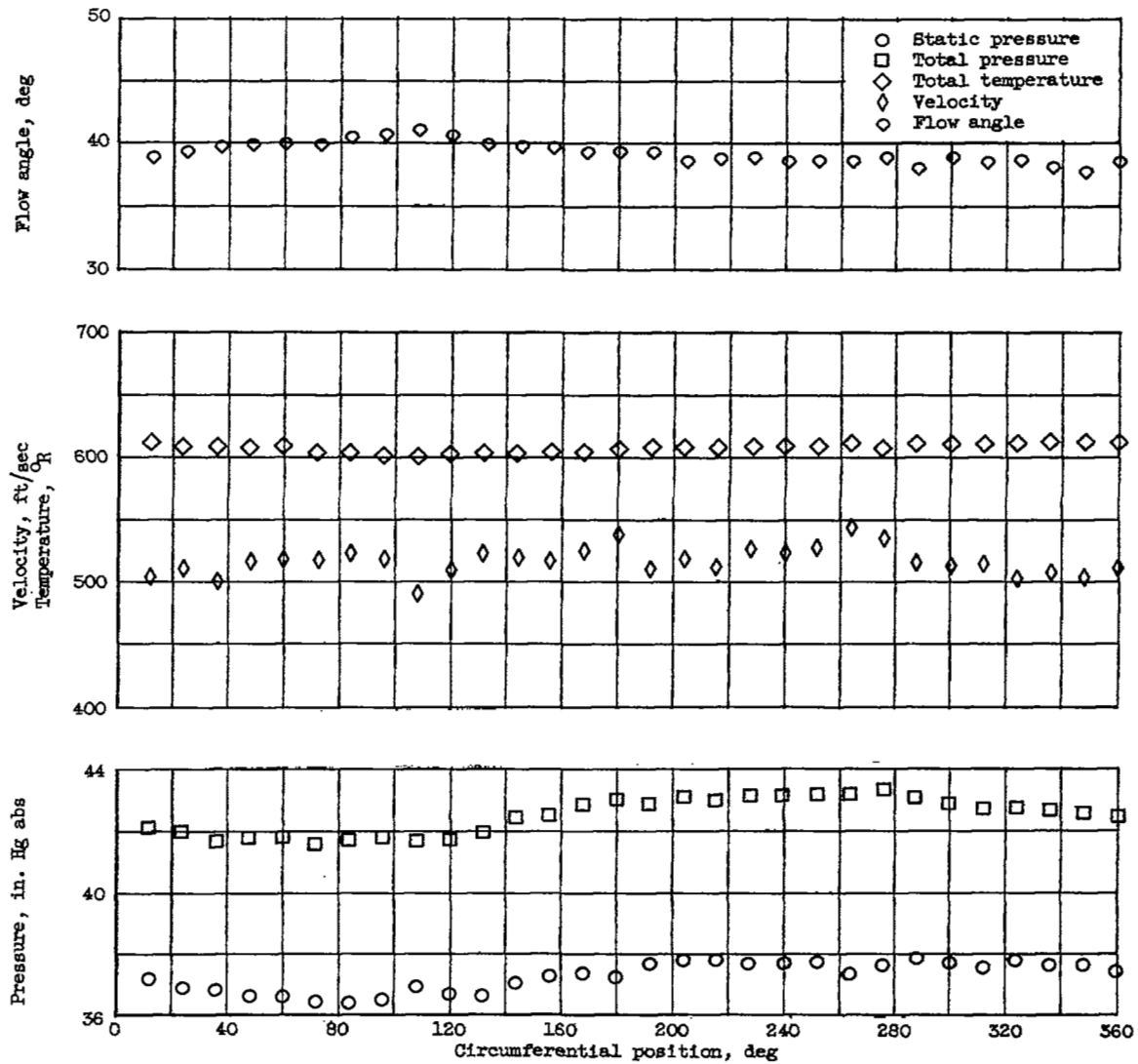
Figure 7. - Continued. Variation of distorted-flow patterns with circumferential position. 70-Percent speed.

4710



(j) 10-Percent passage depth (tip); station 5.

Figure 7. - Continued. Variation of distorted-flow patterns with circumferential position. 70-Percent speed.

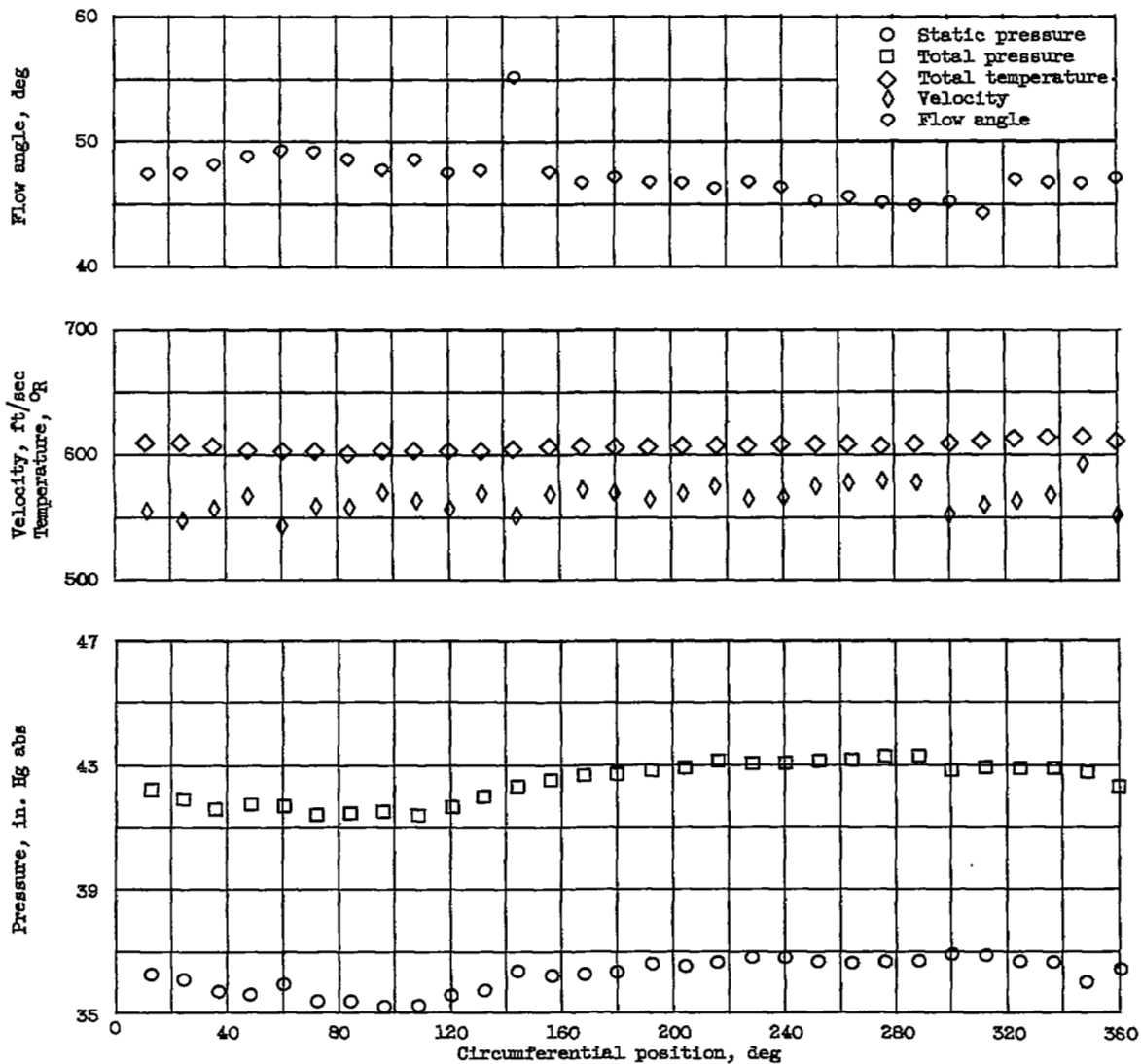


(k) 50-Percent passage depth (mean); station 5.

Figure 7. - Continued. Variation of distorted-flow patterns with circumferential position. 70-Percent speed.

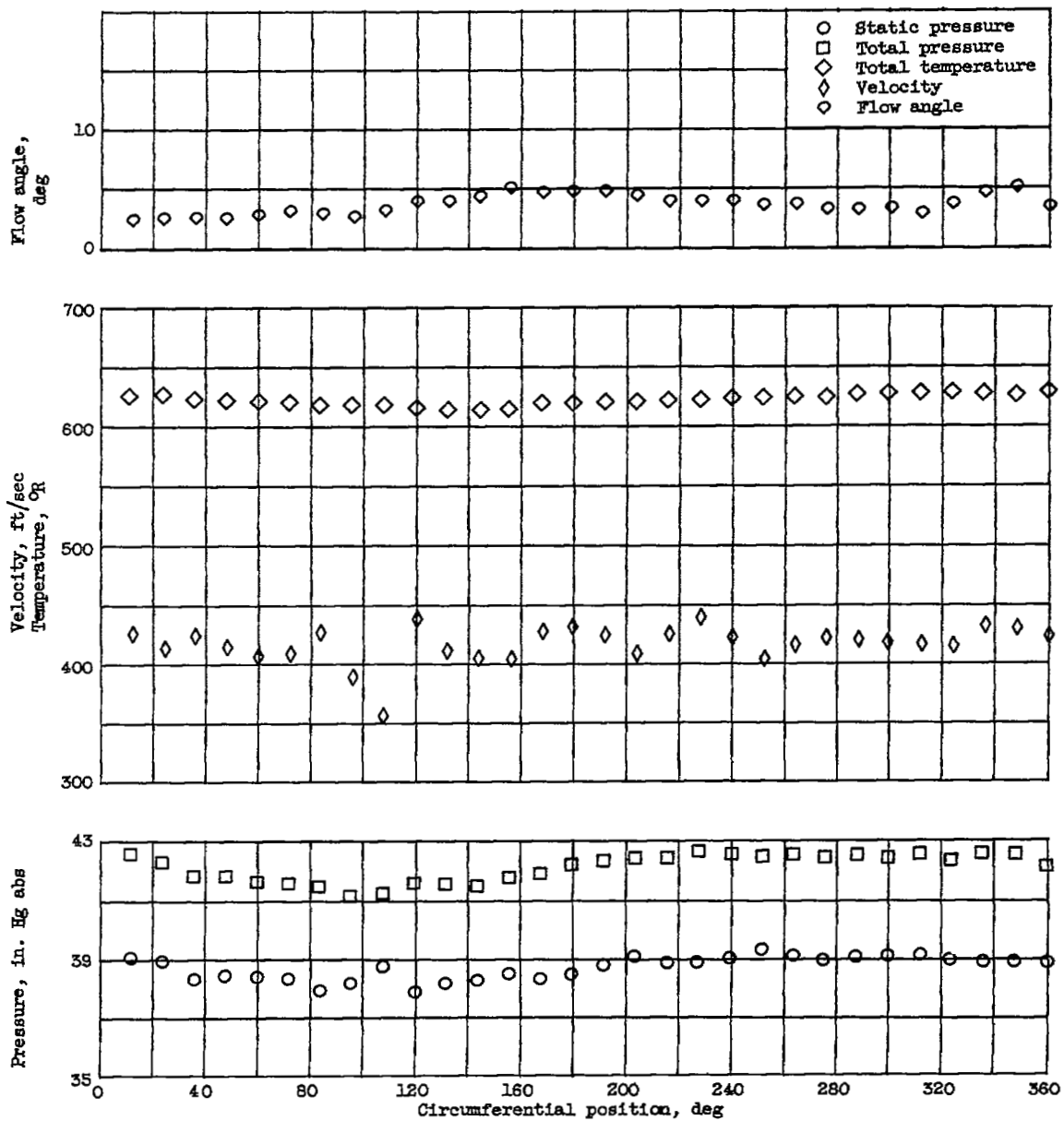
4710

CB-5



(1) 90-Percent passage depth (hub); station 5.

Figure 7. - Continued. Variation of distorted-flow patterns with circumferential position. 70-Percent speed.

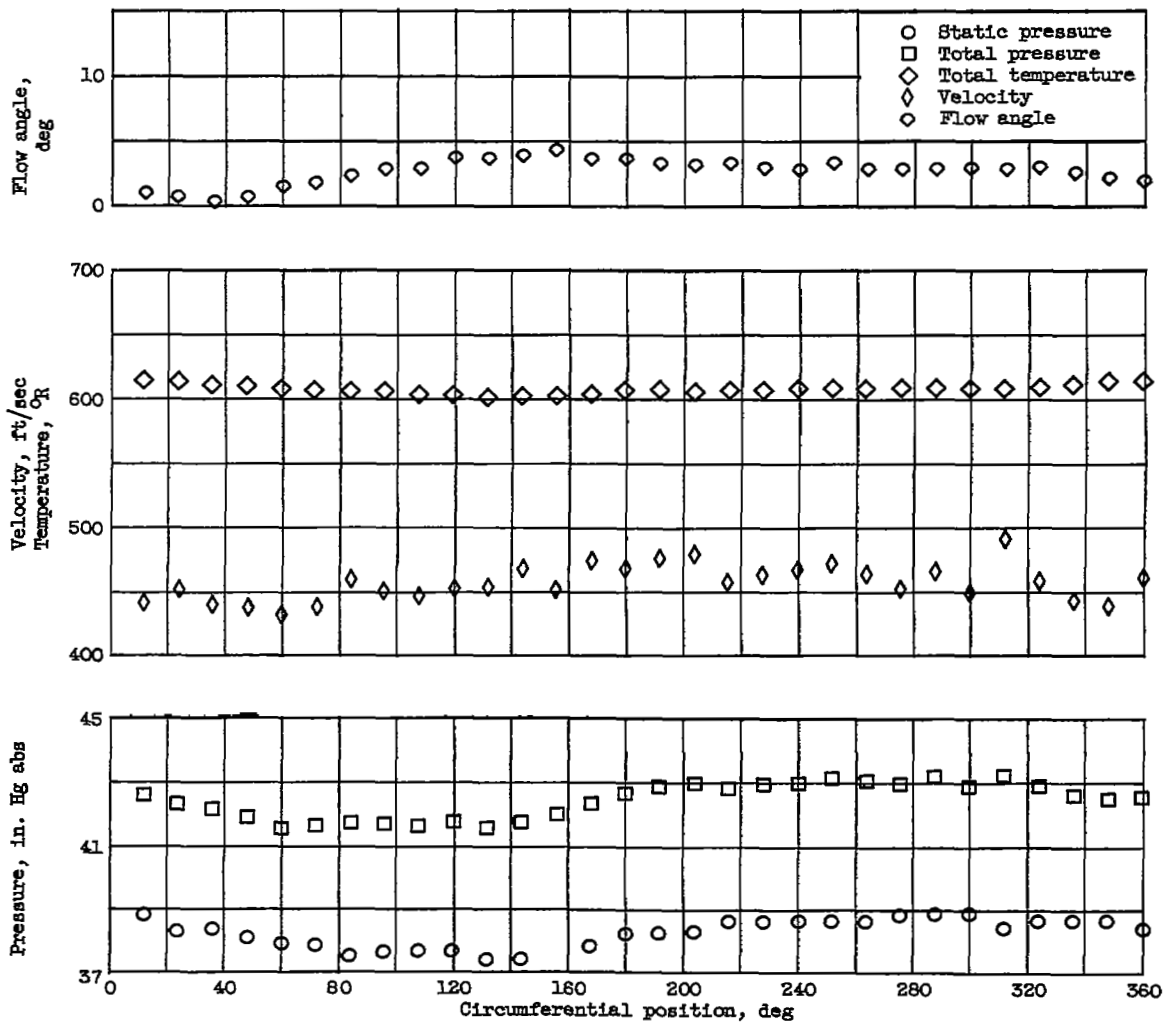


(m) 10-Percent passage depth (tip); station 6.

Figure 7. - Continued. Variation of distorted-flow patterns with circumferential position. 70-Percent speed.

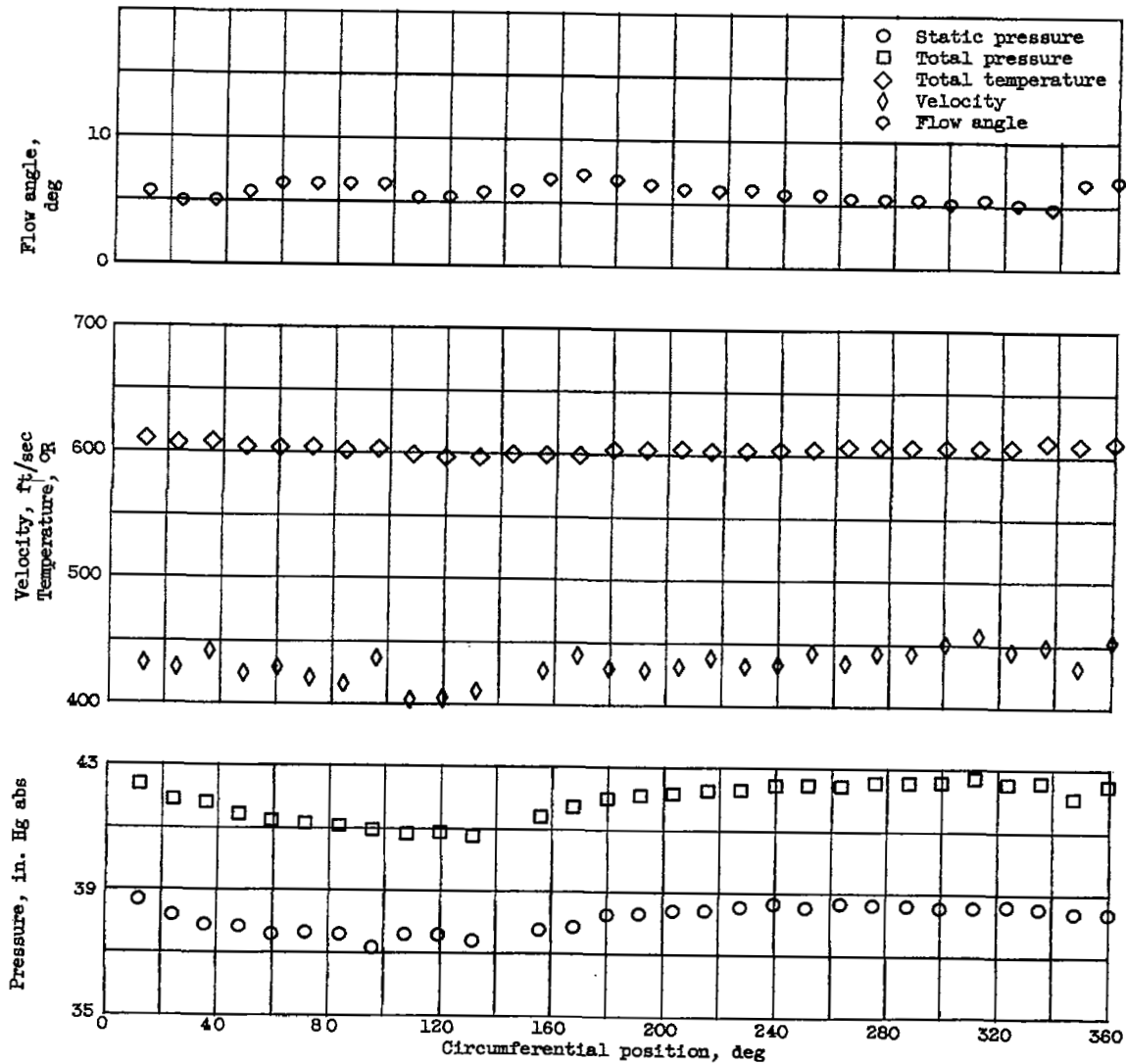
4710

CB-5 back



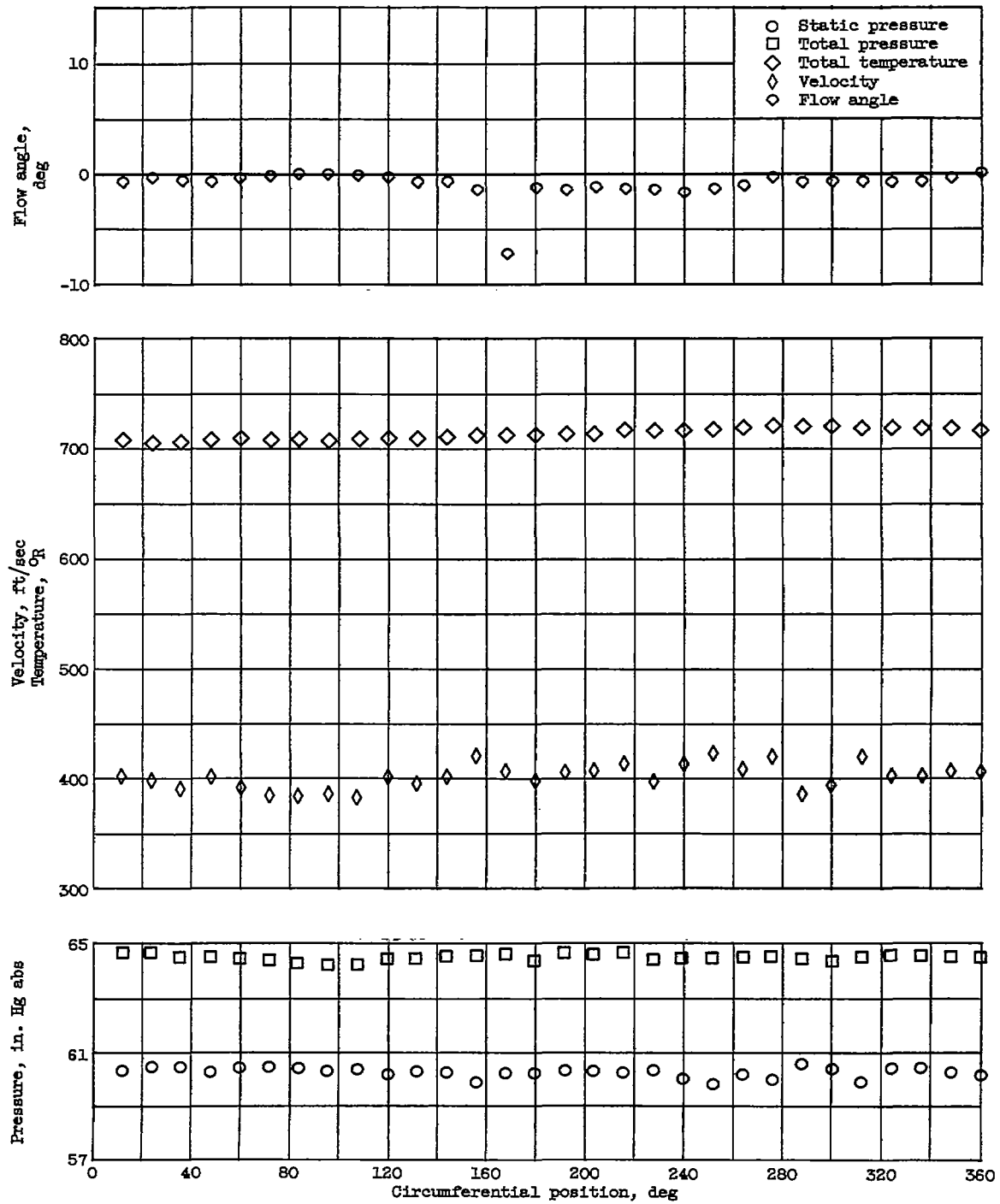
(n) 50-Percent passage depth (mean); station 6.

Figure 7. - Continued. Variation of distorted-flow patterns with circumferential position. 70-Percent speed.



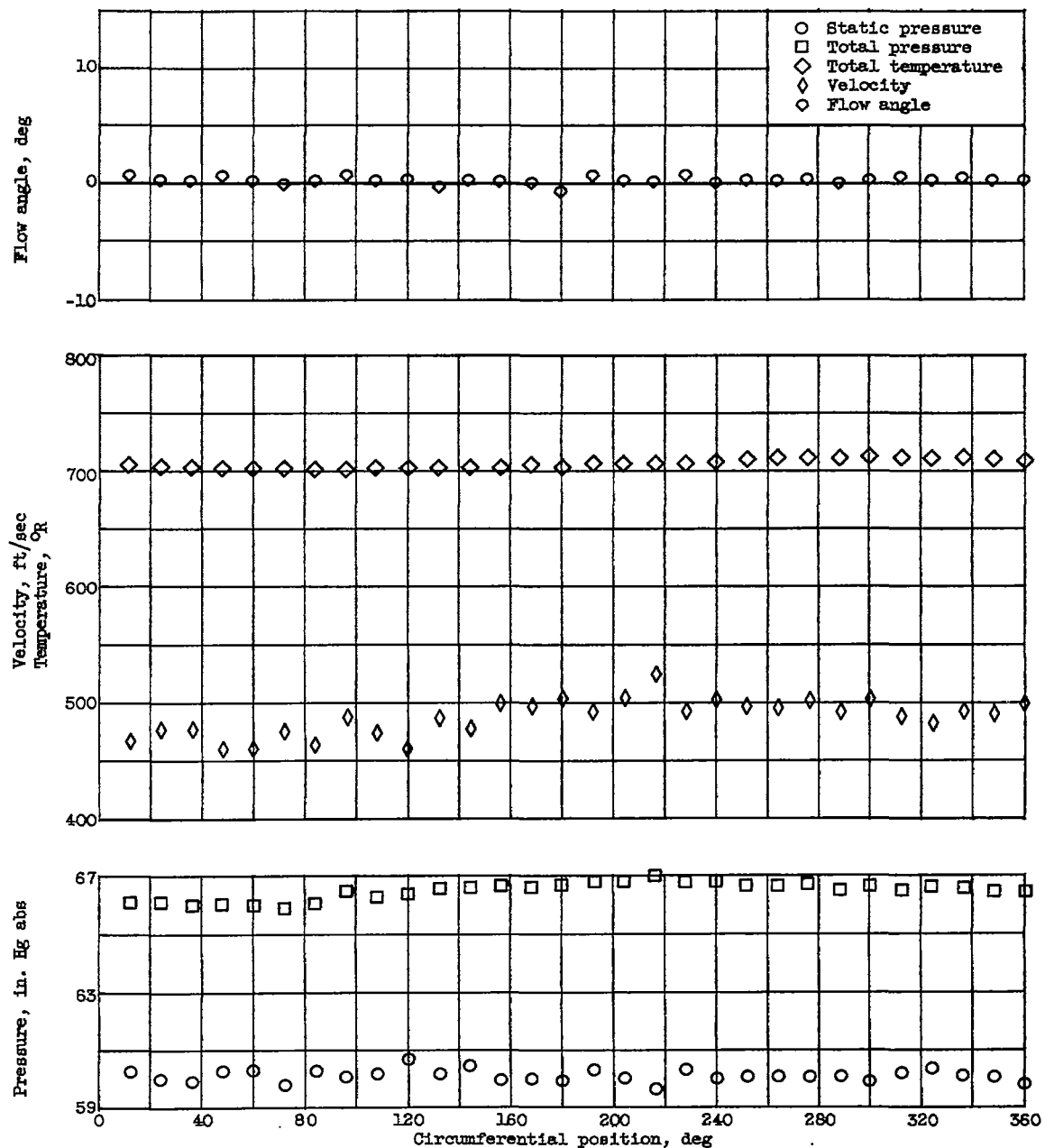
(o) 90-Percent passage depth (hub); station 6.

Figure 7. - Continued. Variation of distorted-flow patterns with circumferential position. 70-Percent speed.



(p) 10-Percent passage depth (tip); station 7.

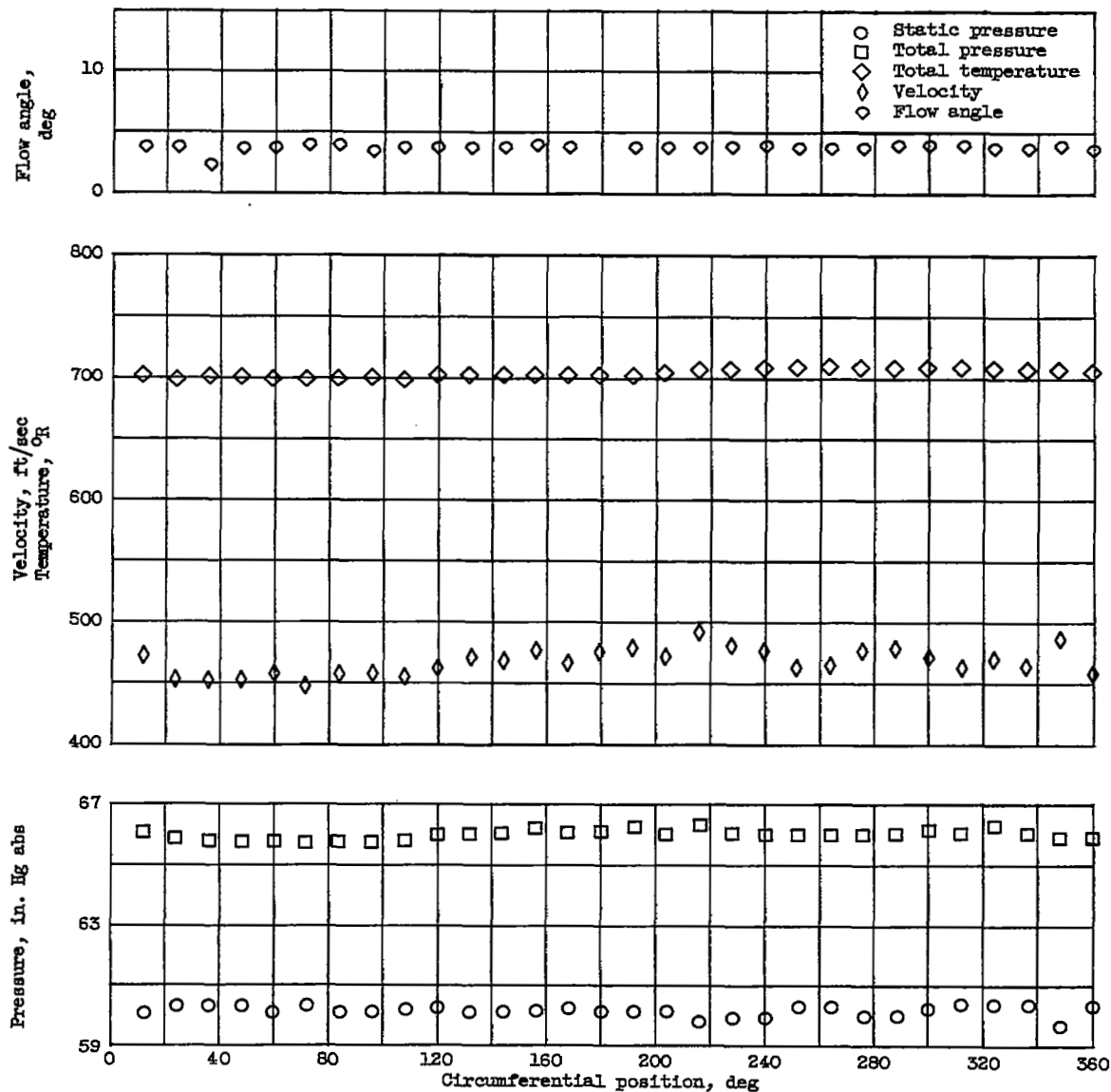
Figure 7. - Continued. Variation of distorted-flow patterns with circumferential position. 70-Percent speed.



(q) 50-Percent passage depth (mean); station 7.

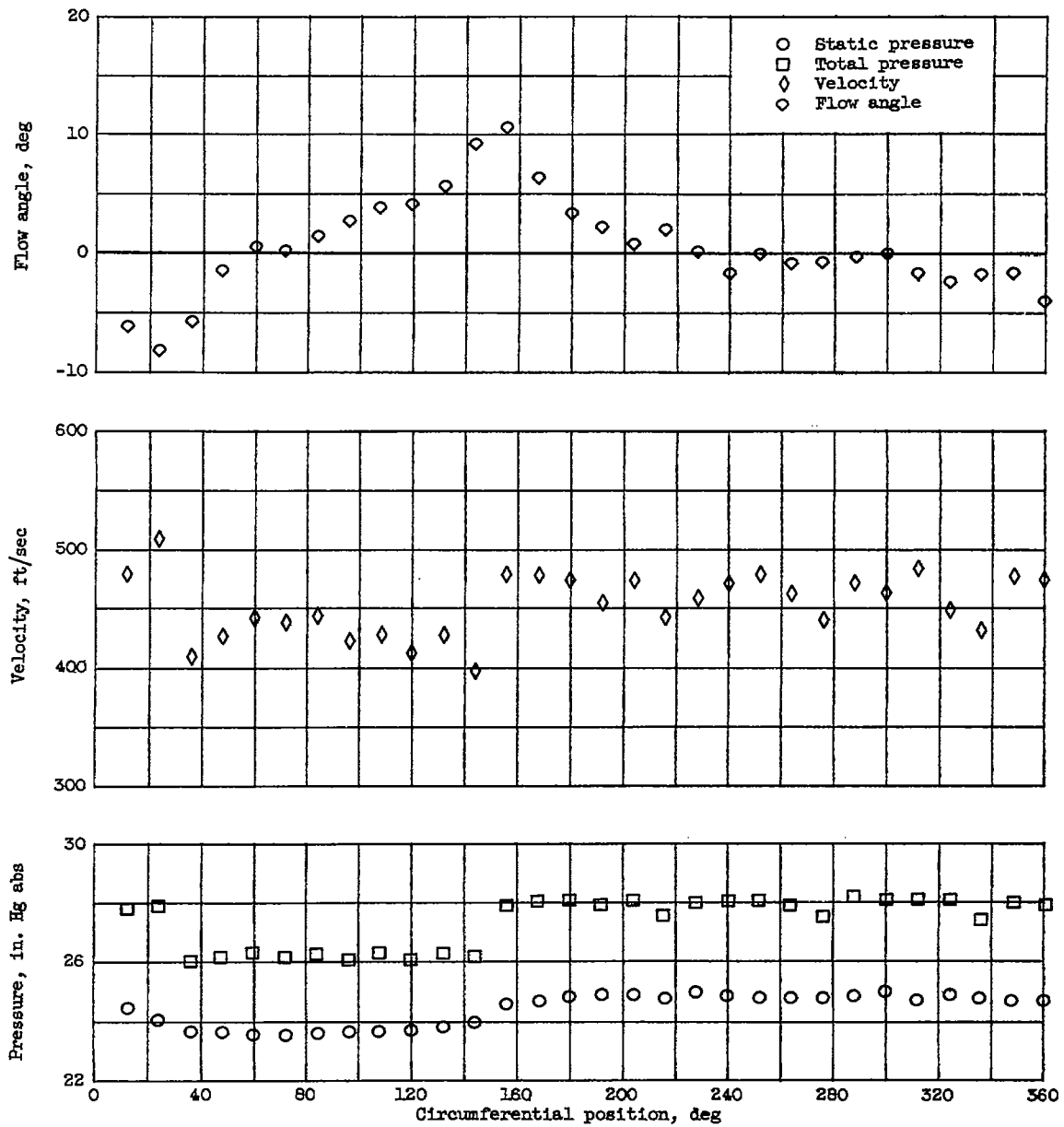
Figure 7. - Continued. Variation of distorted-flow patterns with circumferential position. 70-Percent speed.

4710



(r) 90-Percent passage depth (hub); station 7.

Figure 7. - Concluded. Variation of distorted-flow patterns with circumferential position. 70-Percent speed.

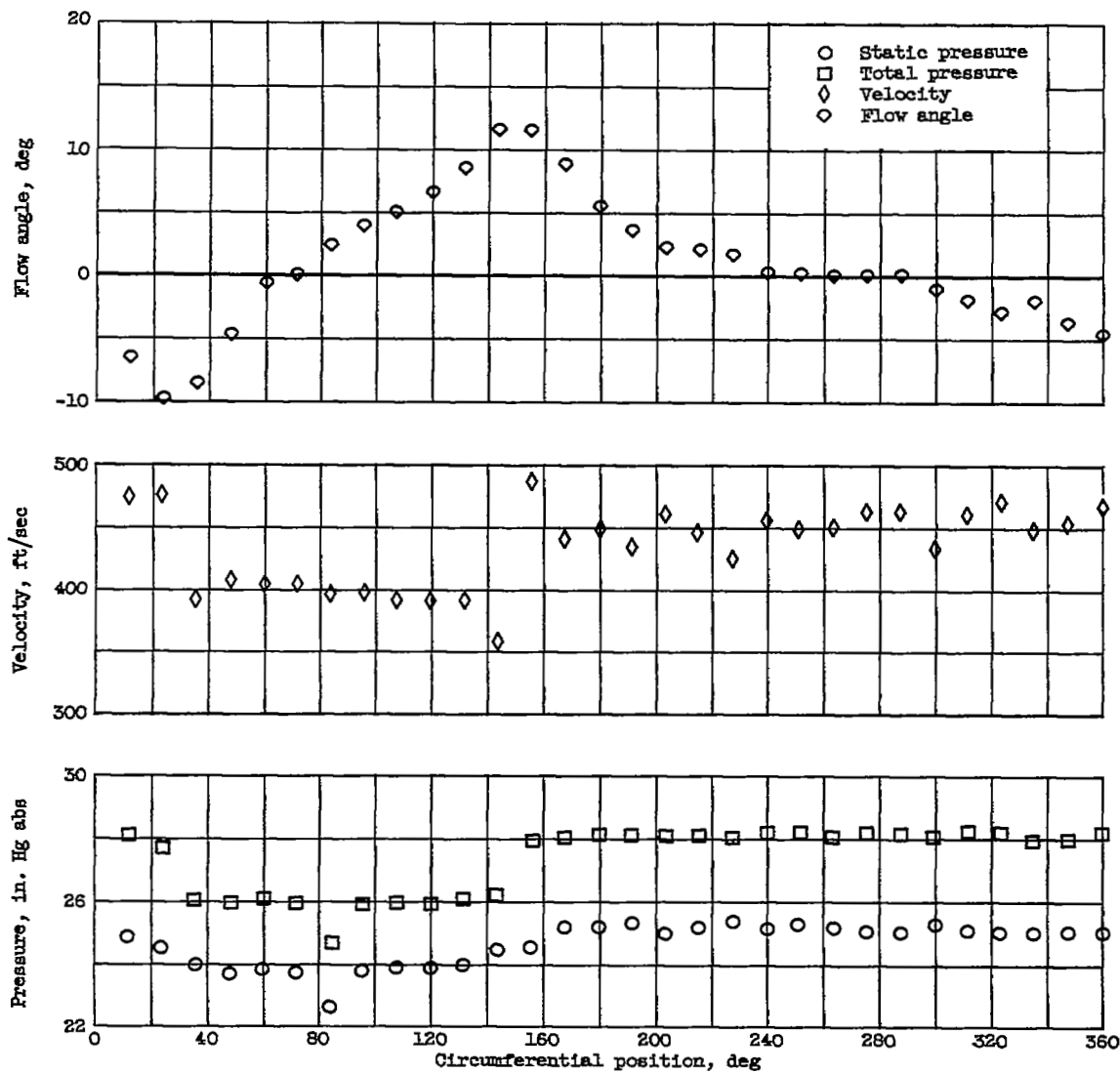


(a) Station 2; tip; absolute total temperature, 540° R.

Figure 8. - Variation of distorted-flow patterns with circumferential position. 80-Percent speed.

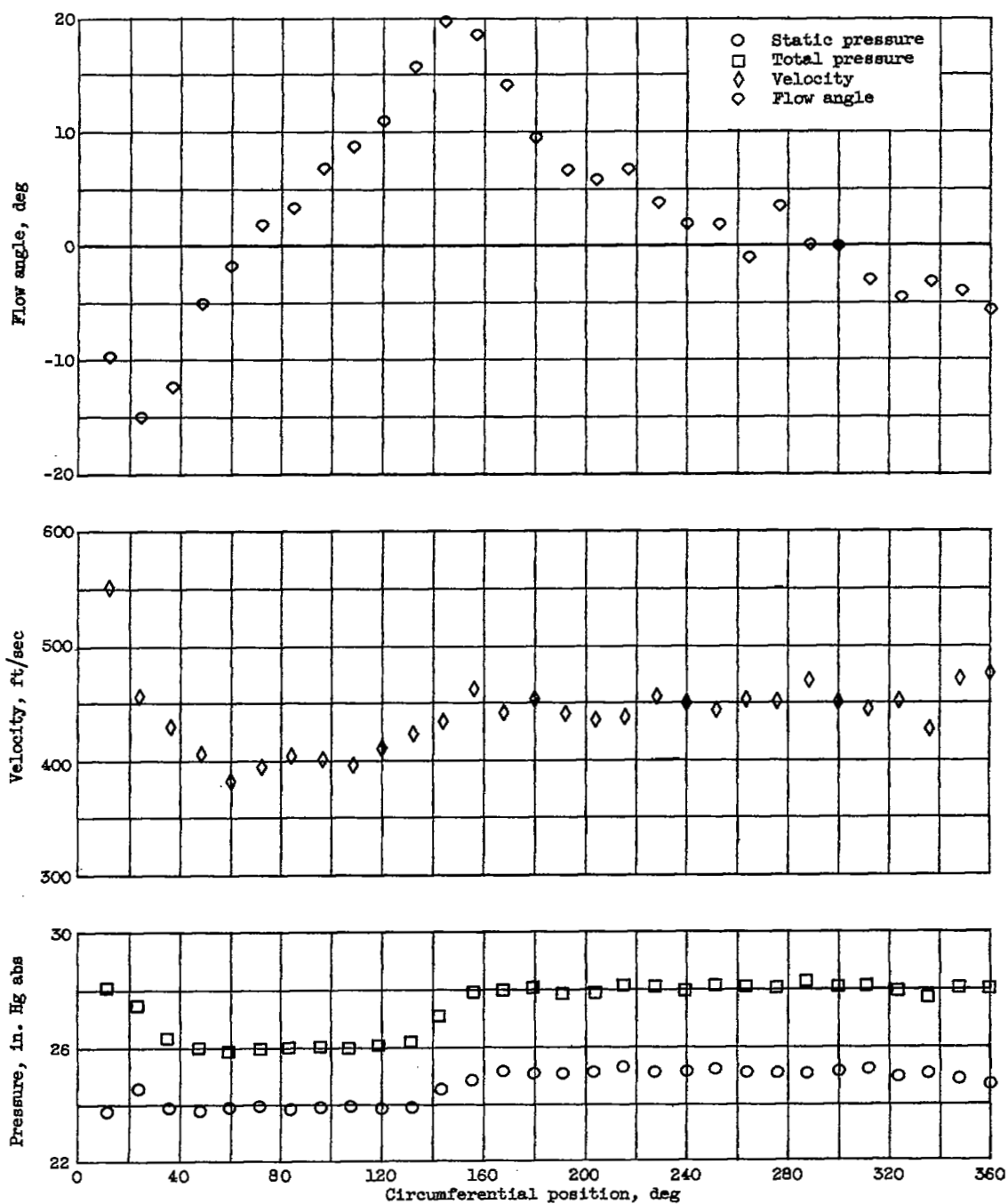
4710

CB-6



(b) Station 2; mean; absolute total temperature, 542° R.

Figure 8. - Continued. Variation of distorted-flow patterns with circumferential position. 80-Percent speed.

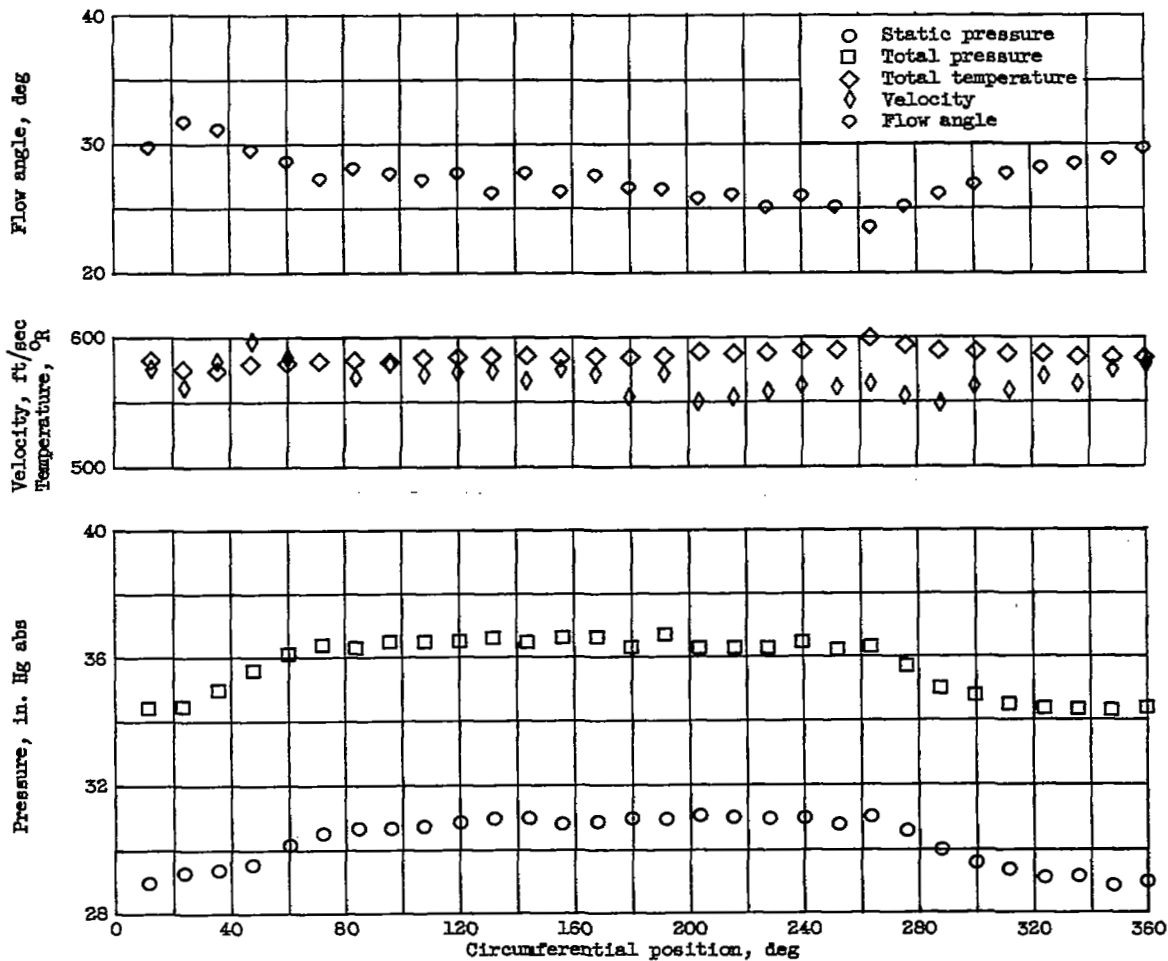


(c) Station 2; hub; absolute total temperature, 545° R.

Figure 8. - Continued. Variation of distorted-flow patterns with circumferential position. 80-Percent speed.

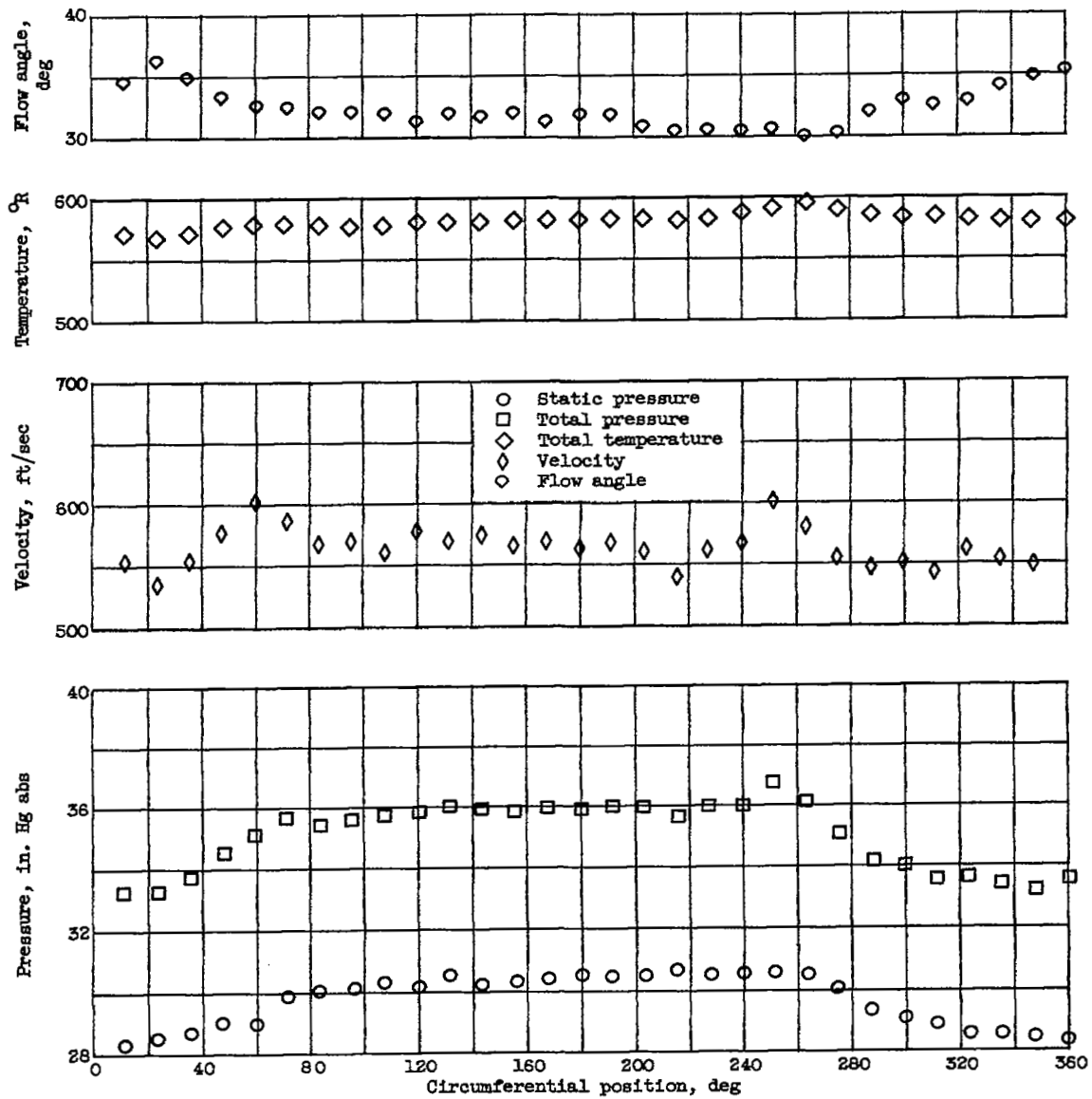
4710

CB-6 back



(d) Station 3; tip.

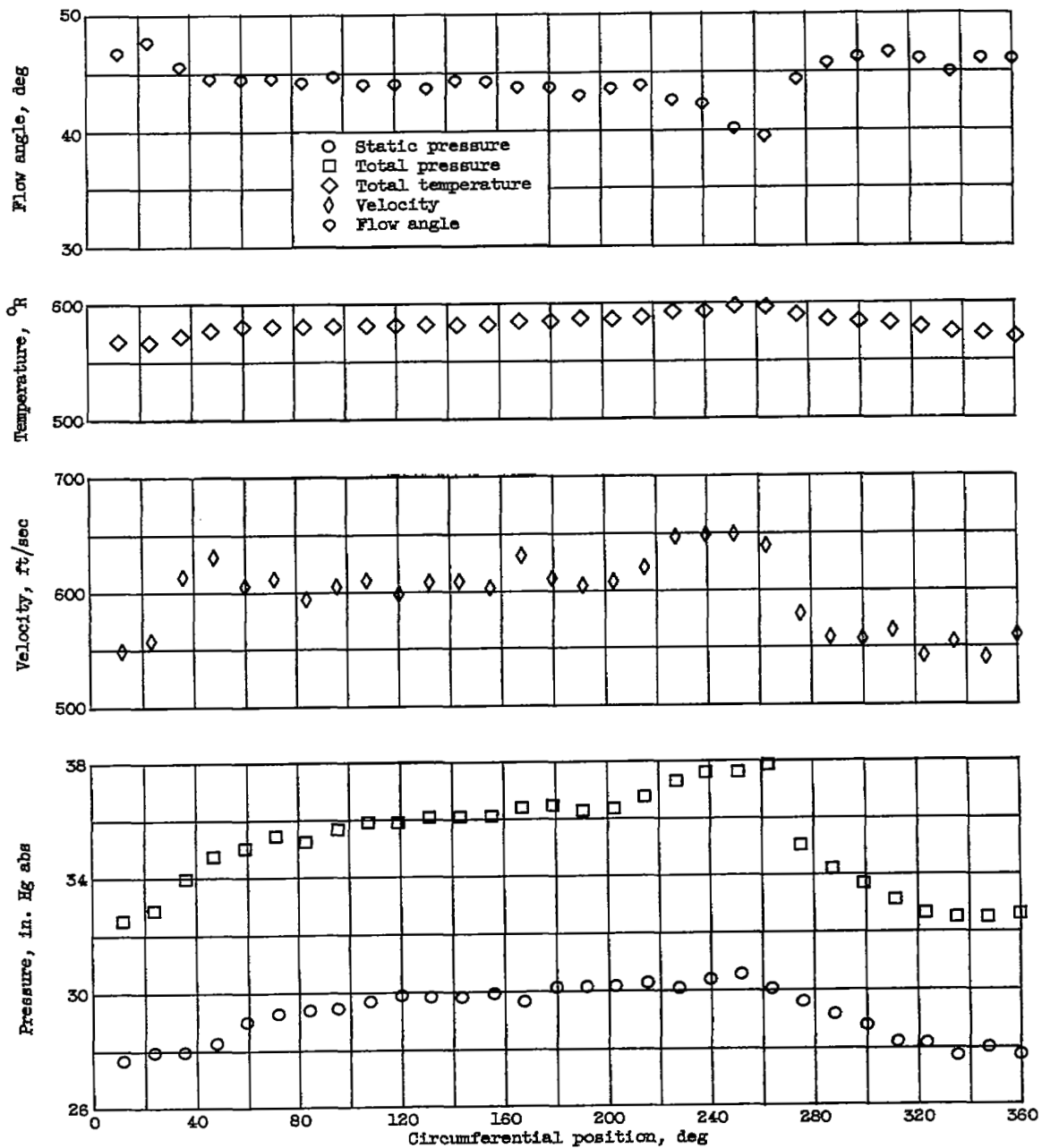
Figure 8. - Continued. Variation of distorted-flow patterns with circumferential position. 80-Percent speed.



(e) Station 3; mean.

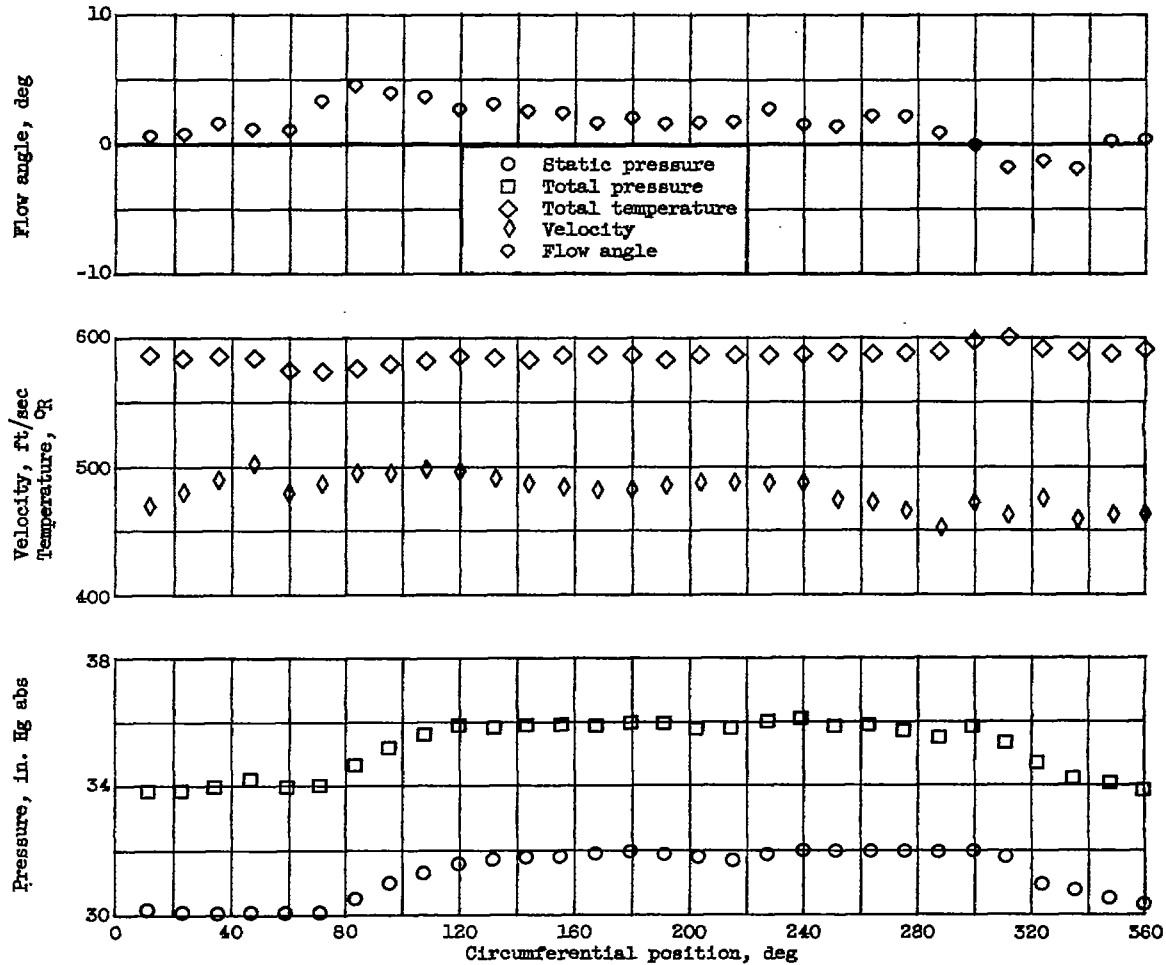
Figure 8. - Continued. Variation of distorted-flow patterns with circumferential position. 80-Percent speed.

4710



(f) Station 3; hub.

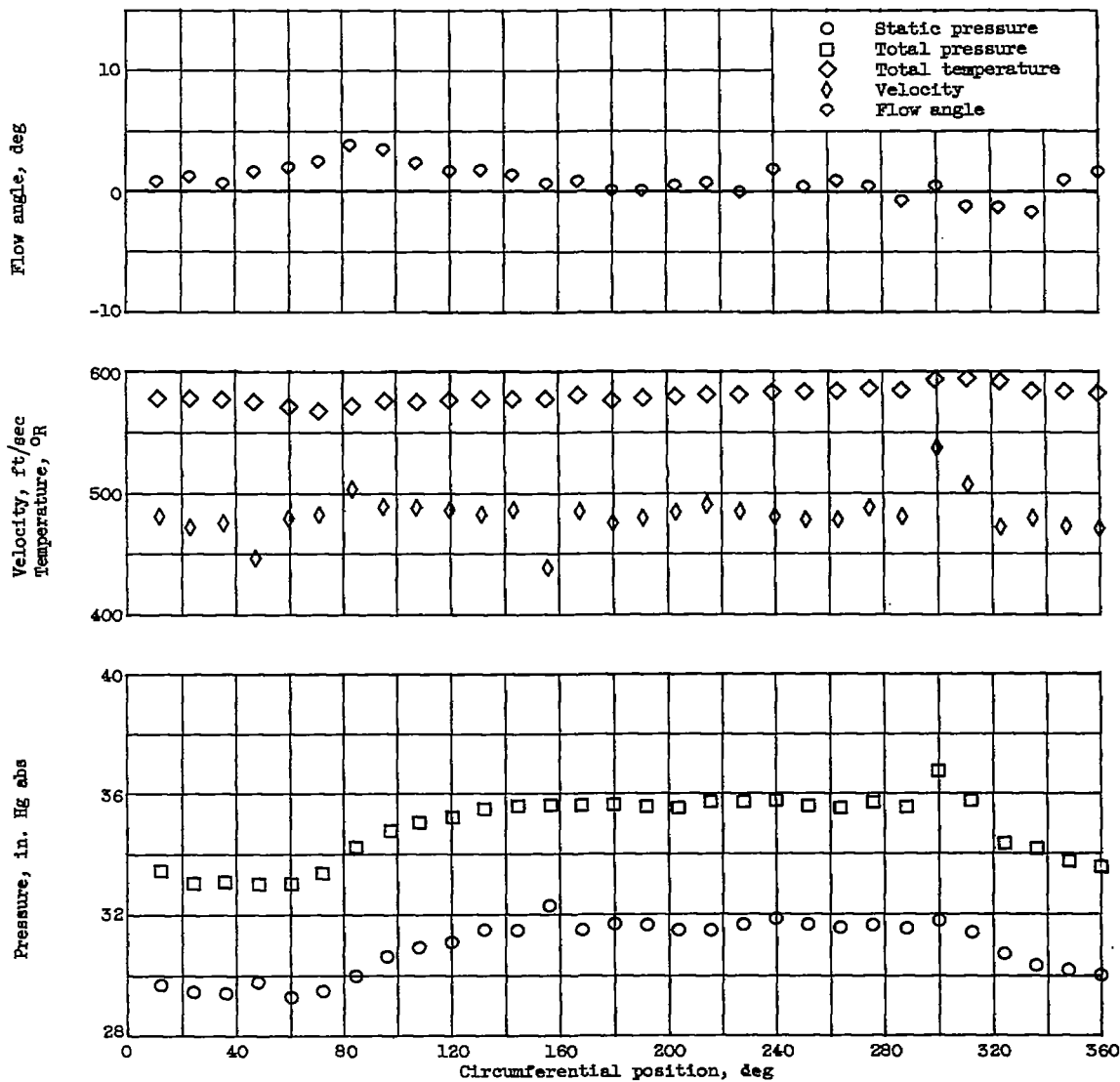
Figure 8. - Continued. Variation of distorted-flow patterns with circumferential position. 80-Percent speed.



(g) Station 4; tip.

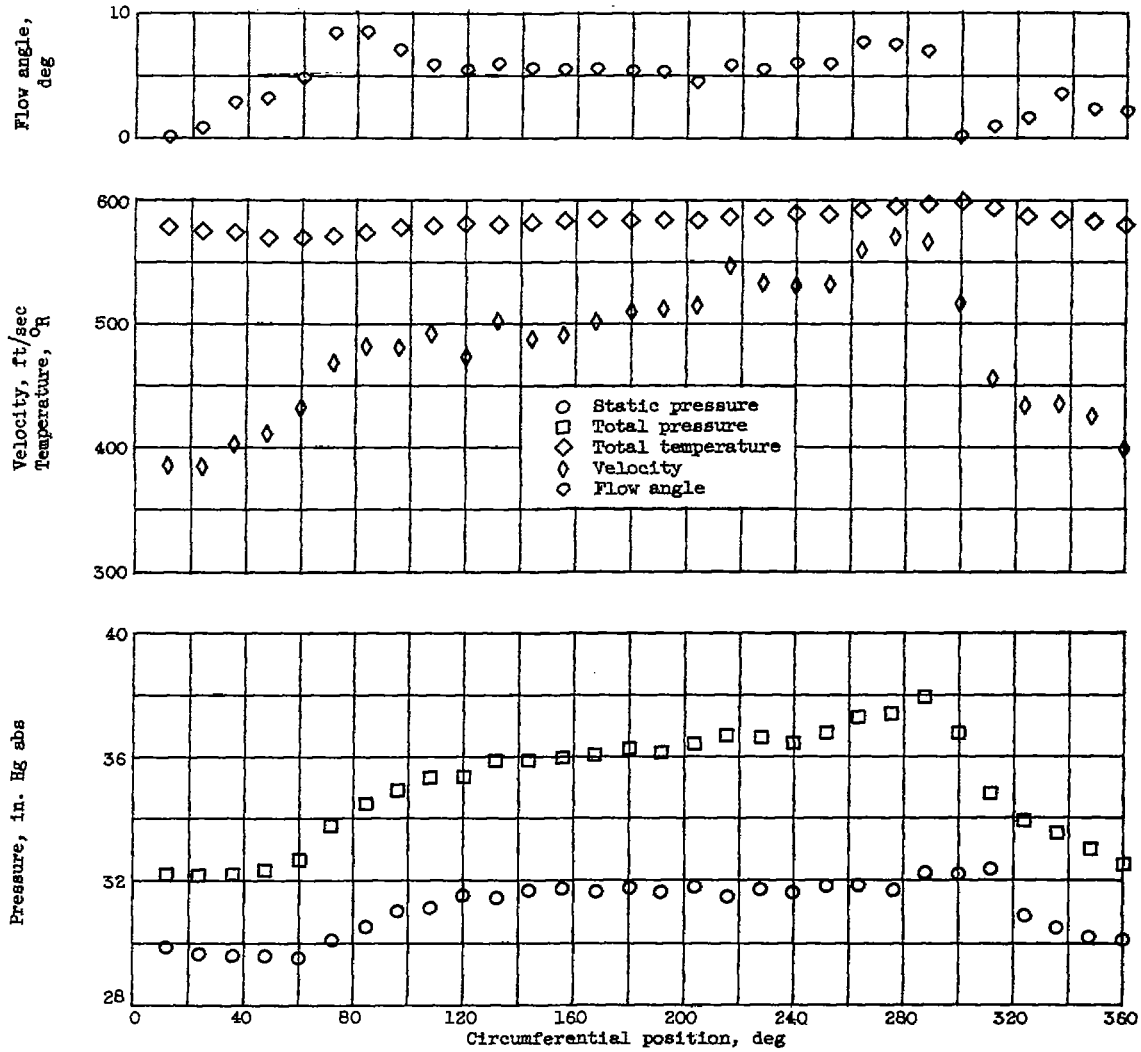
Figure 8. - Continued. Variation of distorted-flow patterns with circumferential position. 80-Percent speed.

4710



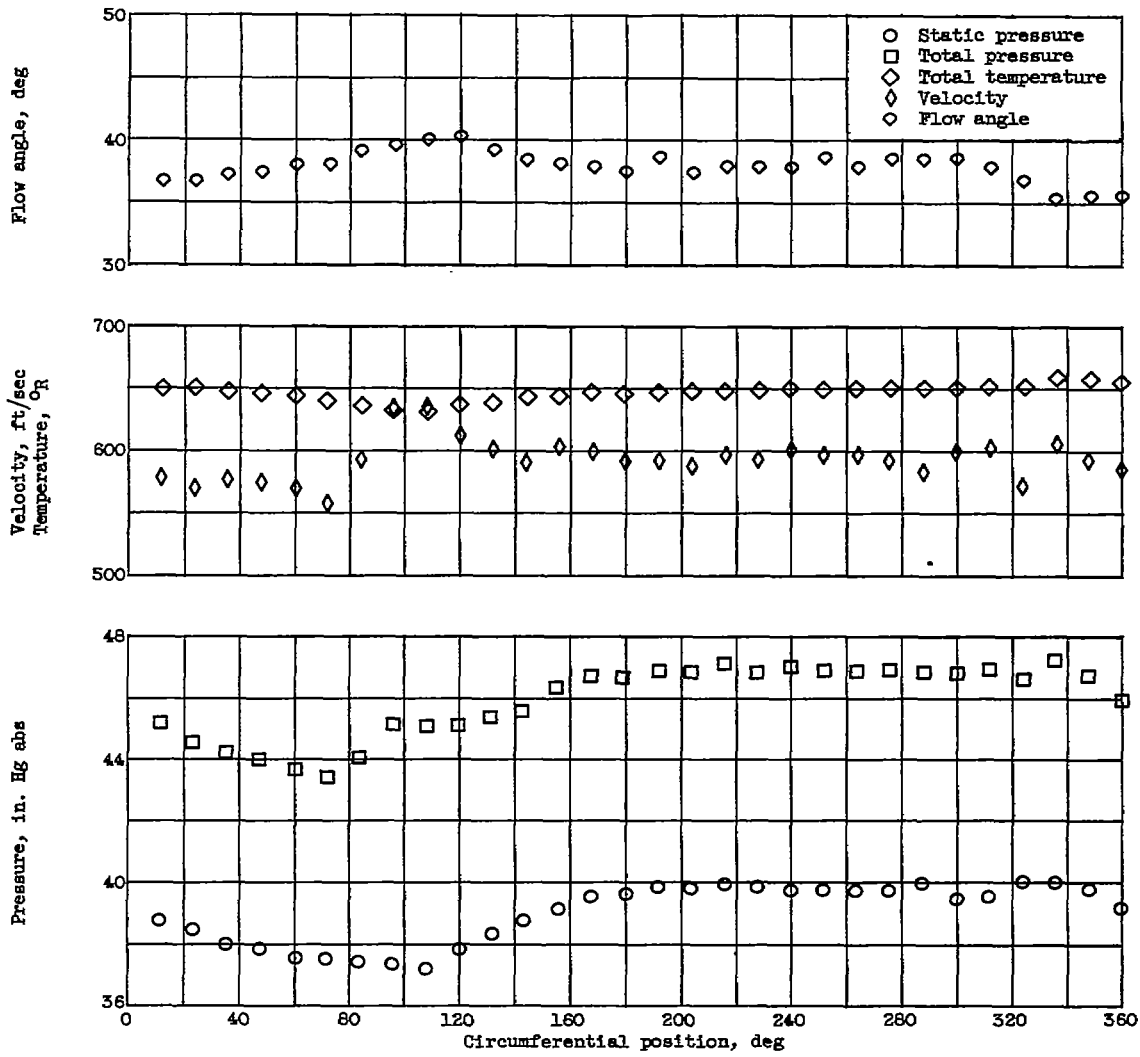
(h) Station 4; mean.

Figure 8. - Continued. Variation of distorted-flow patterns with circumferential position. 80-Percent speed.



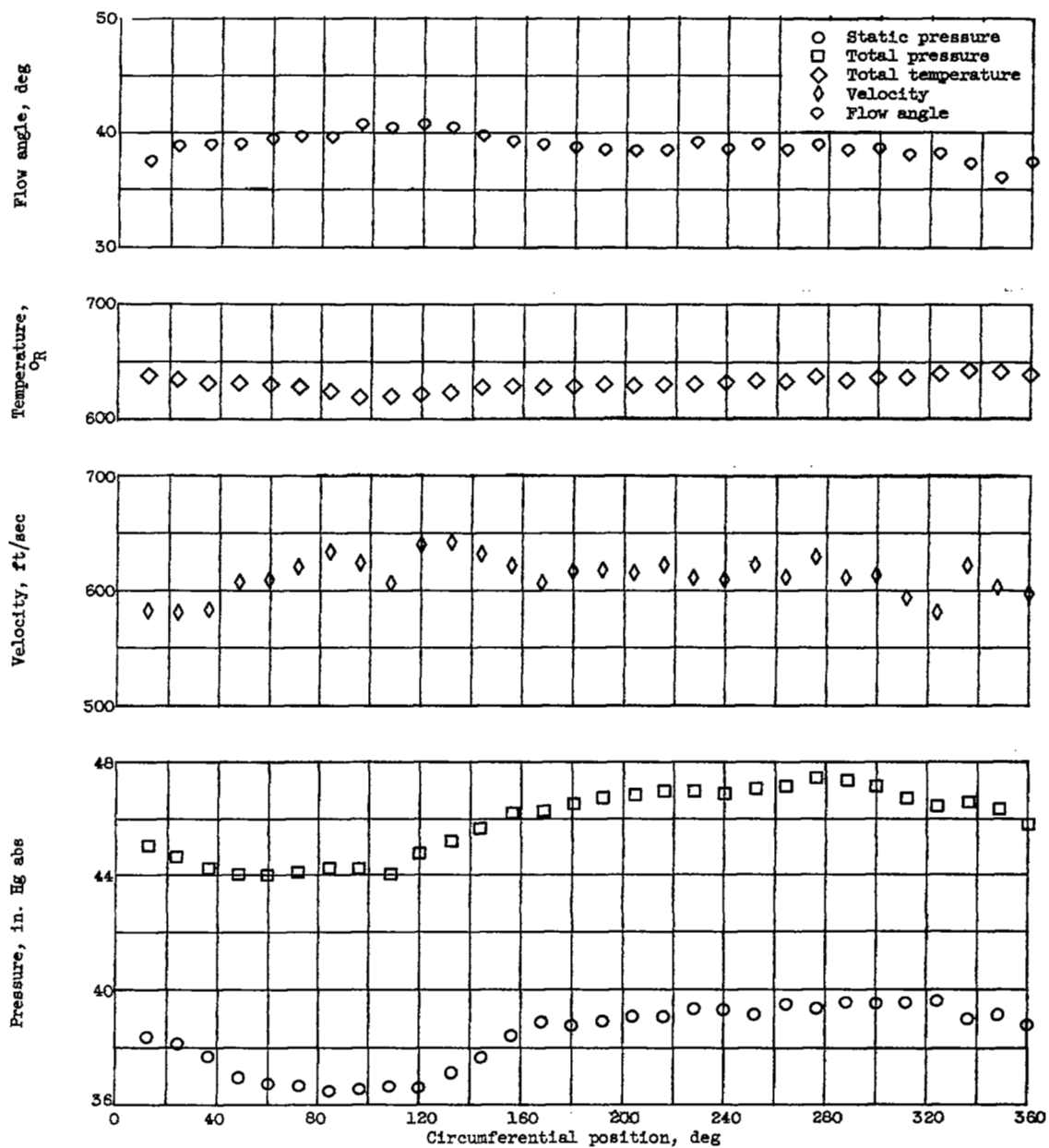
(i) Station 4; hub.

Figure 8. - Continued. Variation of distorted-flow patterns with circumferential position. 80-Percent speed.



(j) Station 5; tip.

Figure 8. - Continued. Variation of distorted-flow patterns with circumferential position. 80-Percent speed.

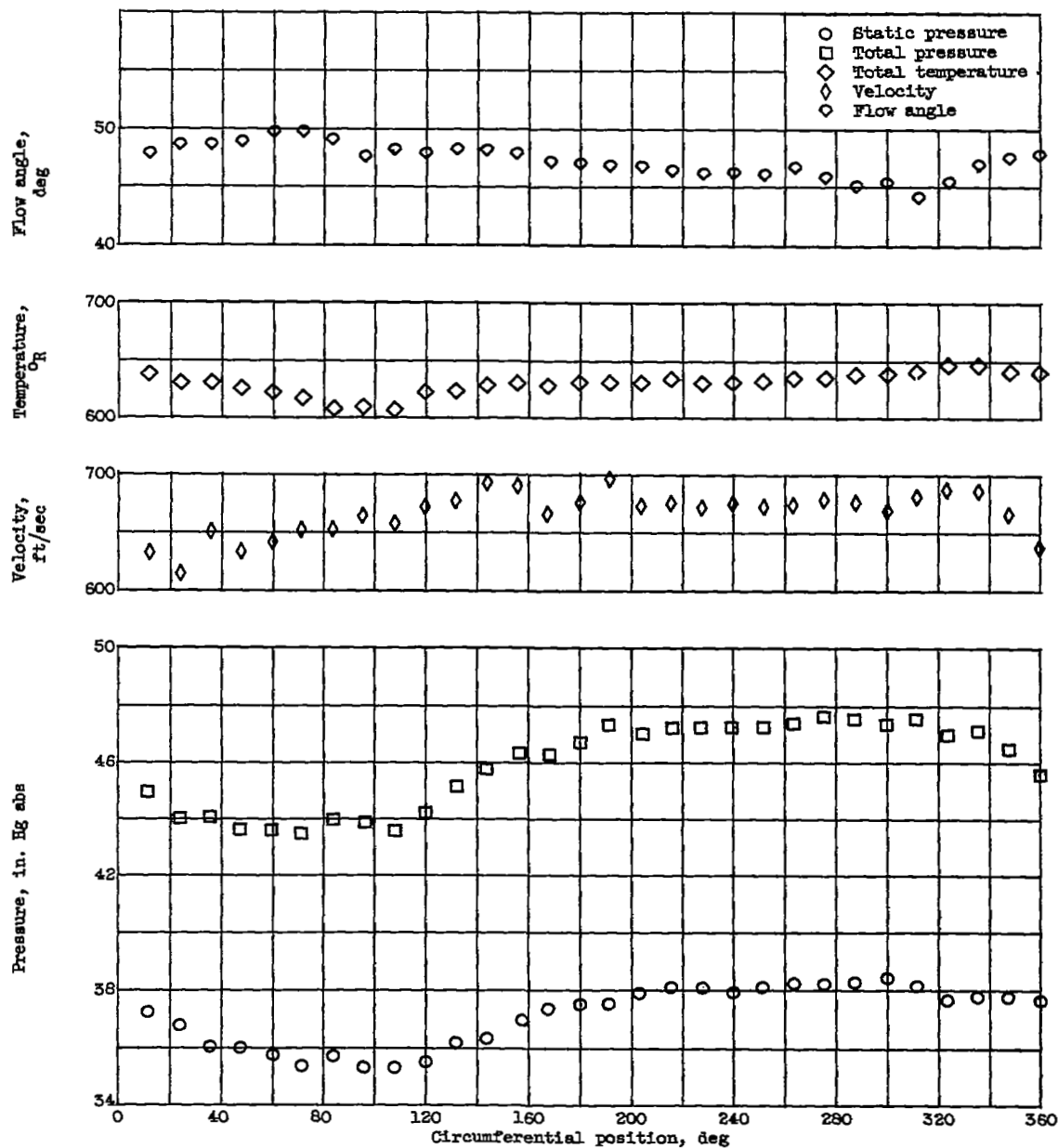


(k) Station 5; mean.

Figure 8. - Continued. Variation of distorted-flow patterns with circumferential position.
80-Percent speed.

4710

CB-7 back



(1) Station 5; hub.

Figure 8. - Continued. Variation of distorted-flow patterns with circumferential position. 80-Percent speed.

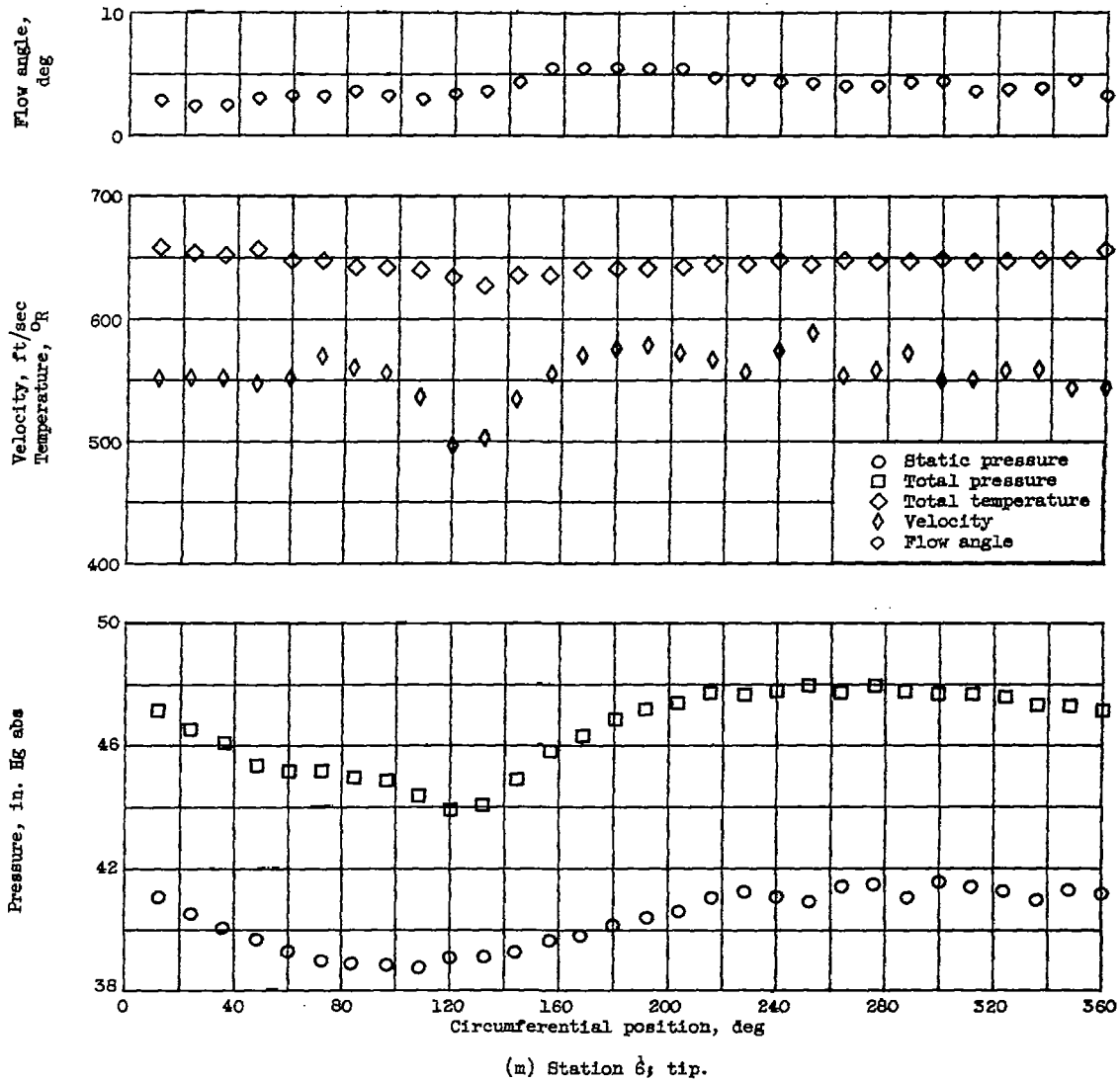
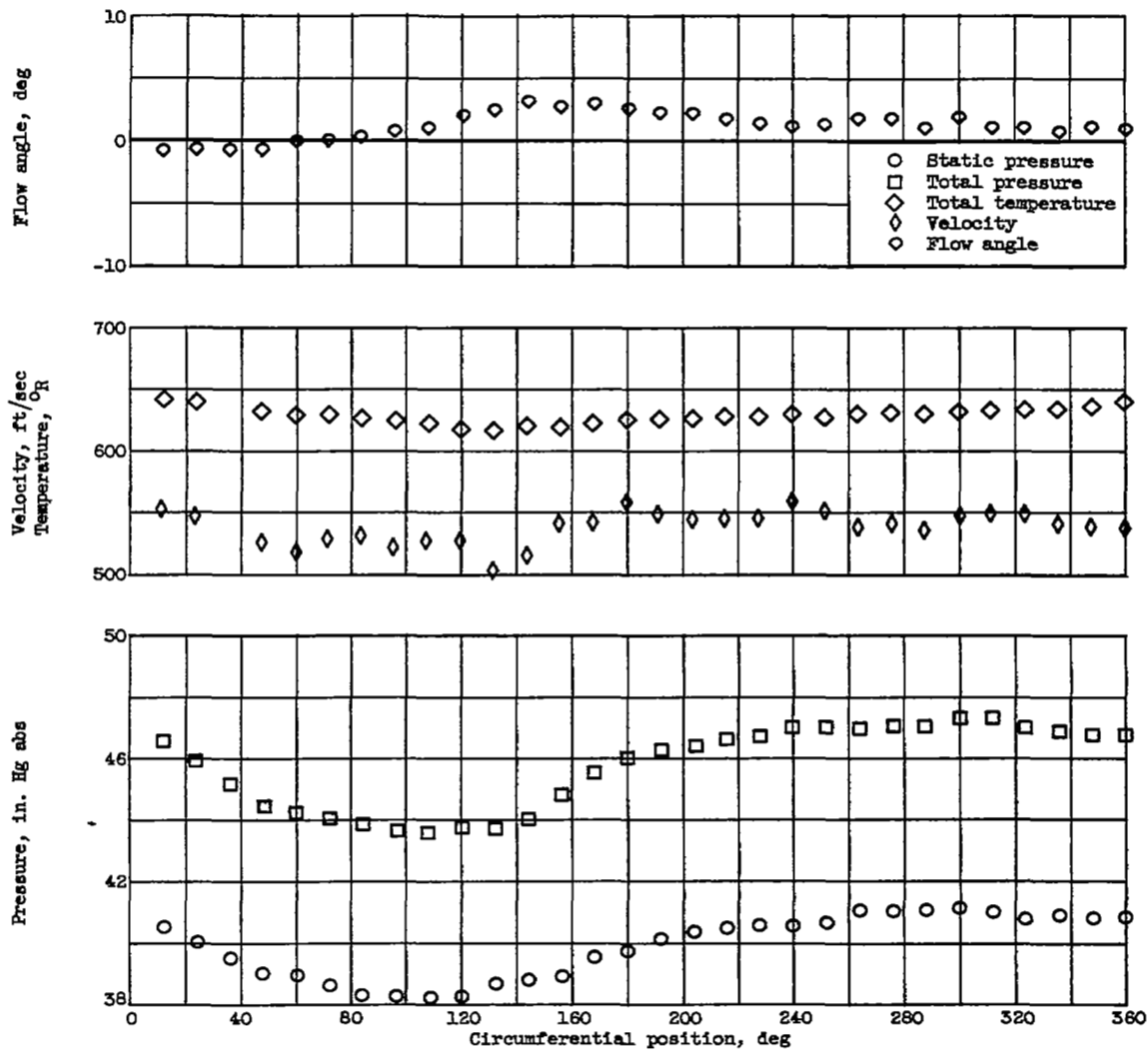
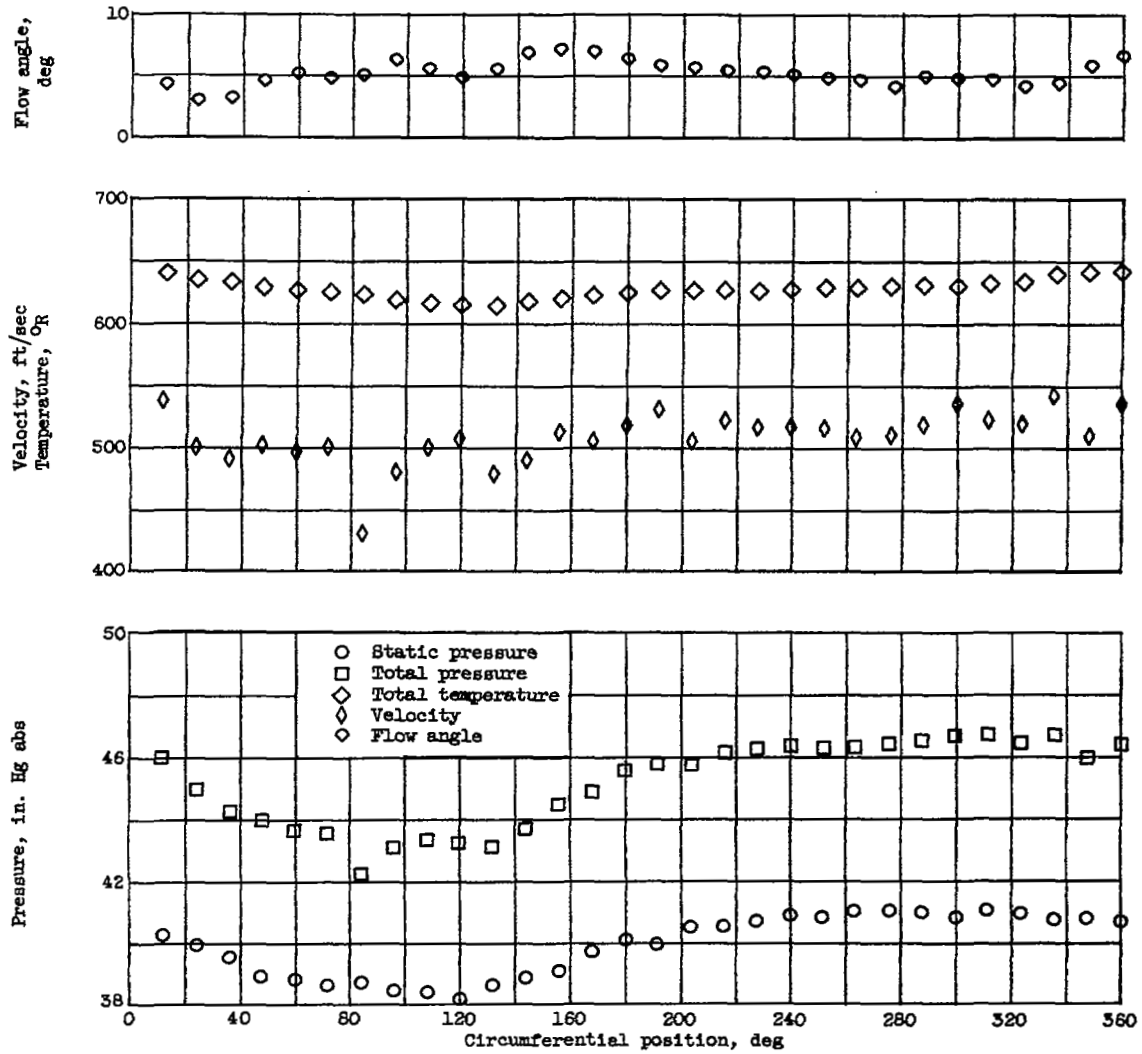


Figure 8. - Continued. Variation of distorted-flow patterns with circumferential position.
80-Percent speed.



(n) Station 6; mean.

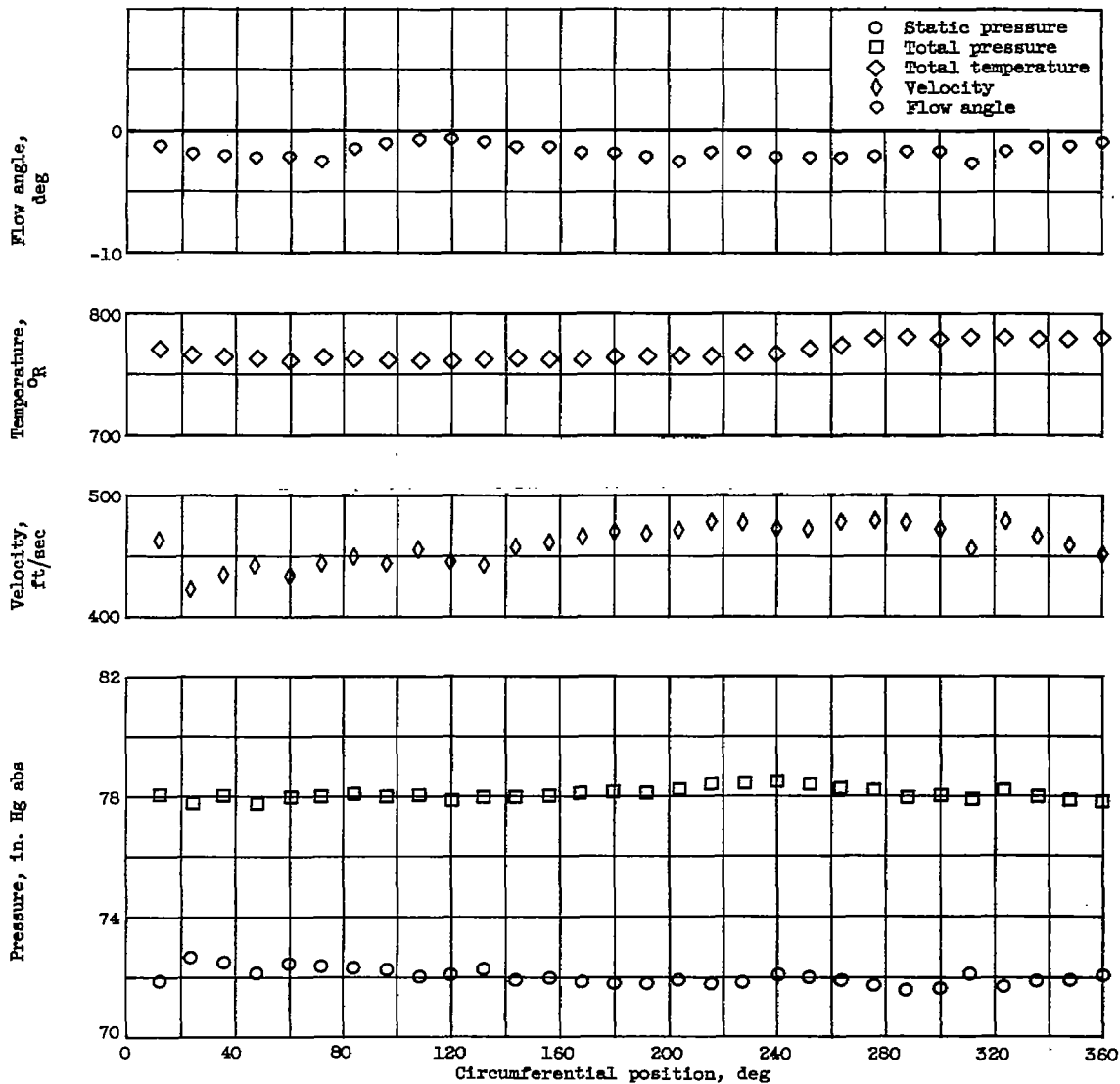
Figure 8. - Continued. Variation of distorted-flow patterns with circumferential position. 80-Percent speed.



(o) Station 6; hub.

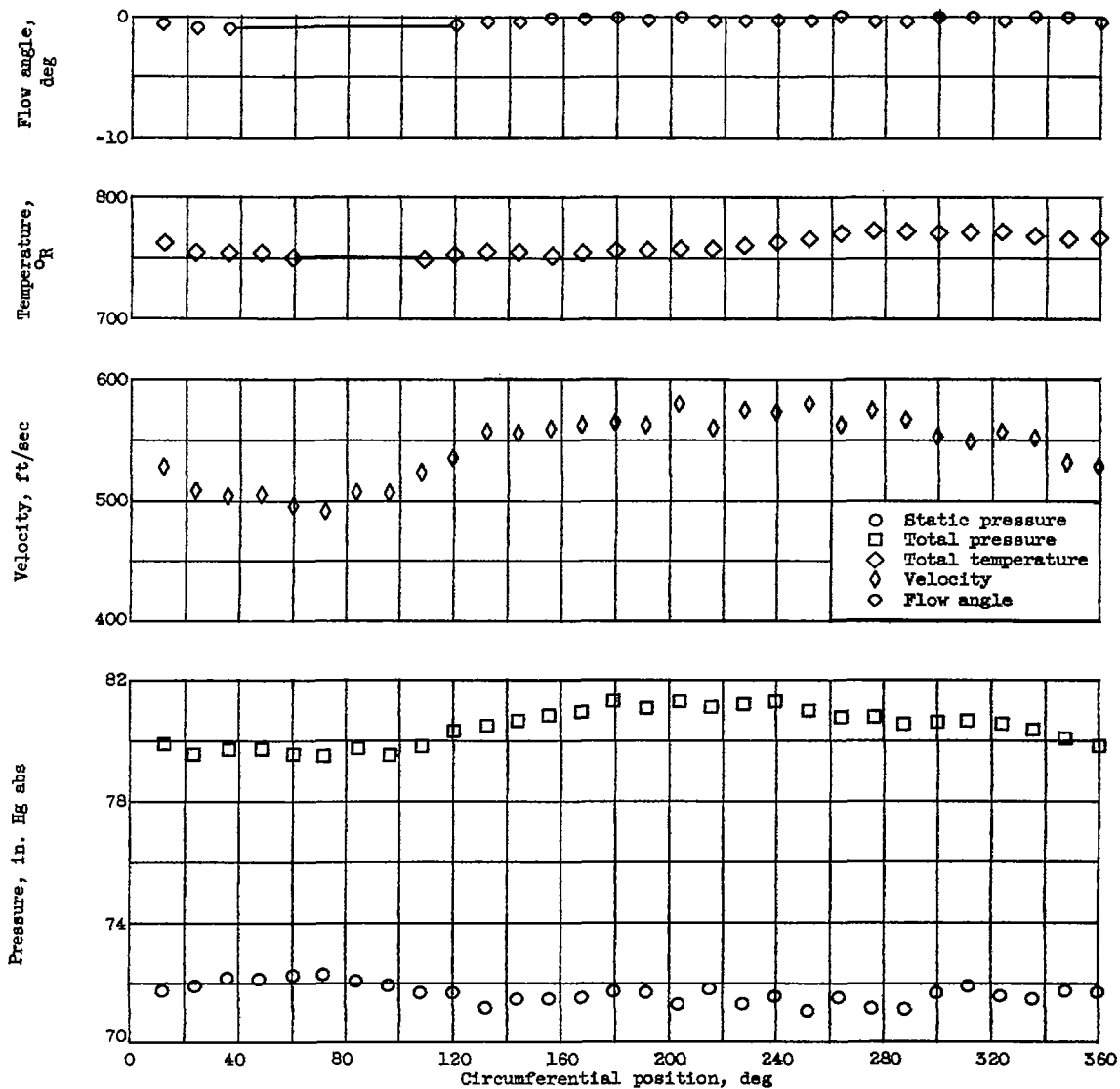
Figure 8. - Continued. Variation of distorted-flow patterns with circumferential position. 80-Percent speed.

4710



(p) Station 7; tip.

Figure 8. - Continued. Variation of distorted-flow patterns with circumferential position. 80-Percent speed.

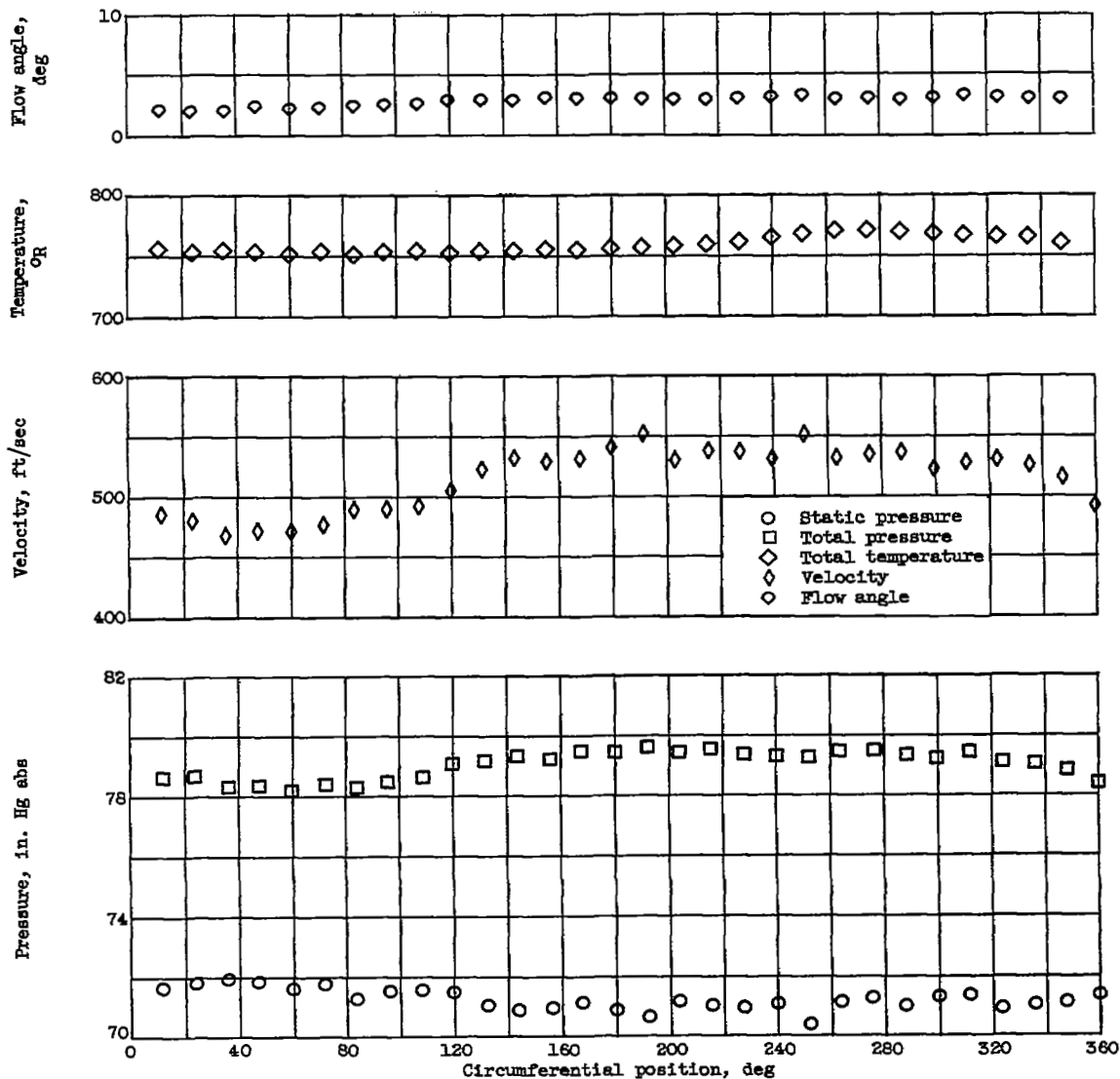


(q) Station 7; mean.

Figure 8. - Continued. Variation of distorted-flow patterns with circumferential position. 80-Percent speed.

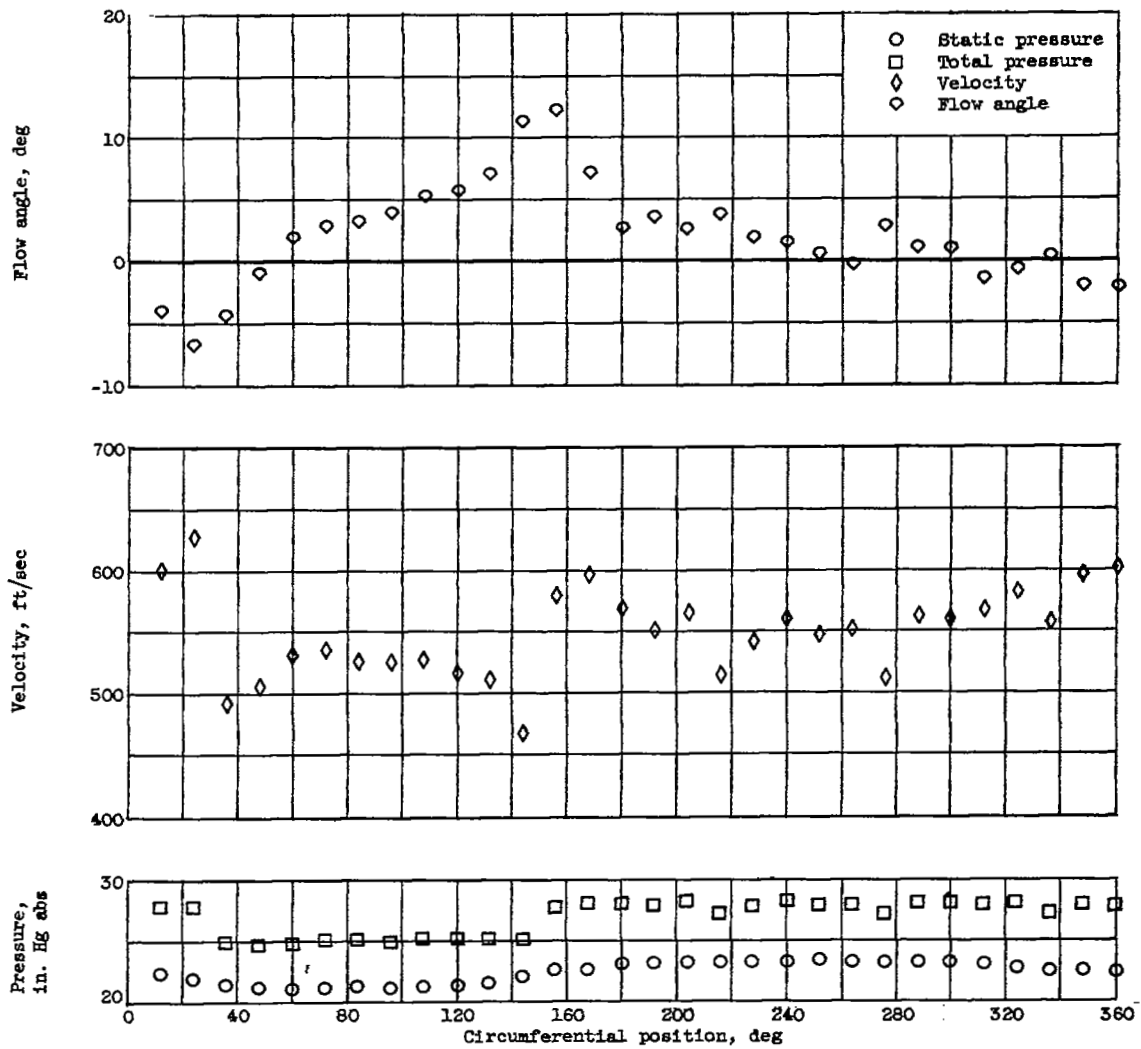
4710

CB-8



(r) Station 7; hub.

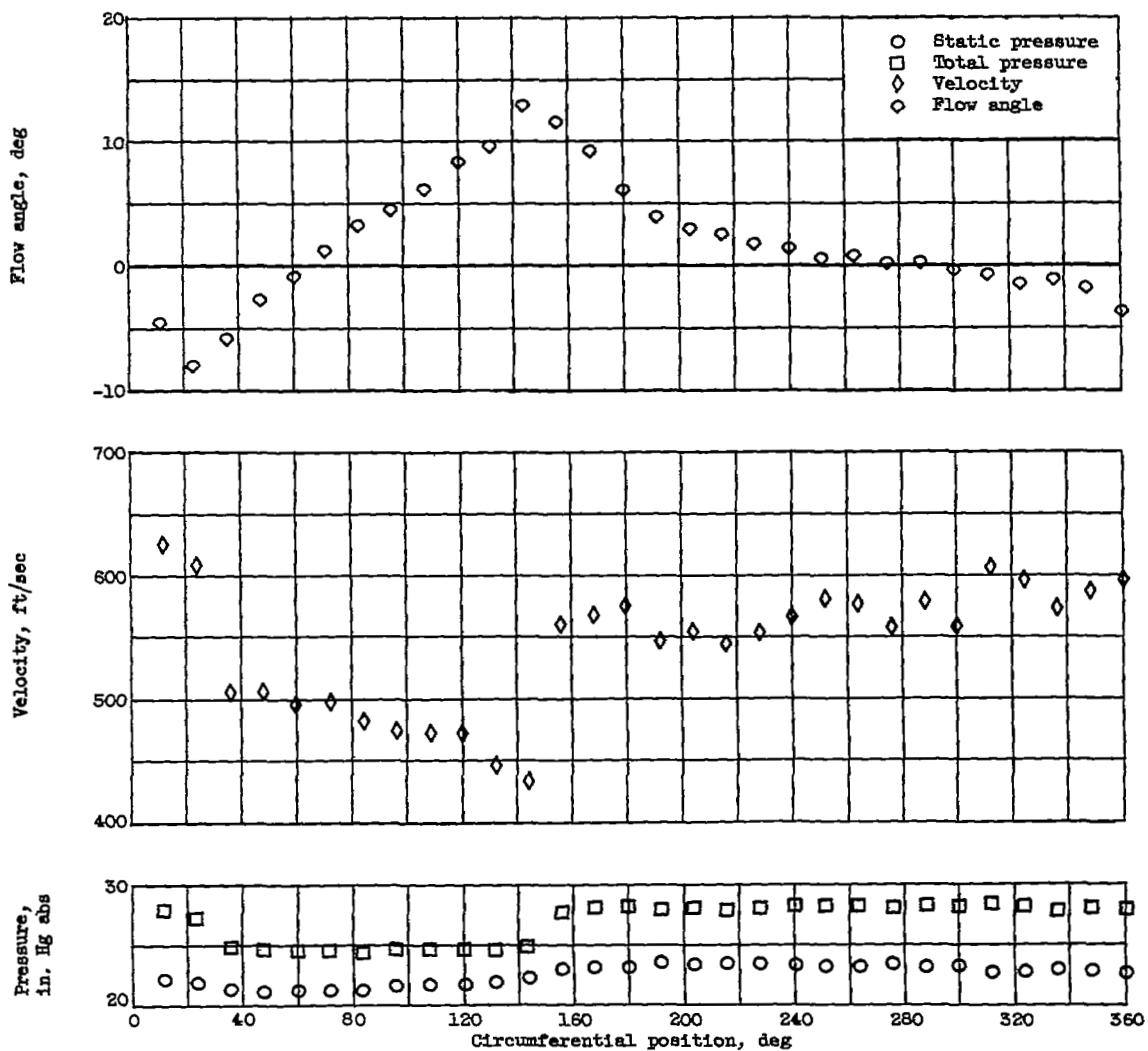
Figure 8. - Concluded. Variation of distorted-flow patterns with circumferential position. 80-Percent speed.



(a) Station 2; tip; absolute total temperature, 517° R.

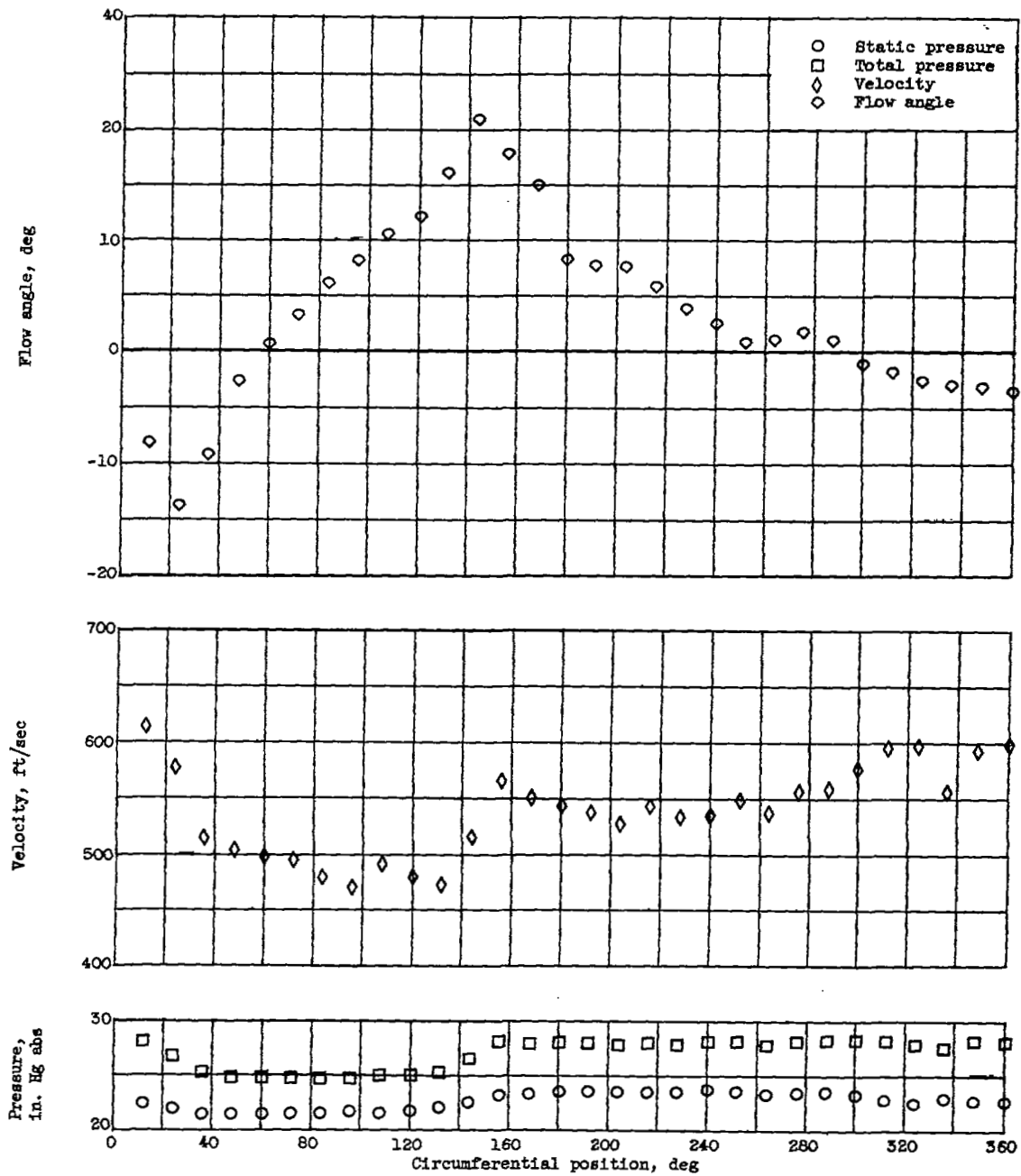
Figure 9. - Variation of distorted-flow patterns with circumferential position. 90-Percent speed.

4710
CB-8 back



(b) Station 2; mean; absolute total temperature, 519° R.

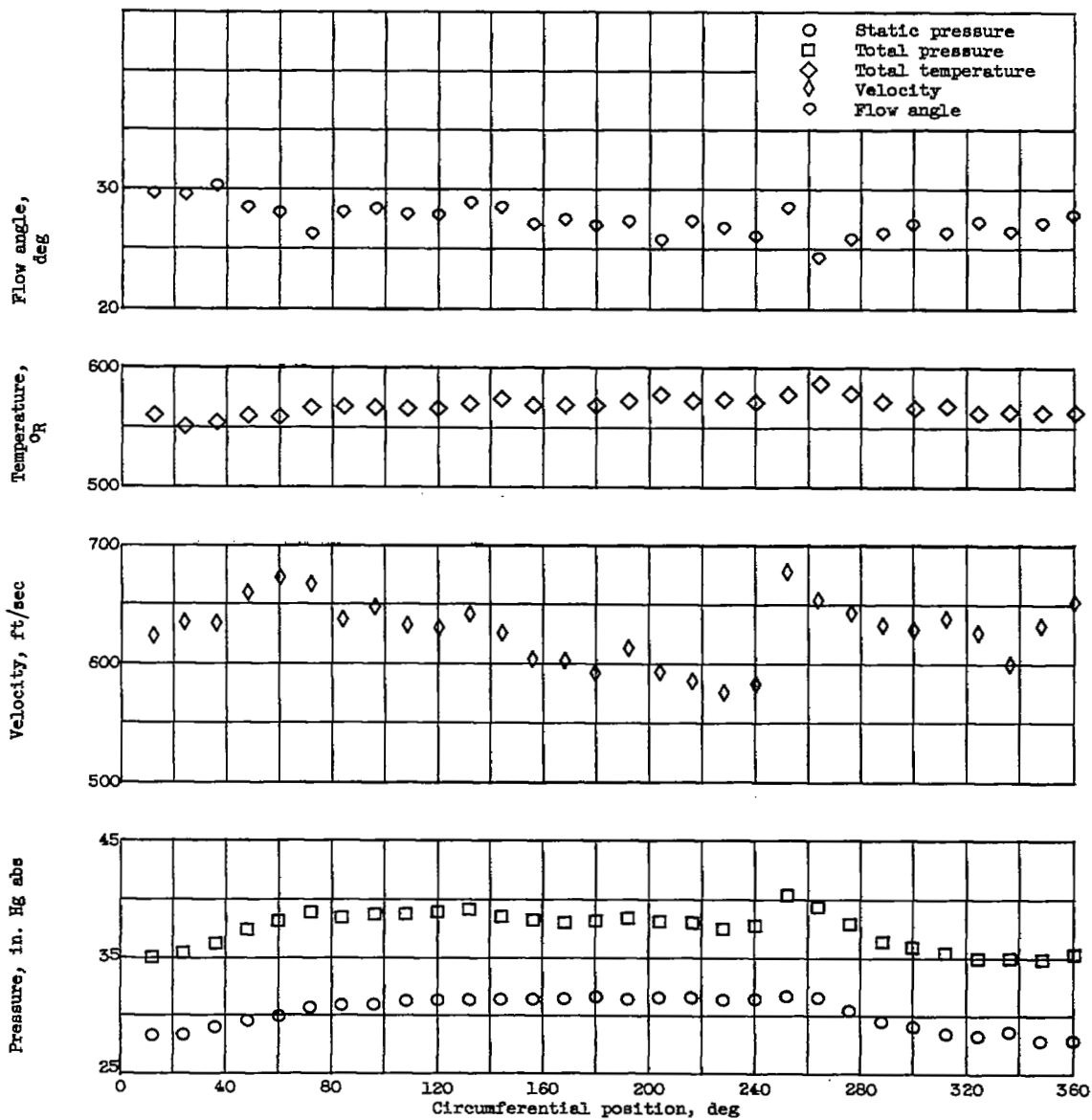
Figure 9. - Continued. Variation of distorted-flow patterns with circumferential position. 90-Percent speed.



(c) Station 2; hub; absolute total temperature, 519° R.

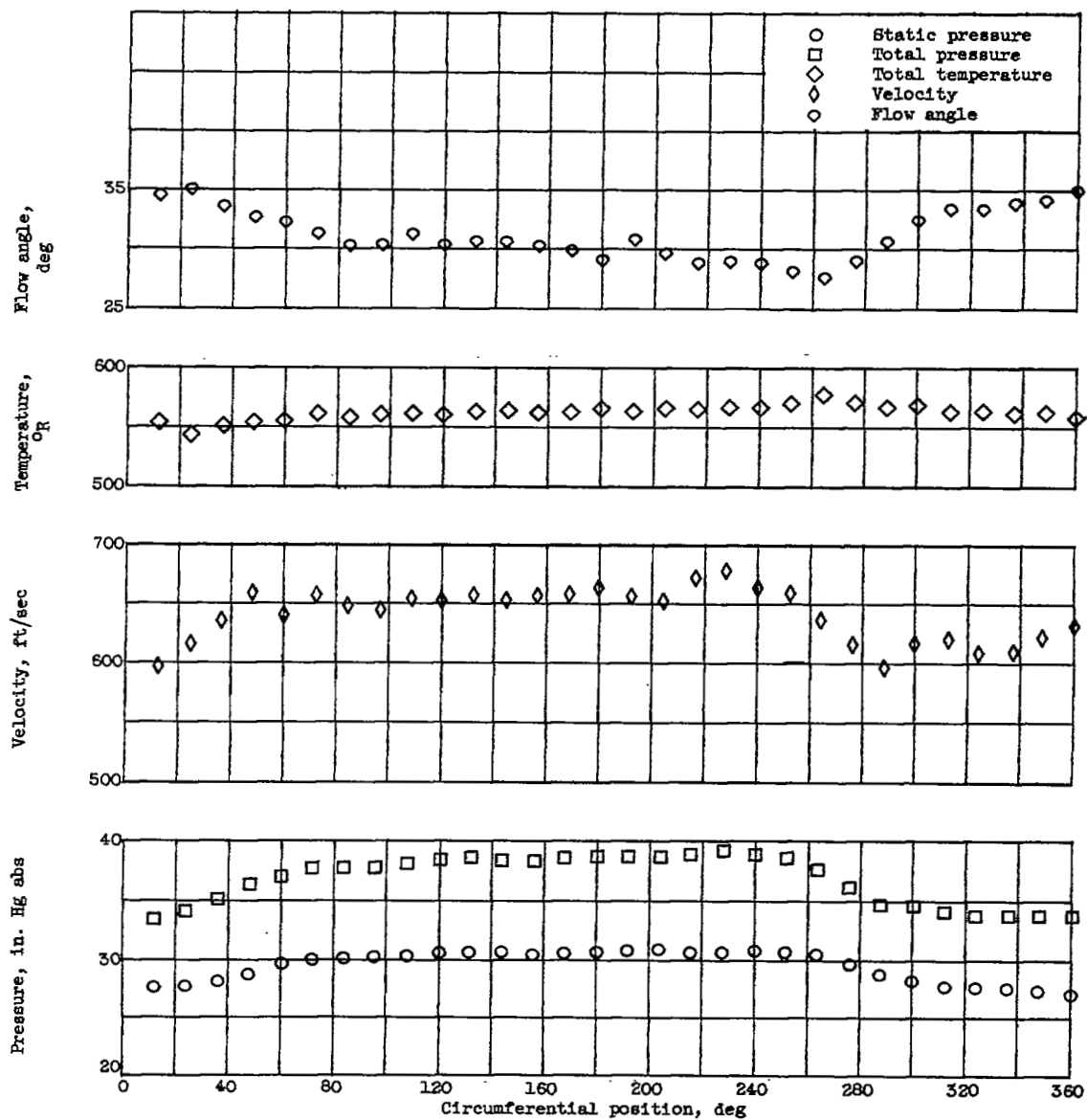
Figure 9. - Continued. Variation of distorted-flow patterns with circumferential position. 90-Percent speed.

4710



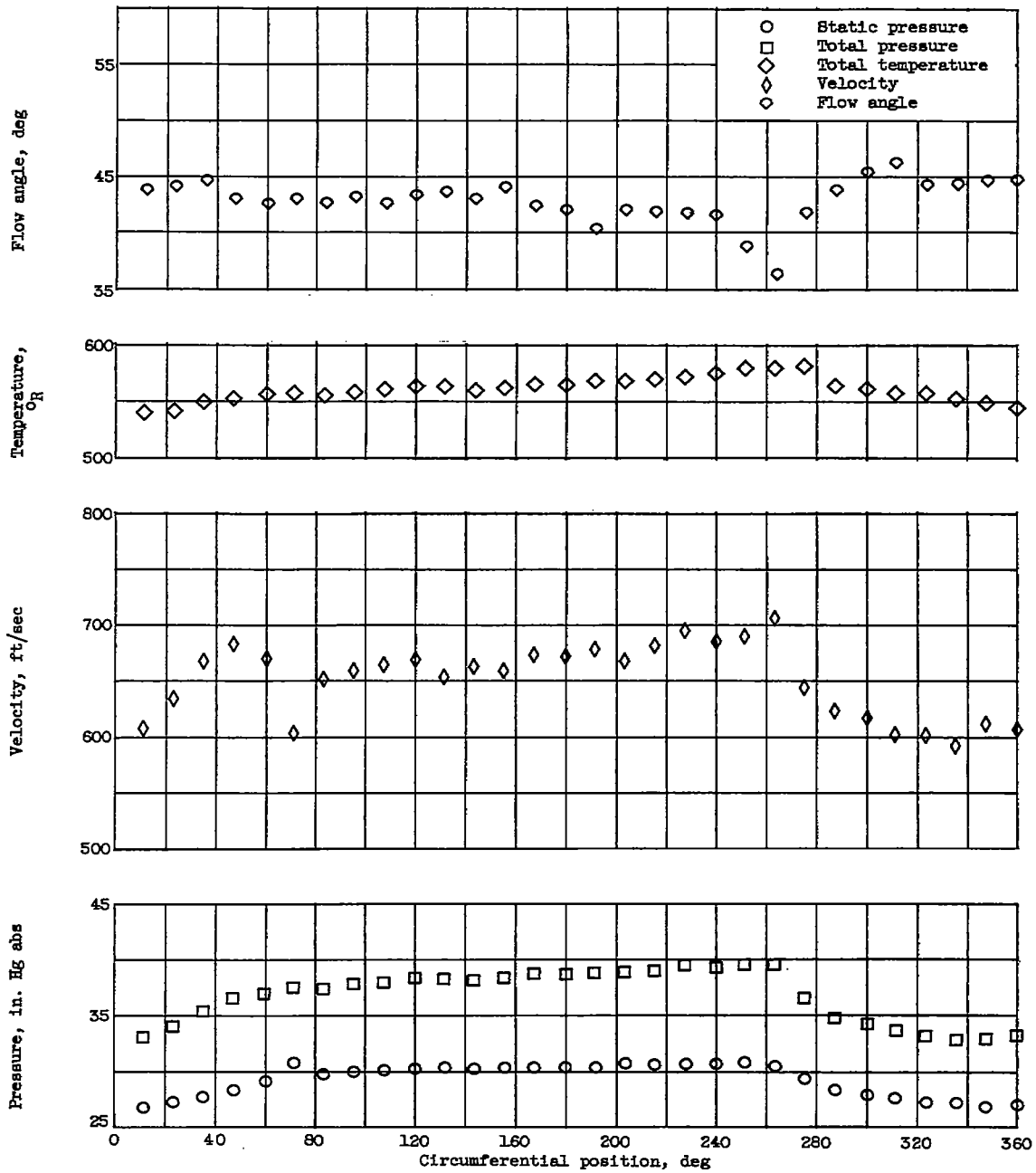
(d) Station 3; tip.

Figure 9. - Continued. Variation of distorted-flow patterns with circumferential position. 90-Percent speed.



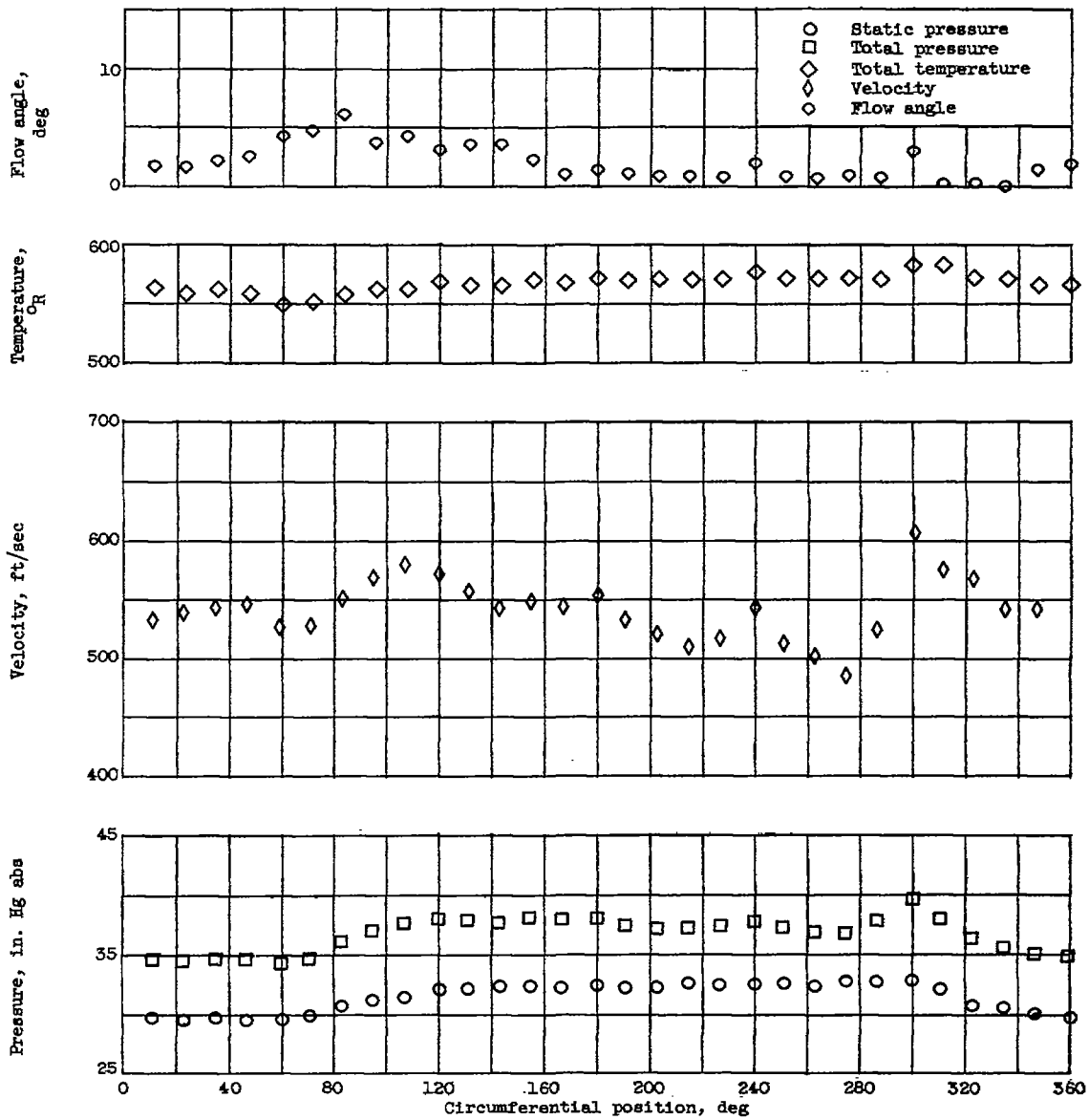
(e) Station 3; mean.

Figure 9. - Continued. Variation of distorted-flow patterns with circumferential position. 90-Percent speed.



(f) Station 3; hub.

Figure 9. - Continued. Variation of distorted-flow patterns with circumferential position. 90-Percent speed.

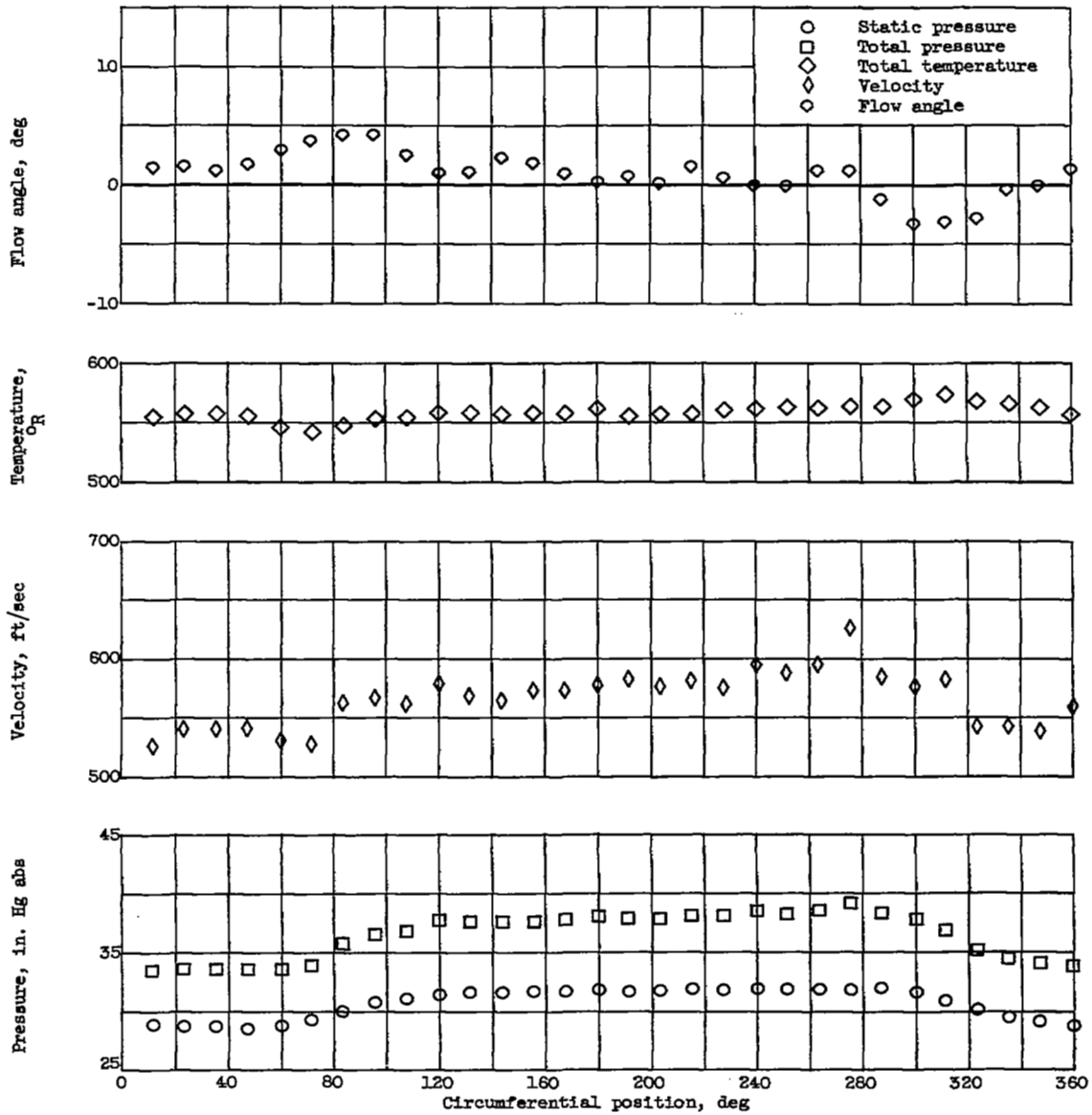


(g) Station 4; tip.

Figure 9. - Continued. Variation of distorted-flow patterns with circumferential position. 90-Percent speed.

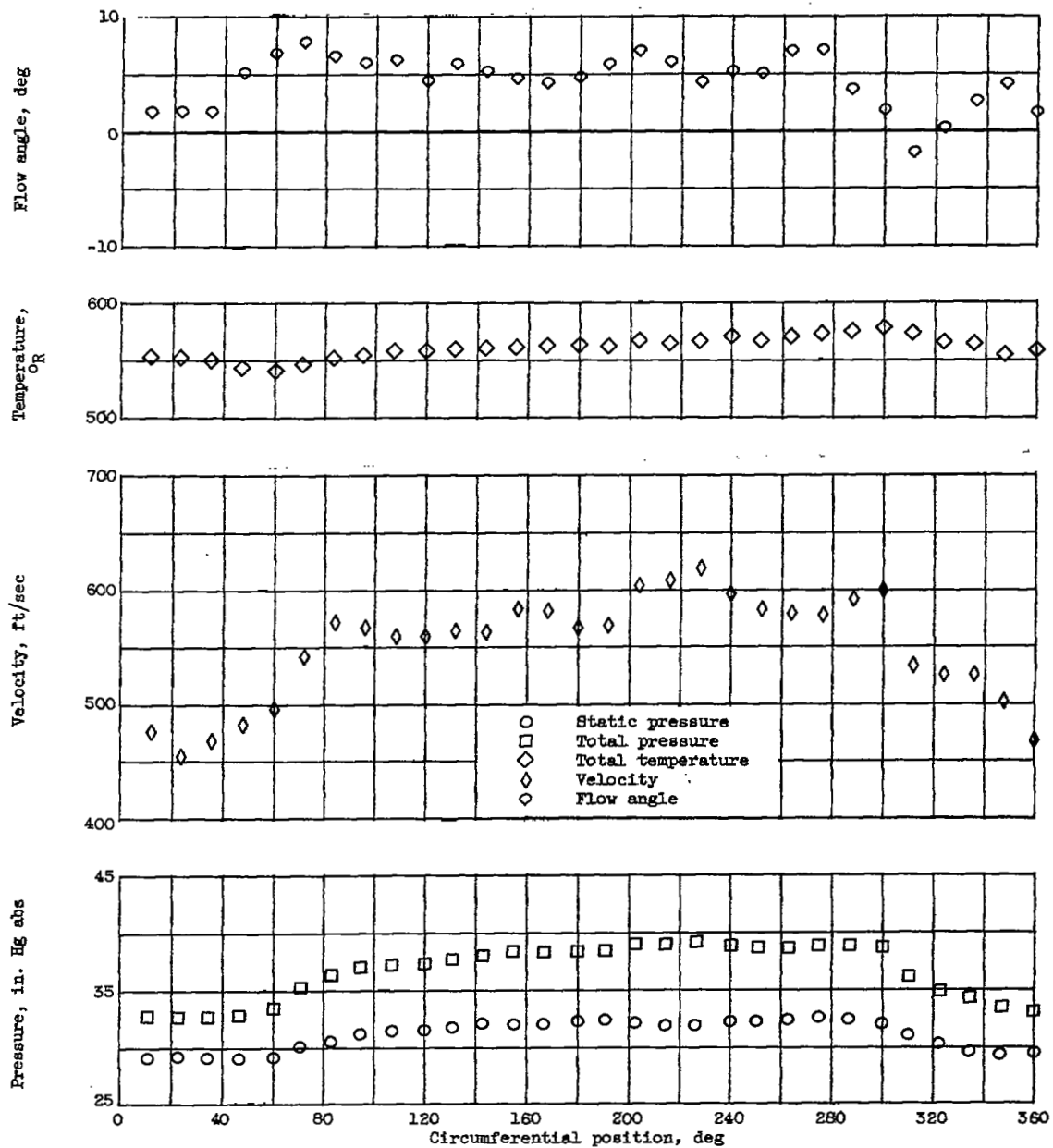
4710

CB-9



(h) Station 4; mean.

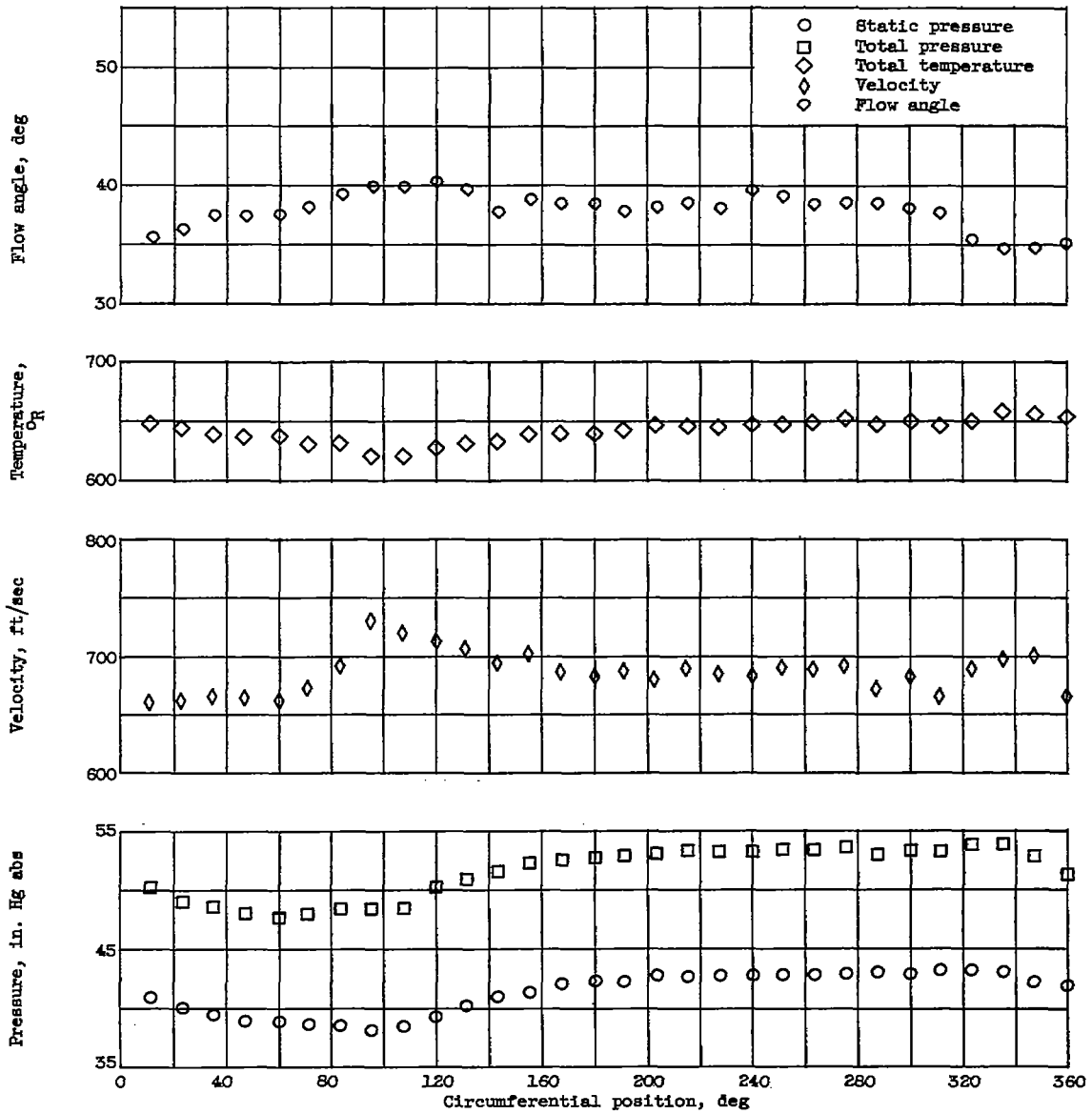
Figure 9. - Continued. Variation of distorted-flow patterns with circumferential position. 90-Percent speed.



(1) Station 4; hub.

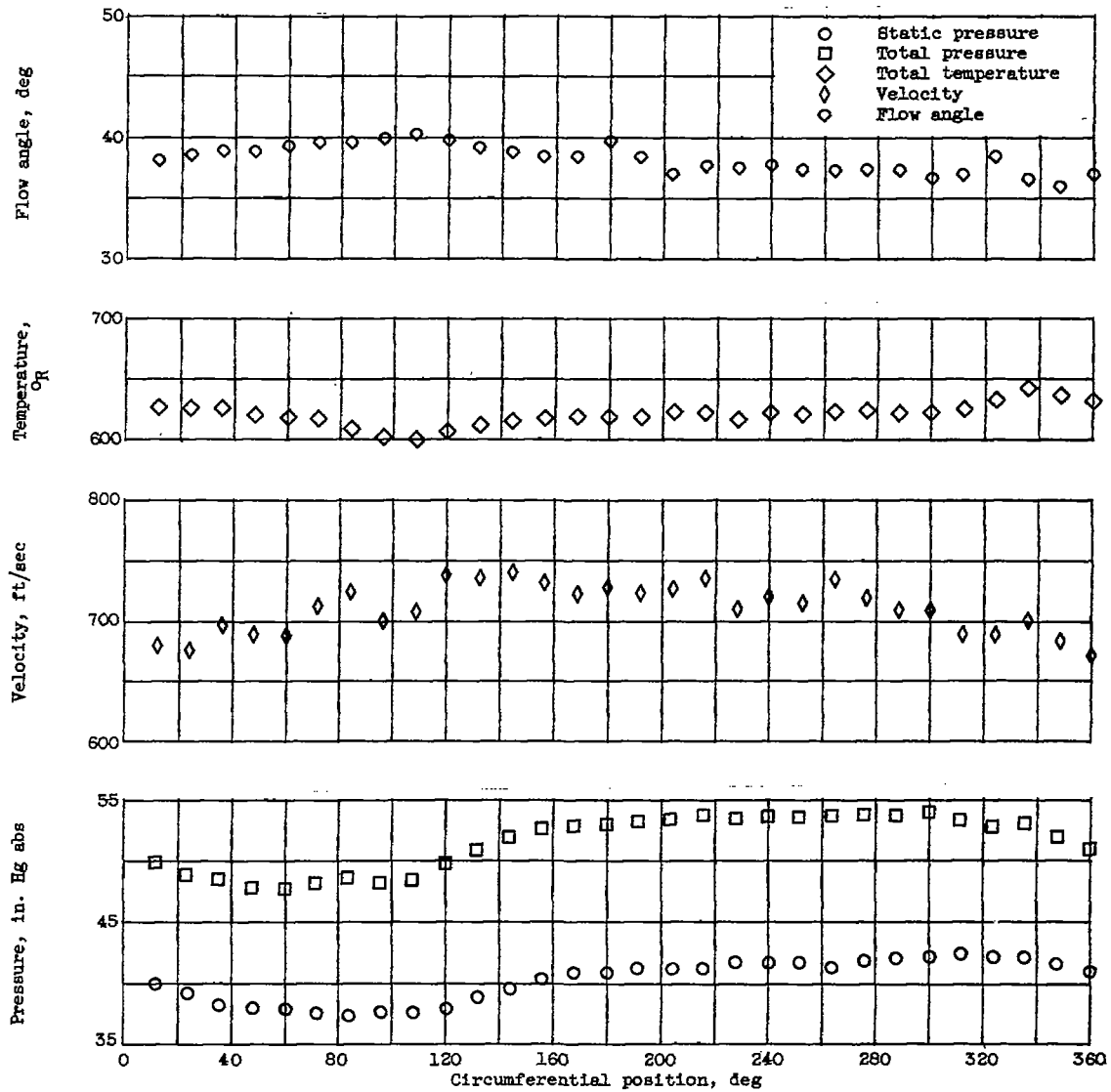
Figure 9. - Continued. Variation of distorted-flow patterns with circumferential position. 90-Percent speed.

4710 CB-9 back



(j) Station 5; tip.

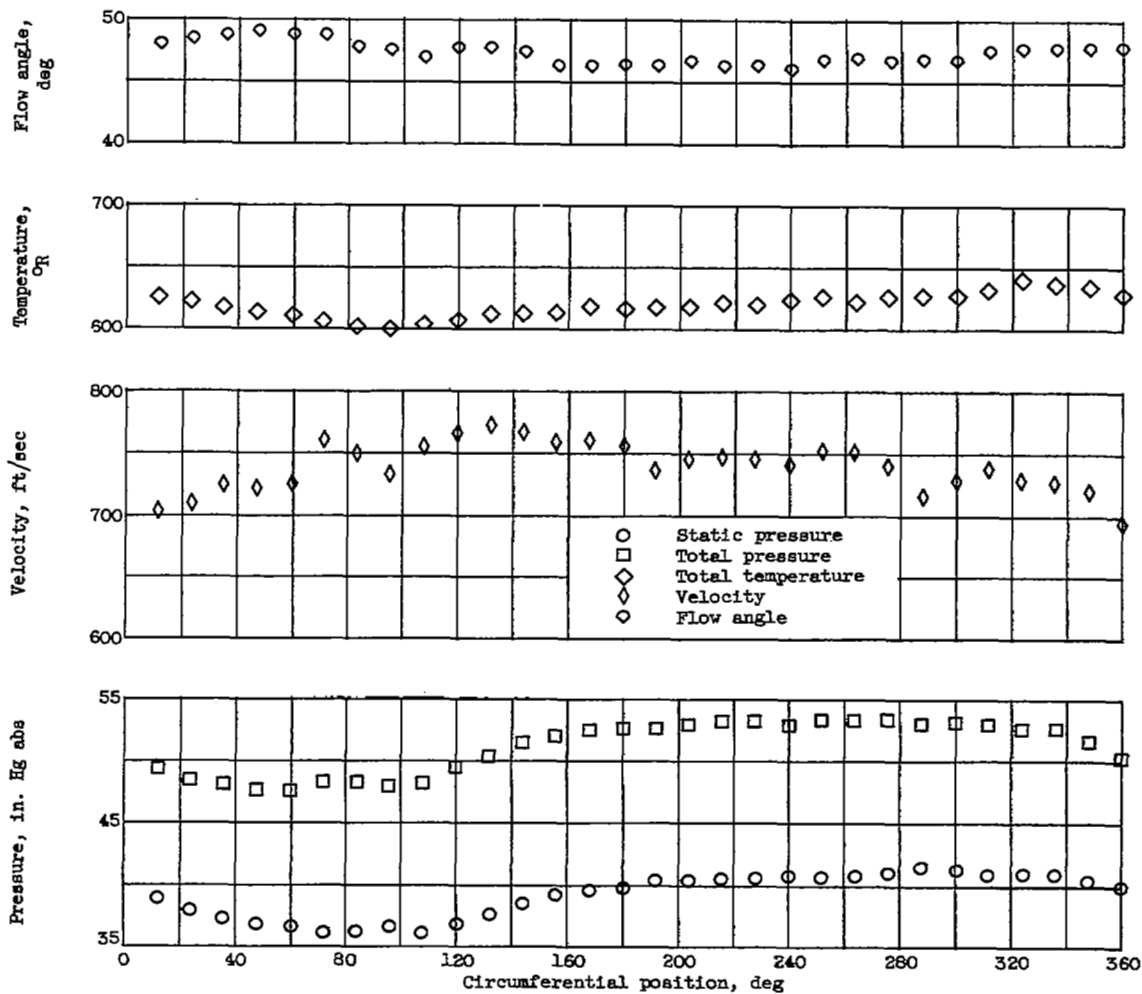
Figure 9. - Continued. Variation of distorted-flow patterns with circumferential position. 90-Percent speed.



(k) Station 5; mean.

Figure 9. - Continued. Variation of distorted-flow patterns with circumferential position. 90-Percent speed.

4710



(1) Station 5; hub.

Figure 9. - Continued. Variation of distorted-flow patterns with circumferential position. 90-Percent speed.

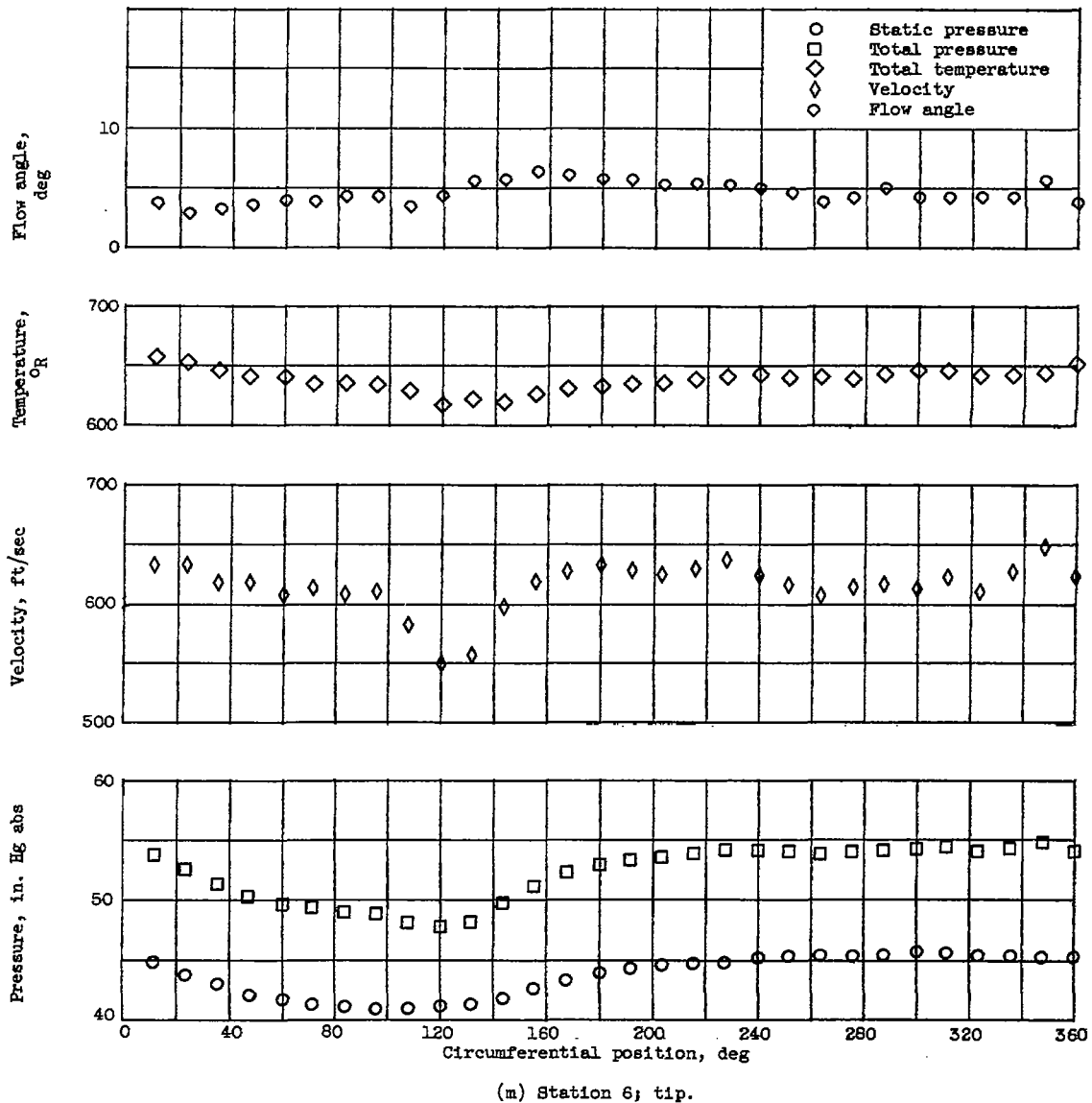
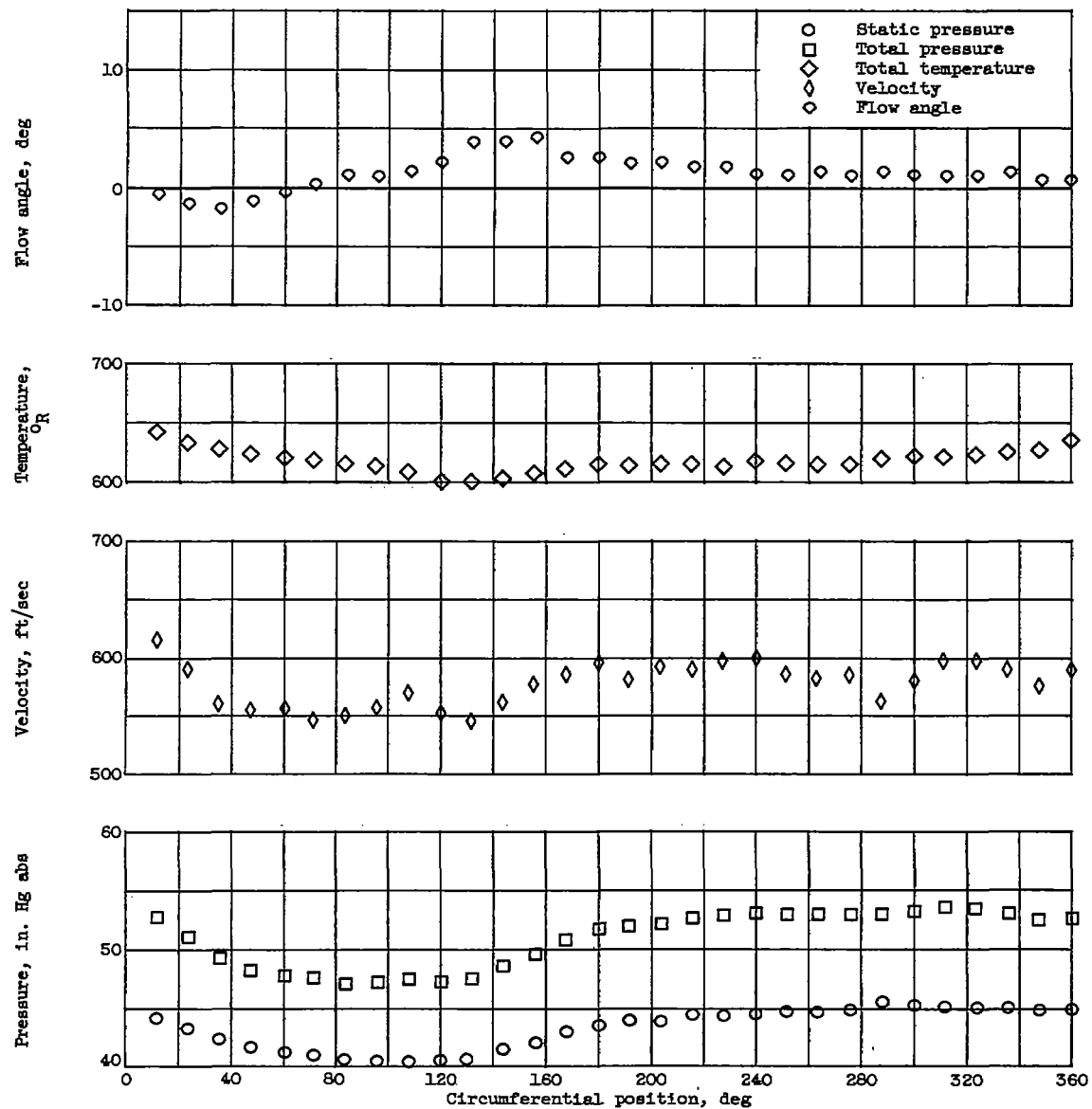


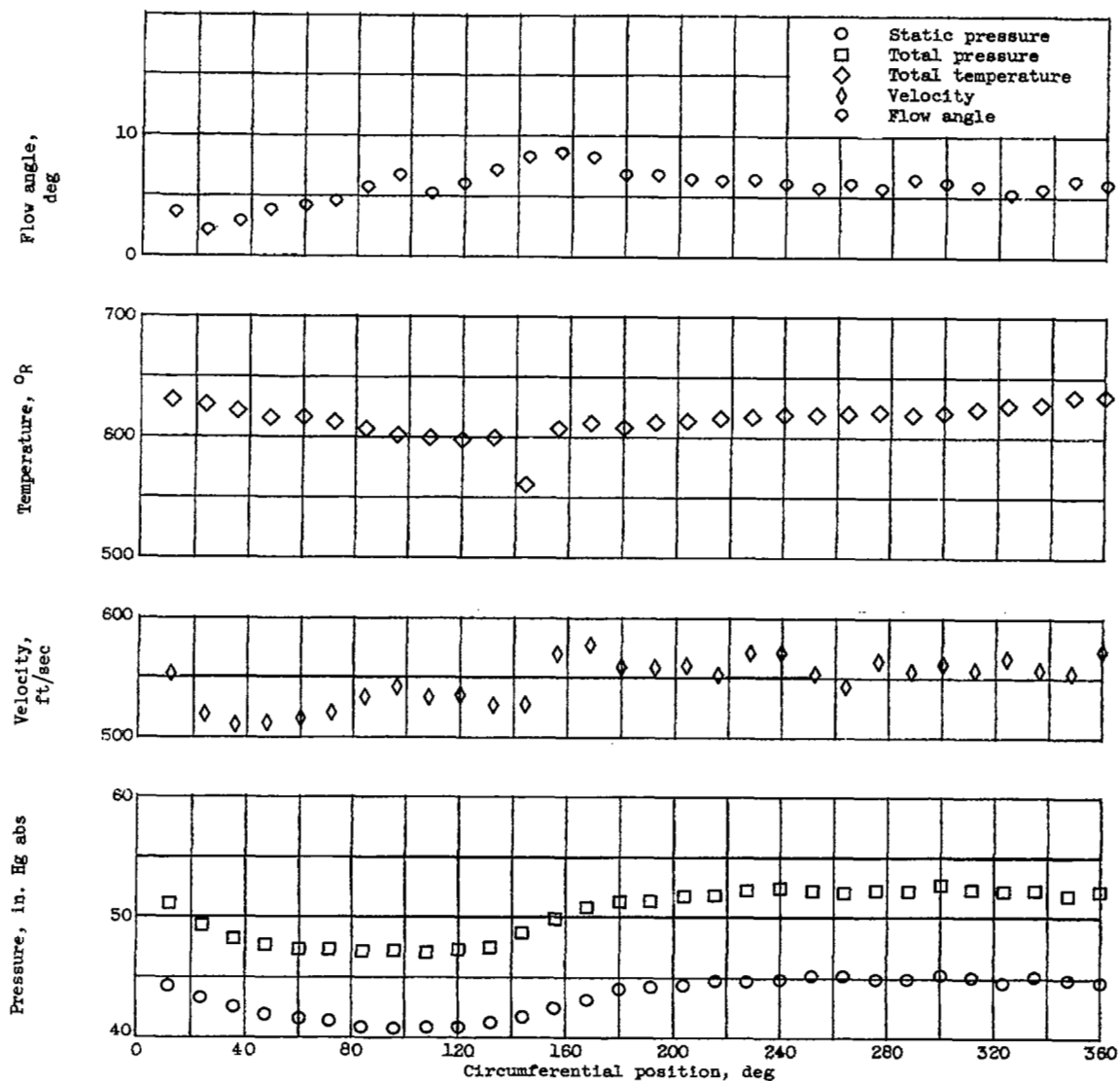
Figure 9. - Continued. Variation of distorted-flow patterns with circumferential position. 90-Percent speed.

4710



(n) Station 6; mean.

Figure 9. - Continued. Variation of distorted-flow patterns with circumferential position. 90-Percent speed.

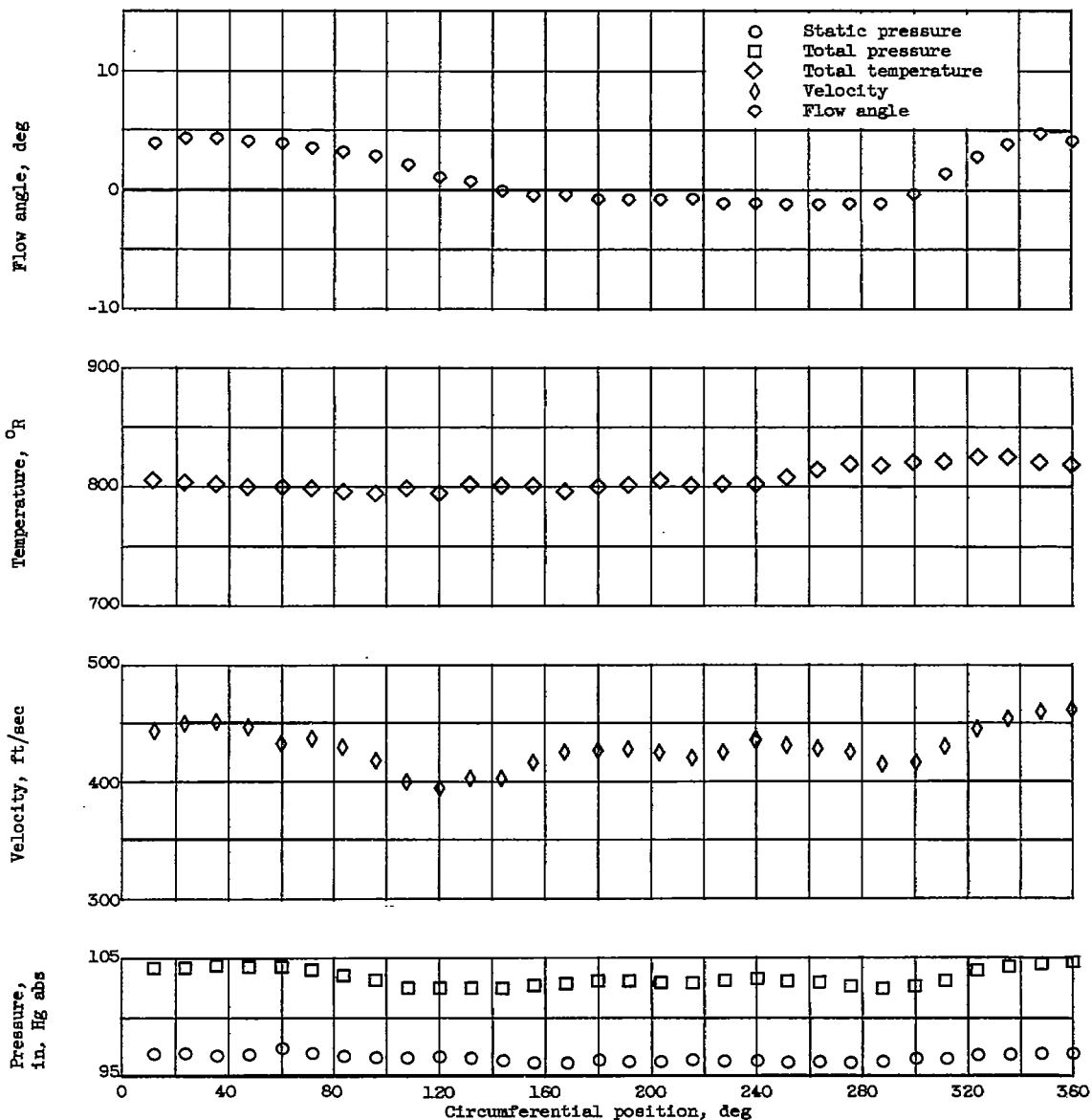


(o) Station 6; hub.

Figure 9. - Continued. Variation of distorted-flow patterns with circumferential position. 90-Percent speed.

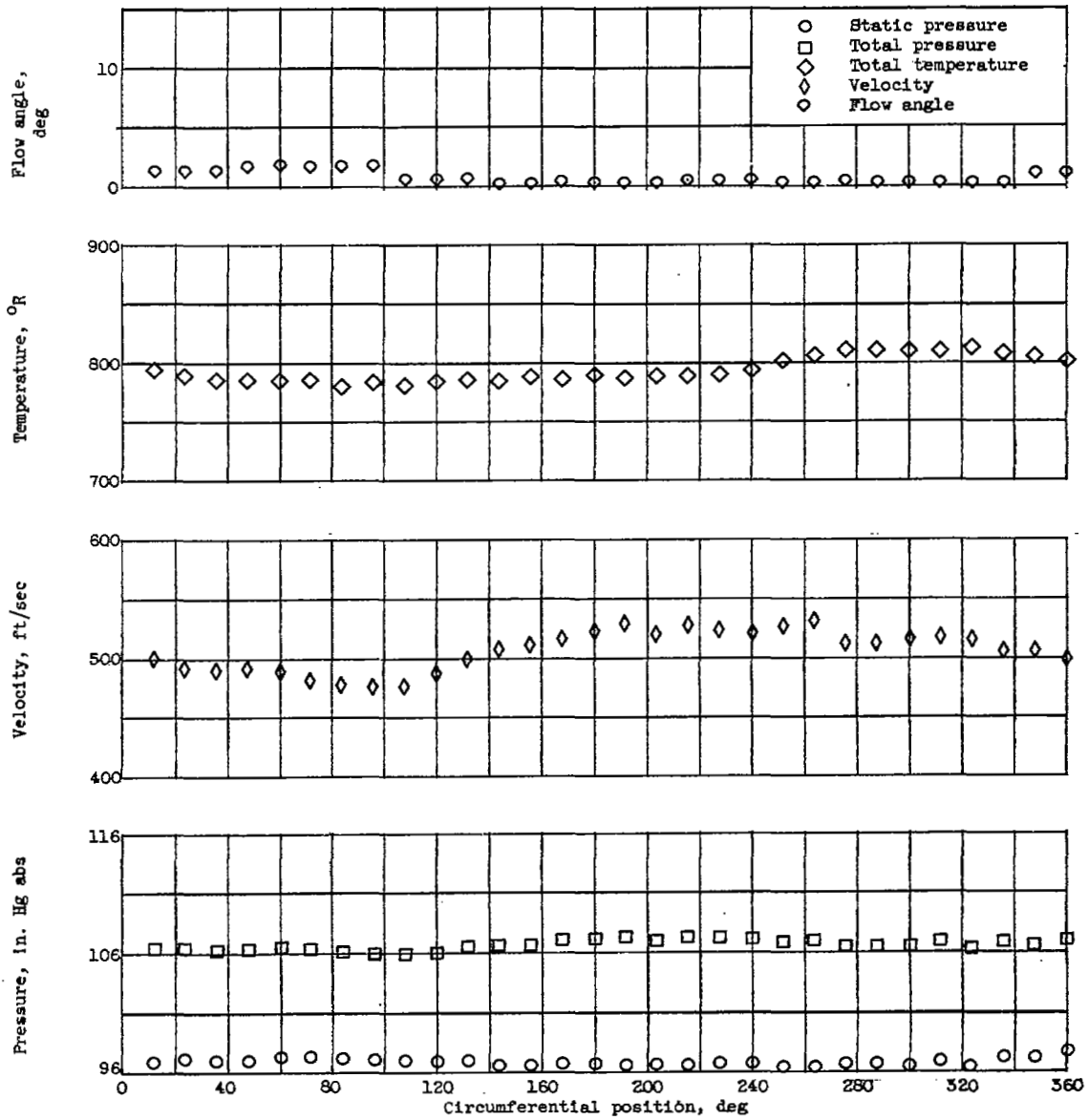
4710

CB-10



(p) Station 7; tip.

Figure 9. - Continued. Variation of distorted-flow patterns with circumferential position. 90-Percent speed.

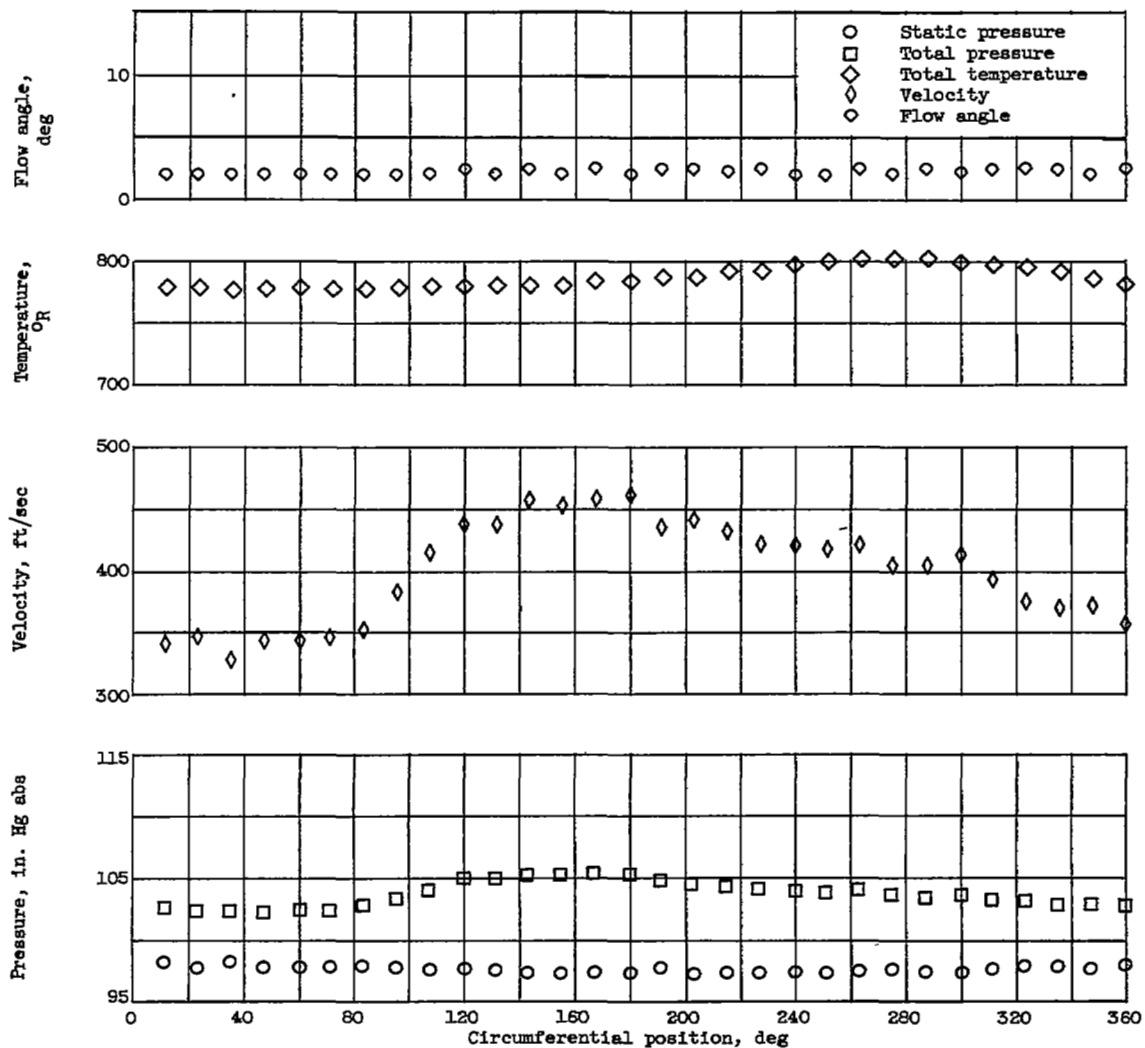


(q) Station 7; mean.

Figure 9. - Continued. Variation of distorted-flow patterns with circumferential position. 90-Percent speed.

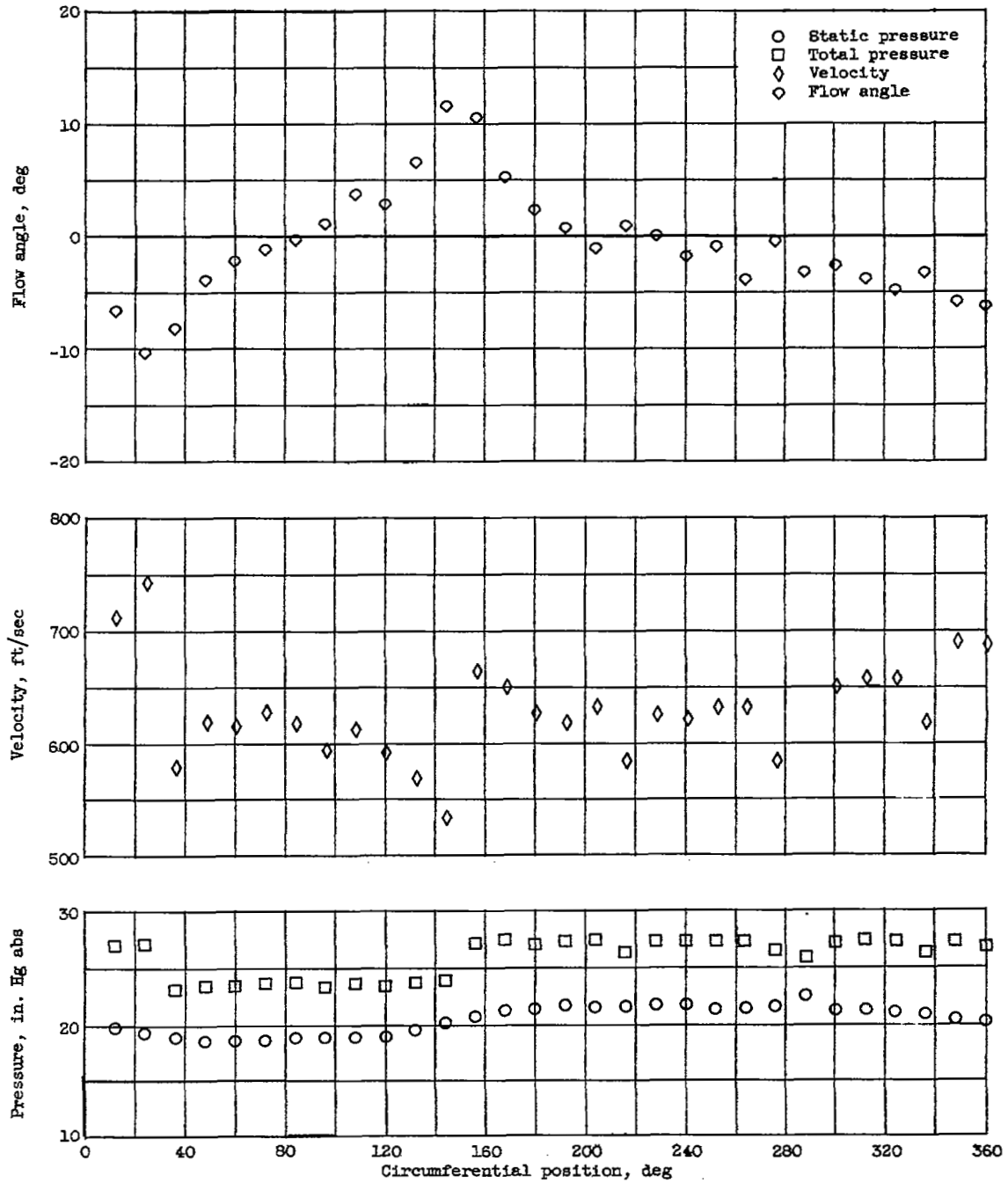
4710

CB-10 back



(r) Station 7; hub.

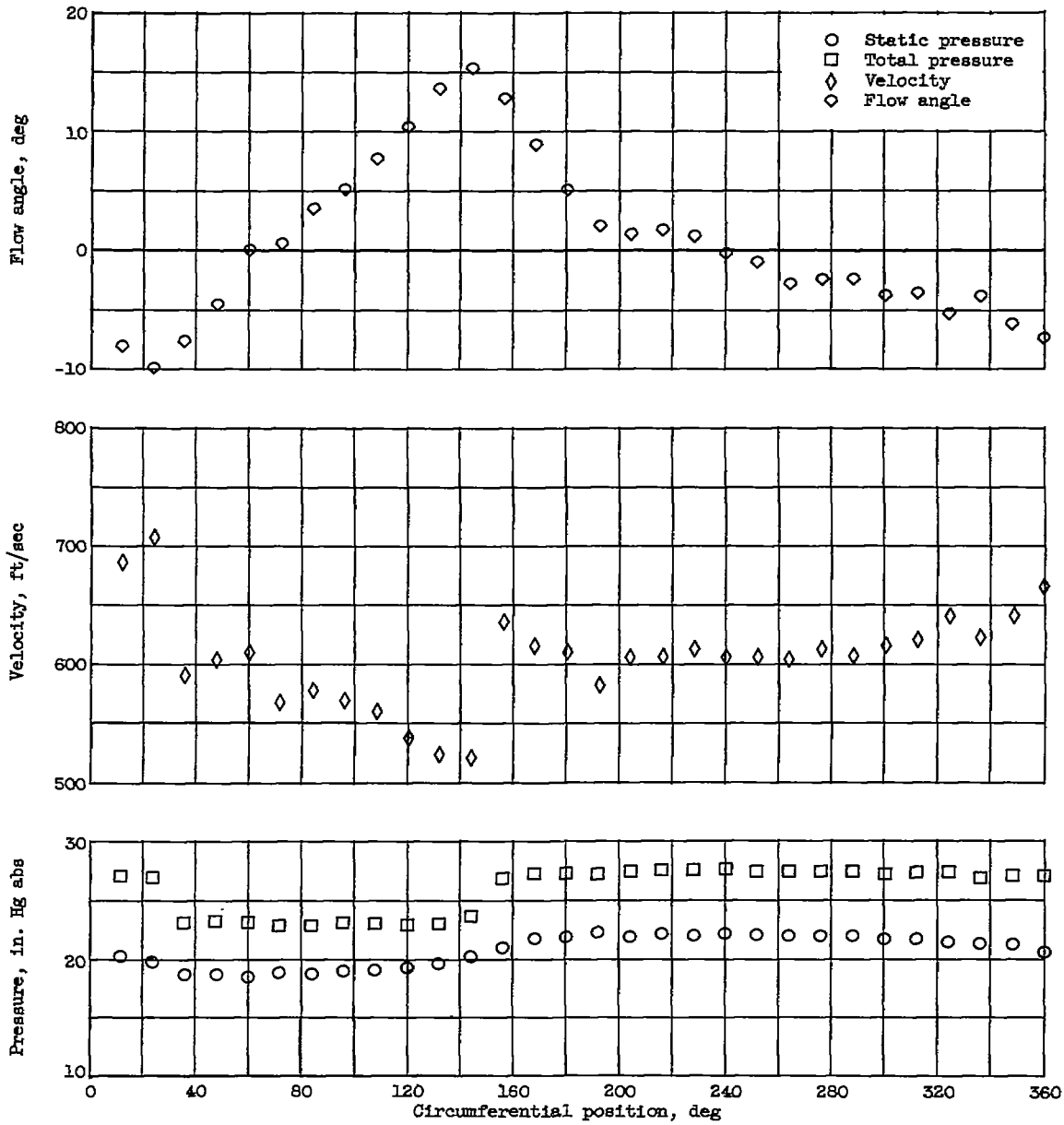
Figure 9. - Concluded. Variation of distorted-flow patterns with circumferential position. 90-Percent speed.



(a) Station 2; tip; absolute total temperature, 501° R.

Figure 10. - Variation of distorted-flow patterns with circumferential position. Design speed.

4710



(b) Station 2; mean; absolute total temperature, 502° R.

Figure 10. - Continued. Variation of distorted-flow patterns with circumferential position. Design speed.

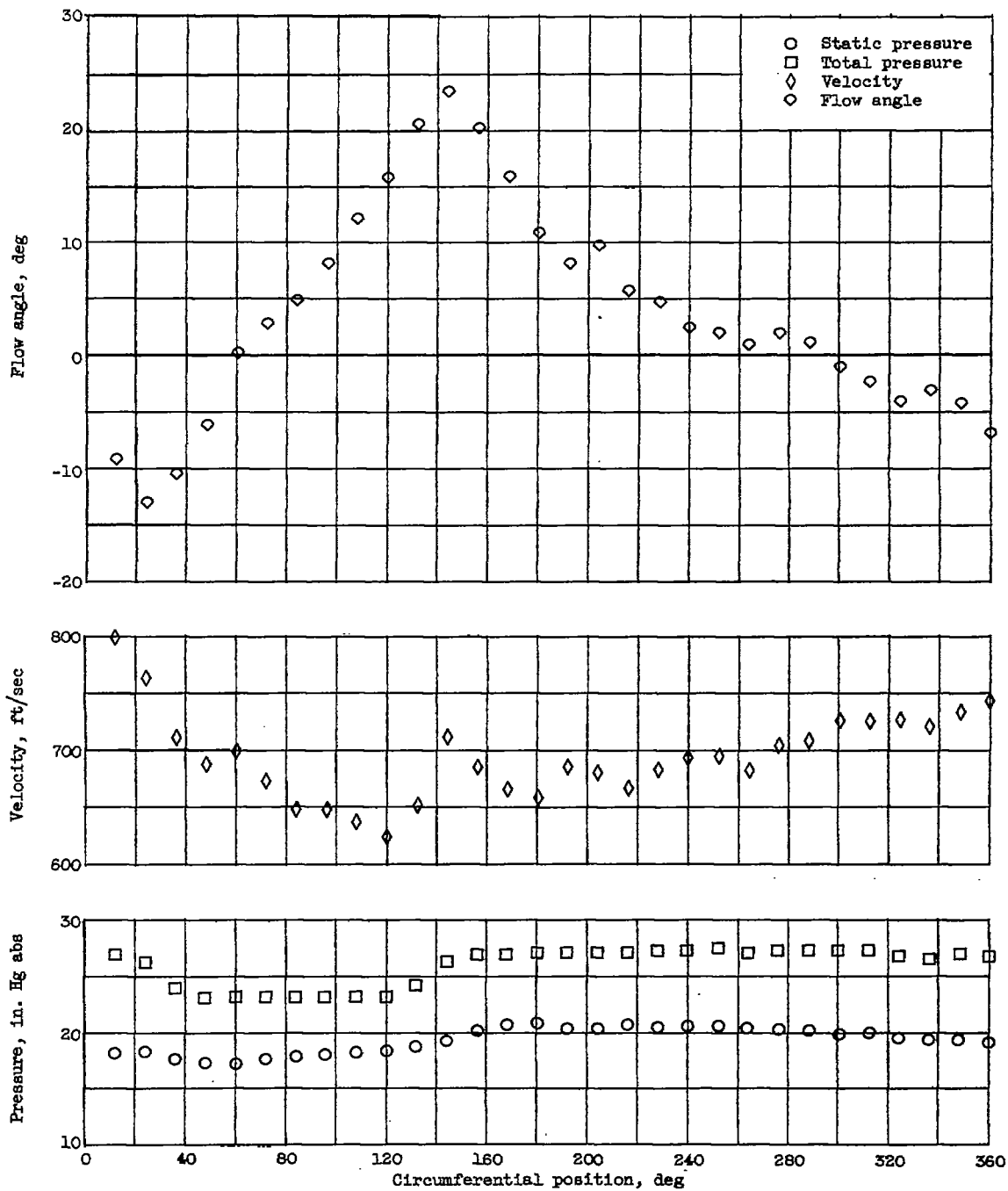
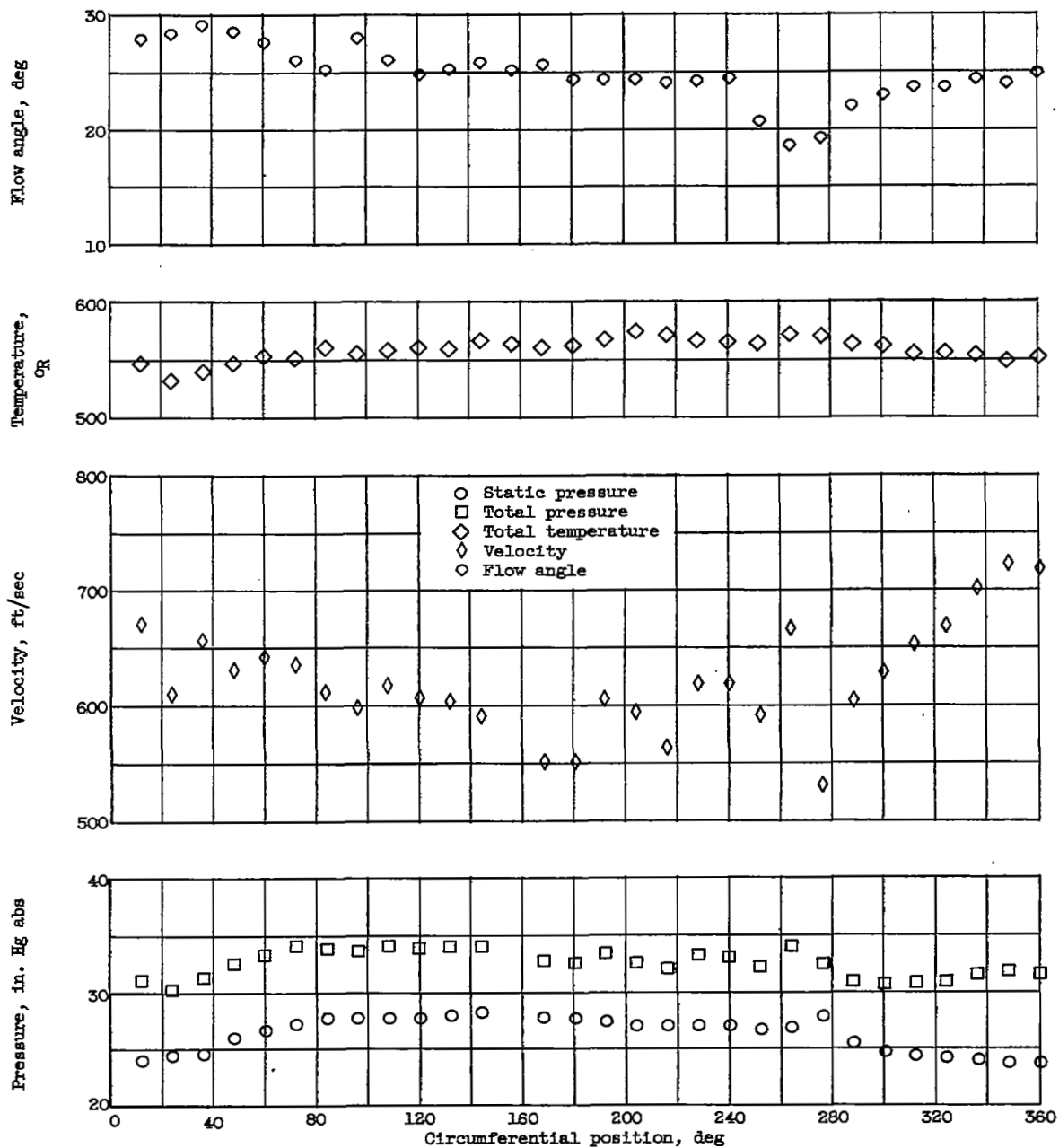
(c) Station 2; hub; absolute total temperature, 504° R.

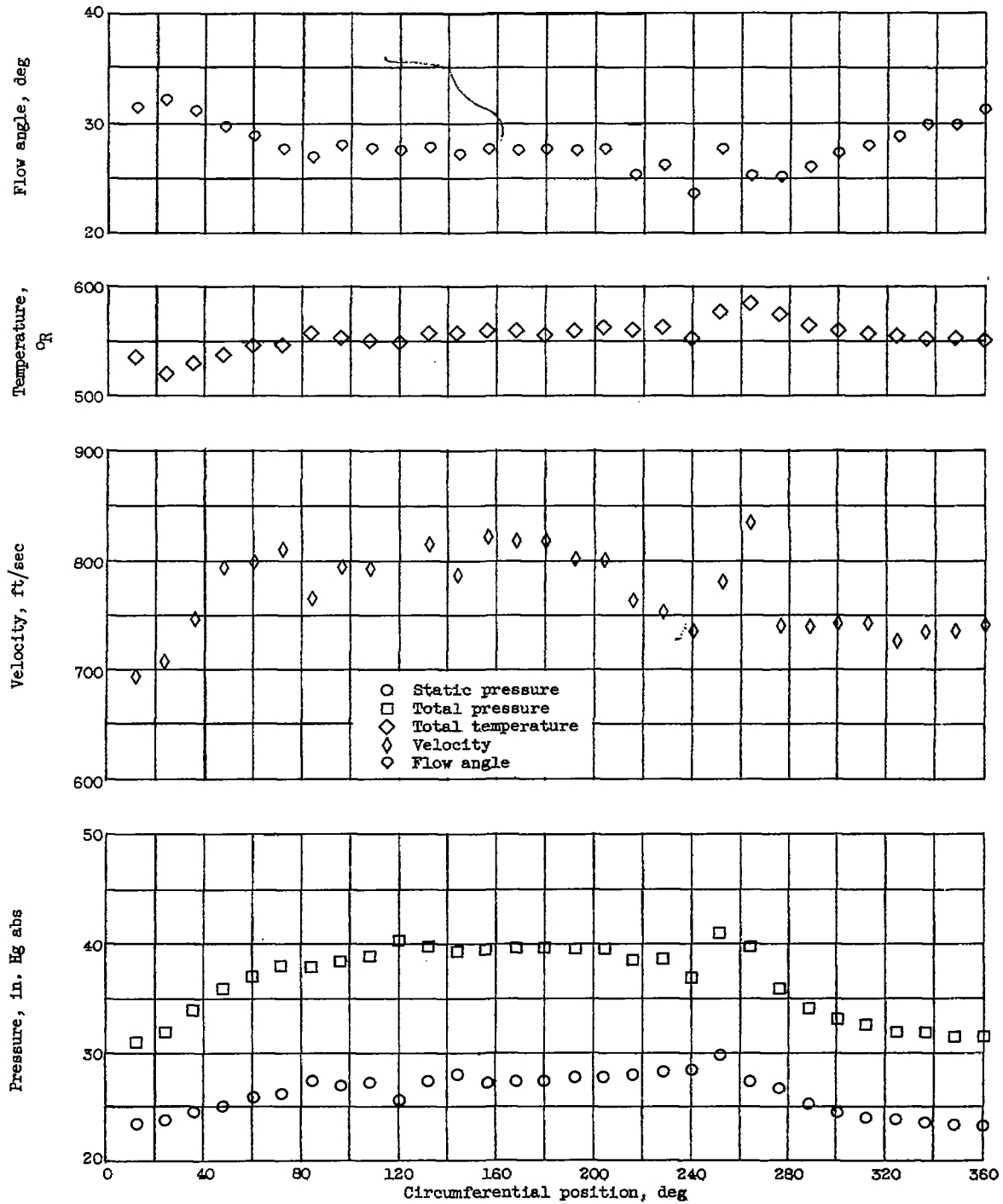
Figure 10. - Continued. Variation of distorted-flow patterns with circumferential position. Design speed.

4710



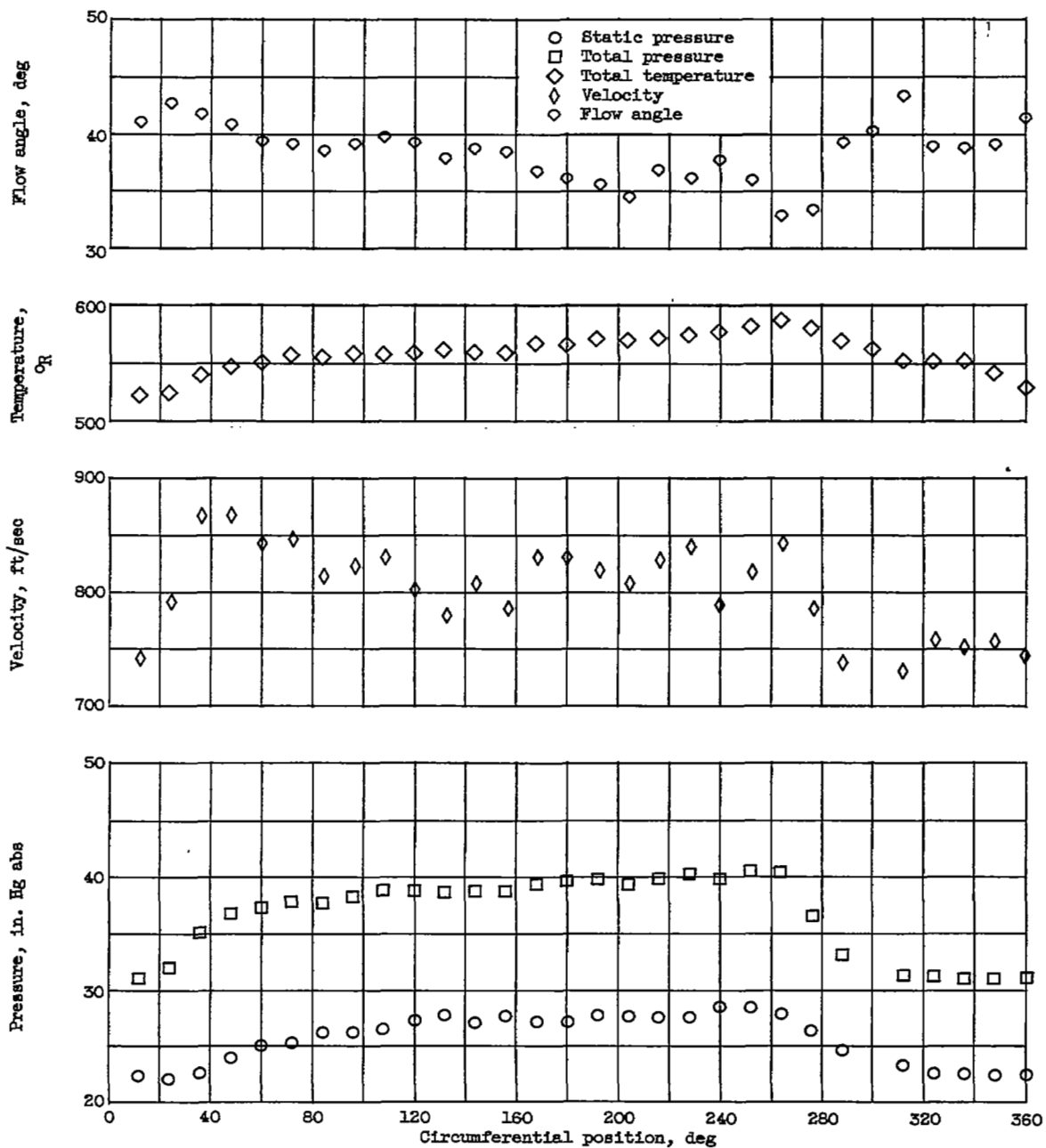
(a) Station 3; tip.

Figure 10. - Continued. Variation of distorted-flow patterns with circumferential position. Design speed.



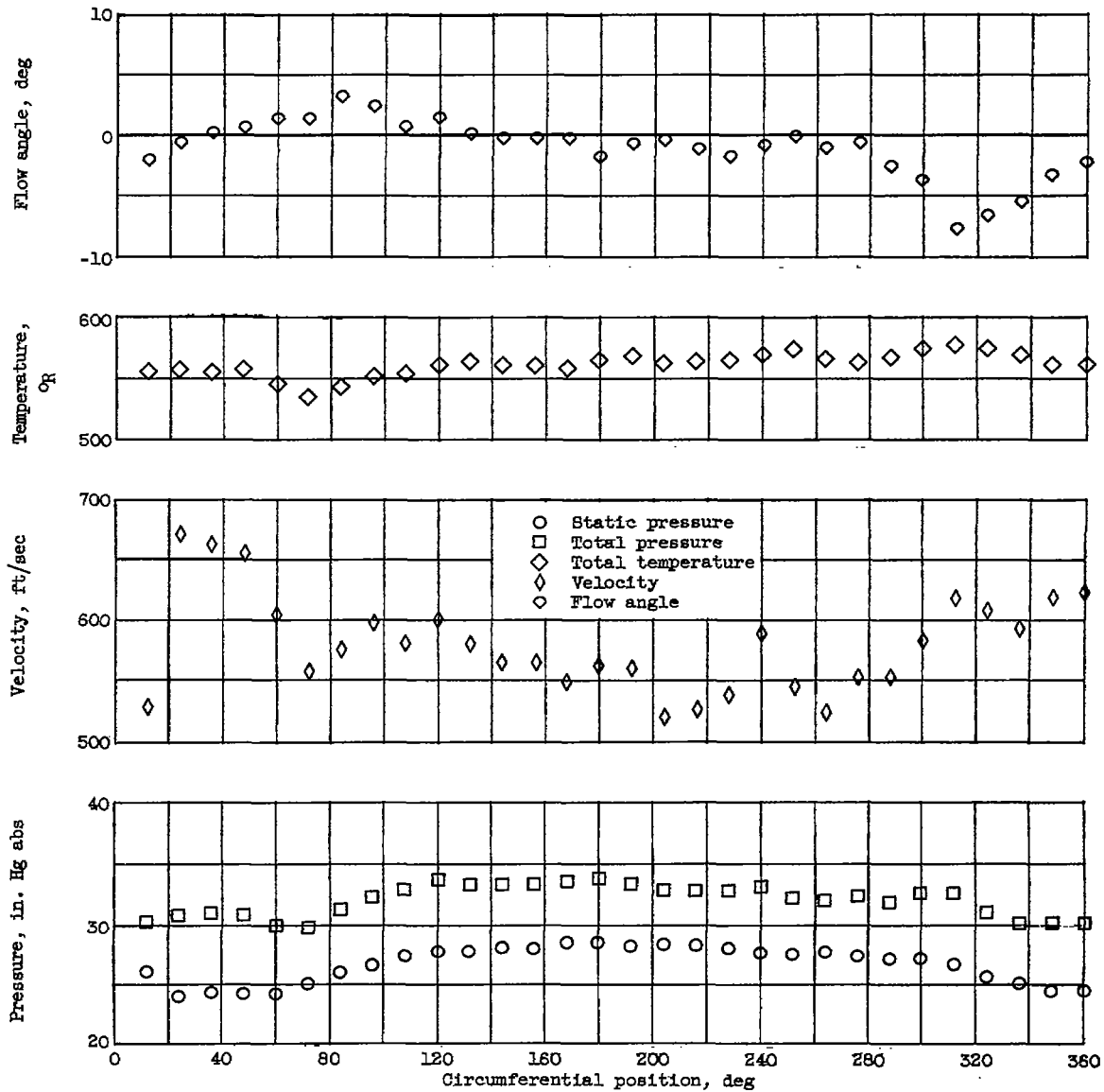
(e) Station 3; mean.

Figure 10. - Continued. Variation of distorted-flow patterns with circumferential position. Design speed.



(f) Station 3; hub.

Figure 10. - Continued. Variation of distorted-flow patterns with circumferential position. Design speed.

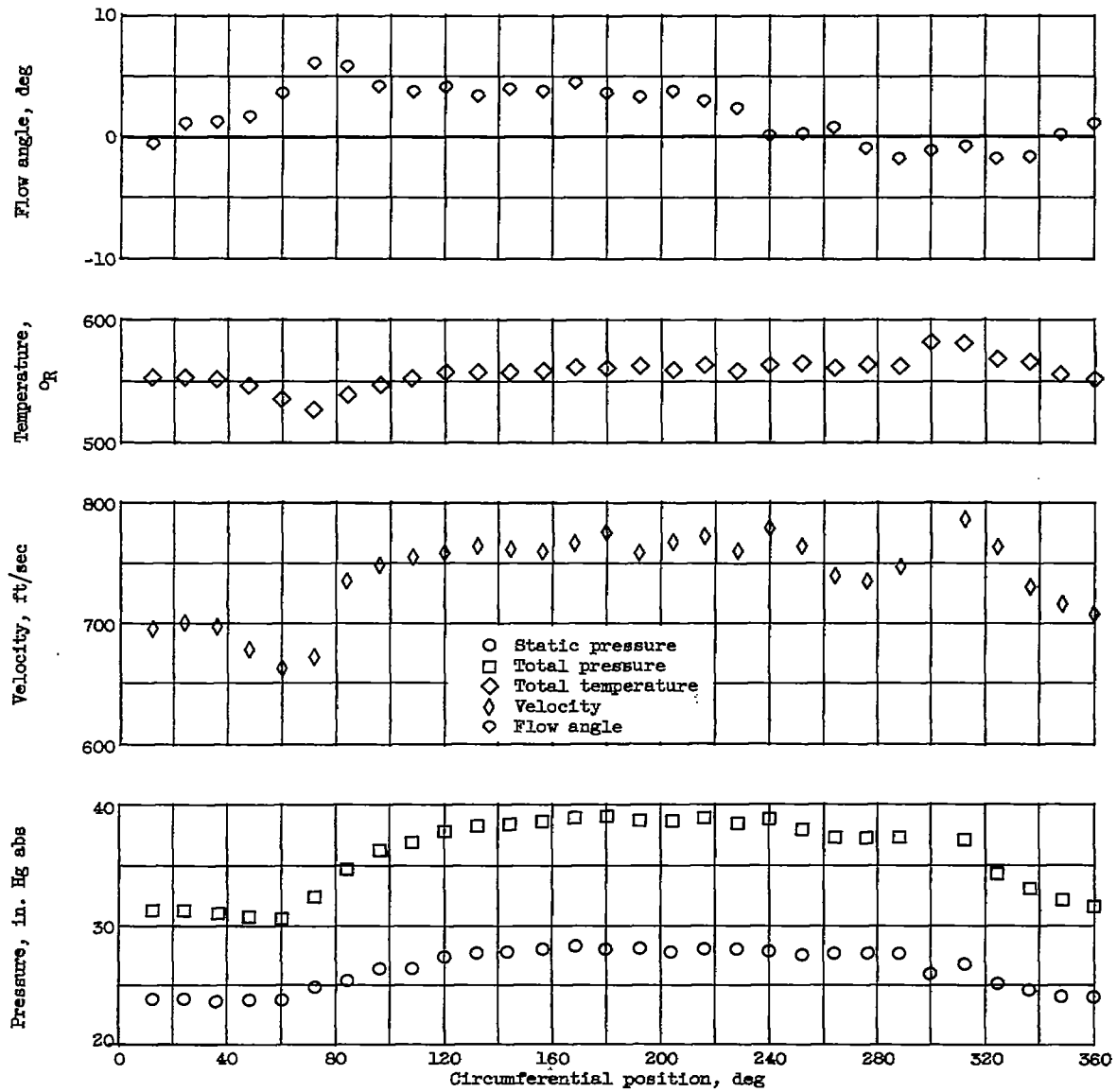


(g) Station 4; tip.

Figure 10. - Continued. Variation of distorted-flow patterns with circumferential position. Design speed.

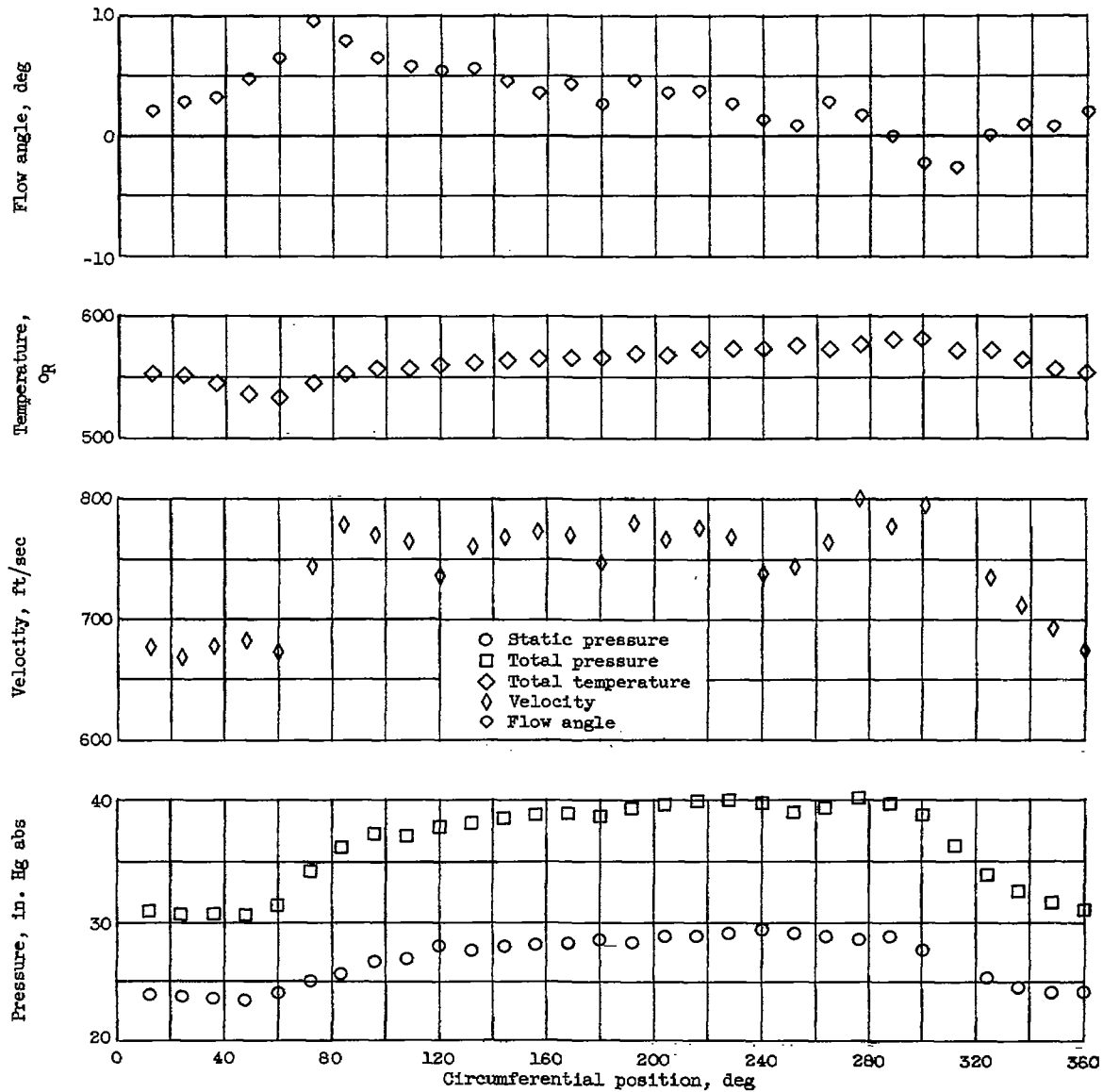
4710

CB-11 back



(h) Station 4; mean.

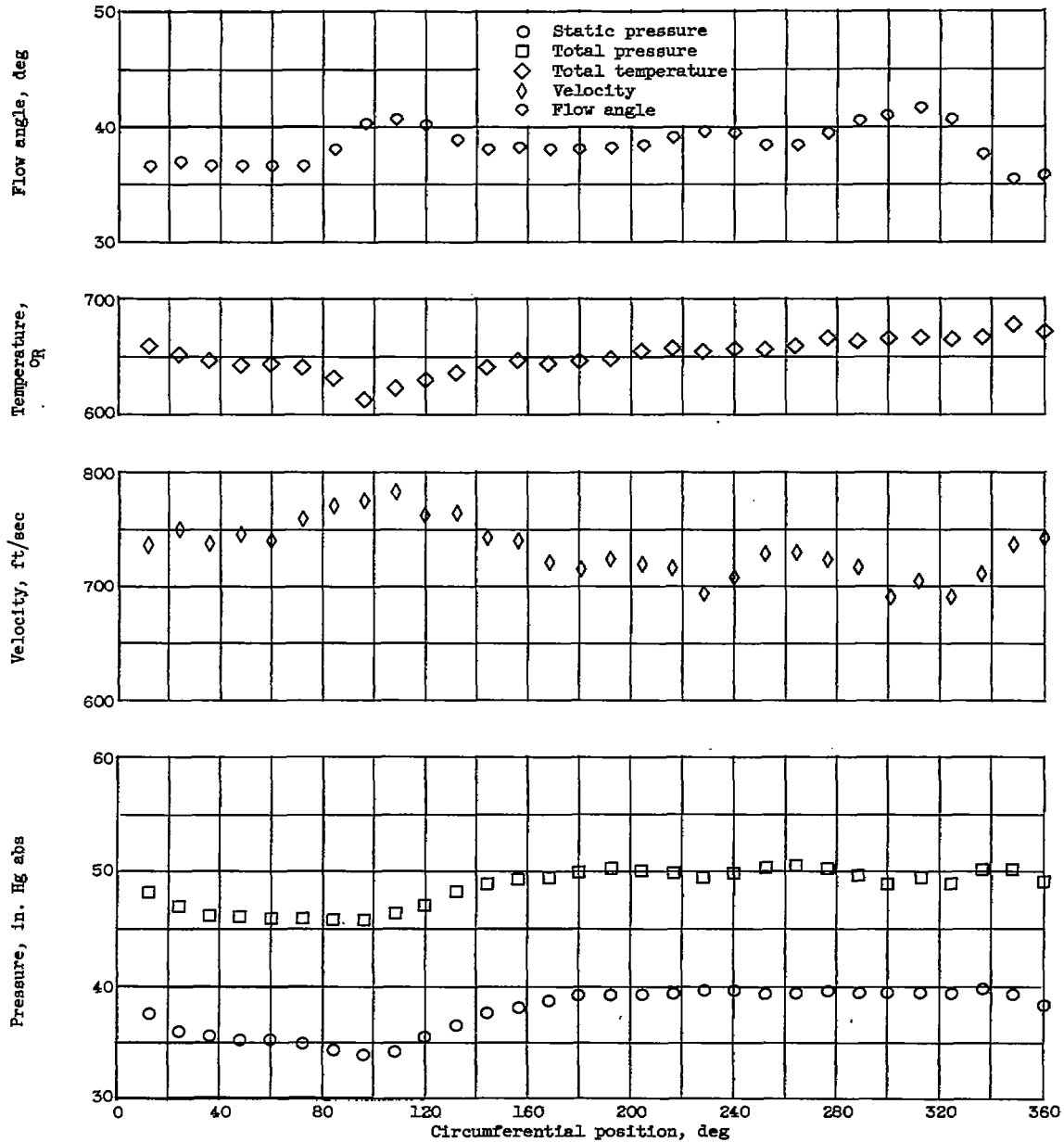
Figure 10. - Continued. Variation of distorted-flow patterns with circumferential position. Design speed.



(i) Station 4; hub.

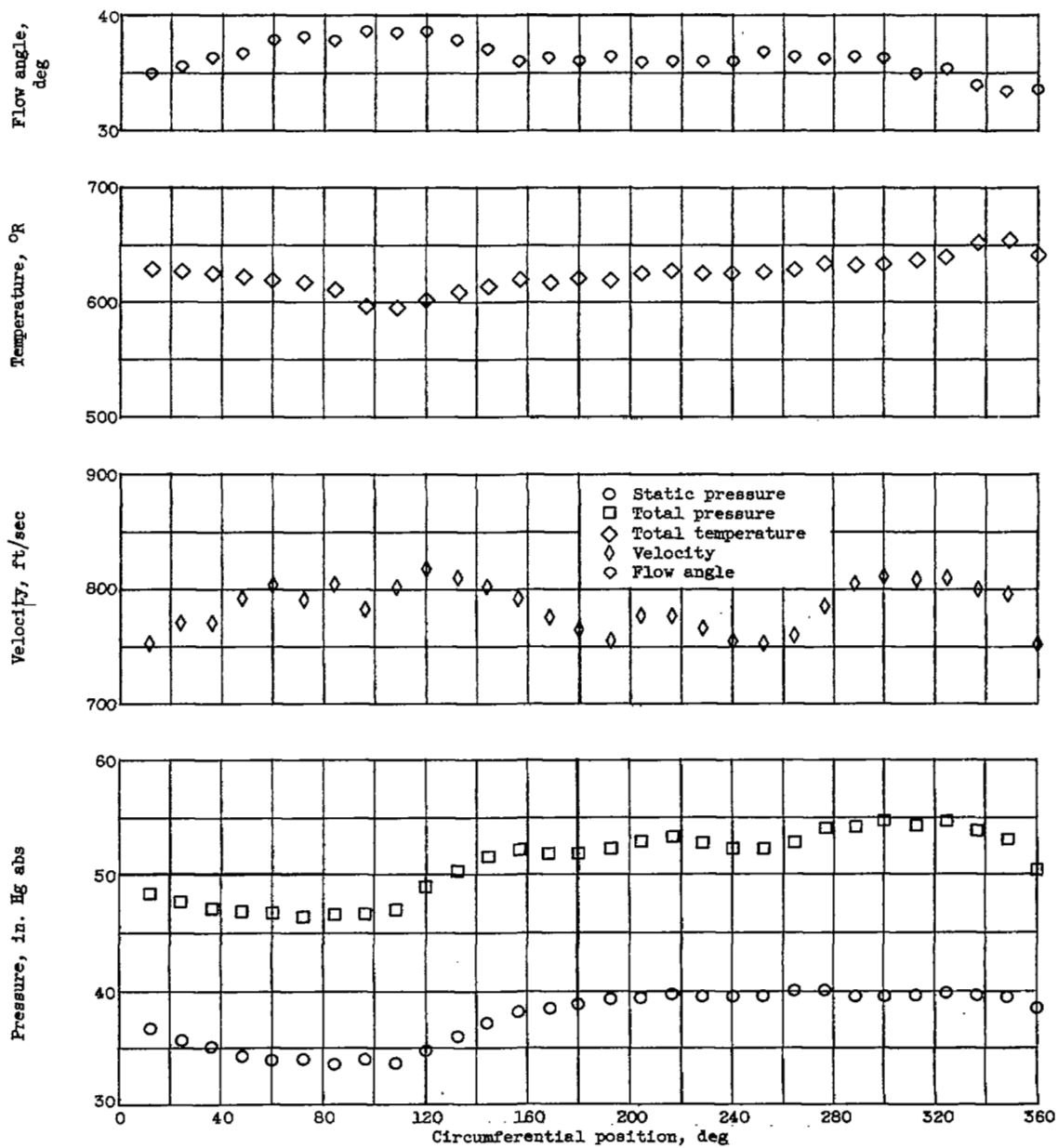
Figure 10. - Continued. Variation of distorted-flow patterns with circumferential position. Design speed.

4710



(j) Station 5; tip.

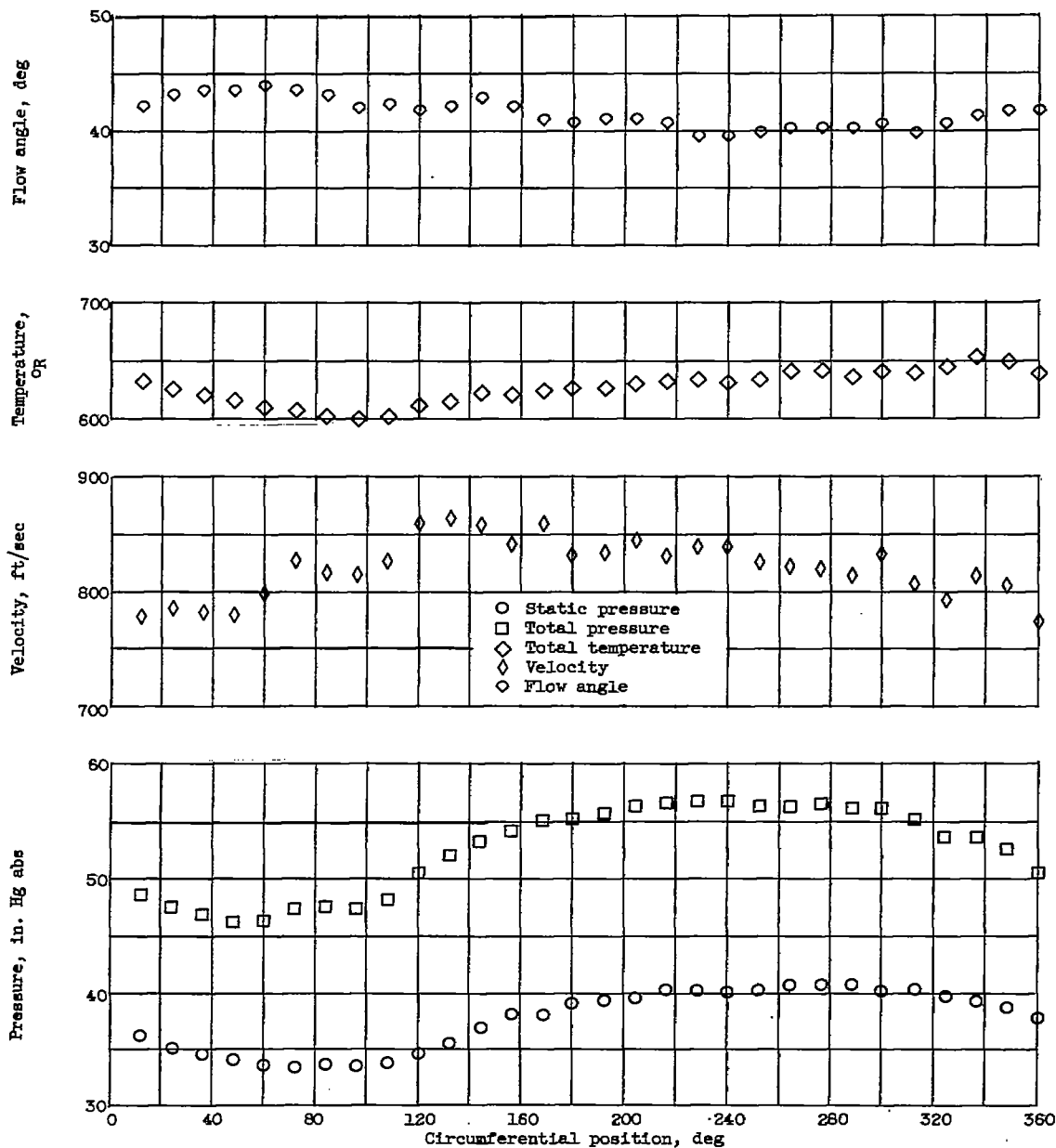
Figure 10. - Continued. Variation of distorted-flow patterns with circumferential position. Design speed.



(k) Station 5; mean.

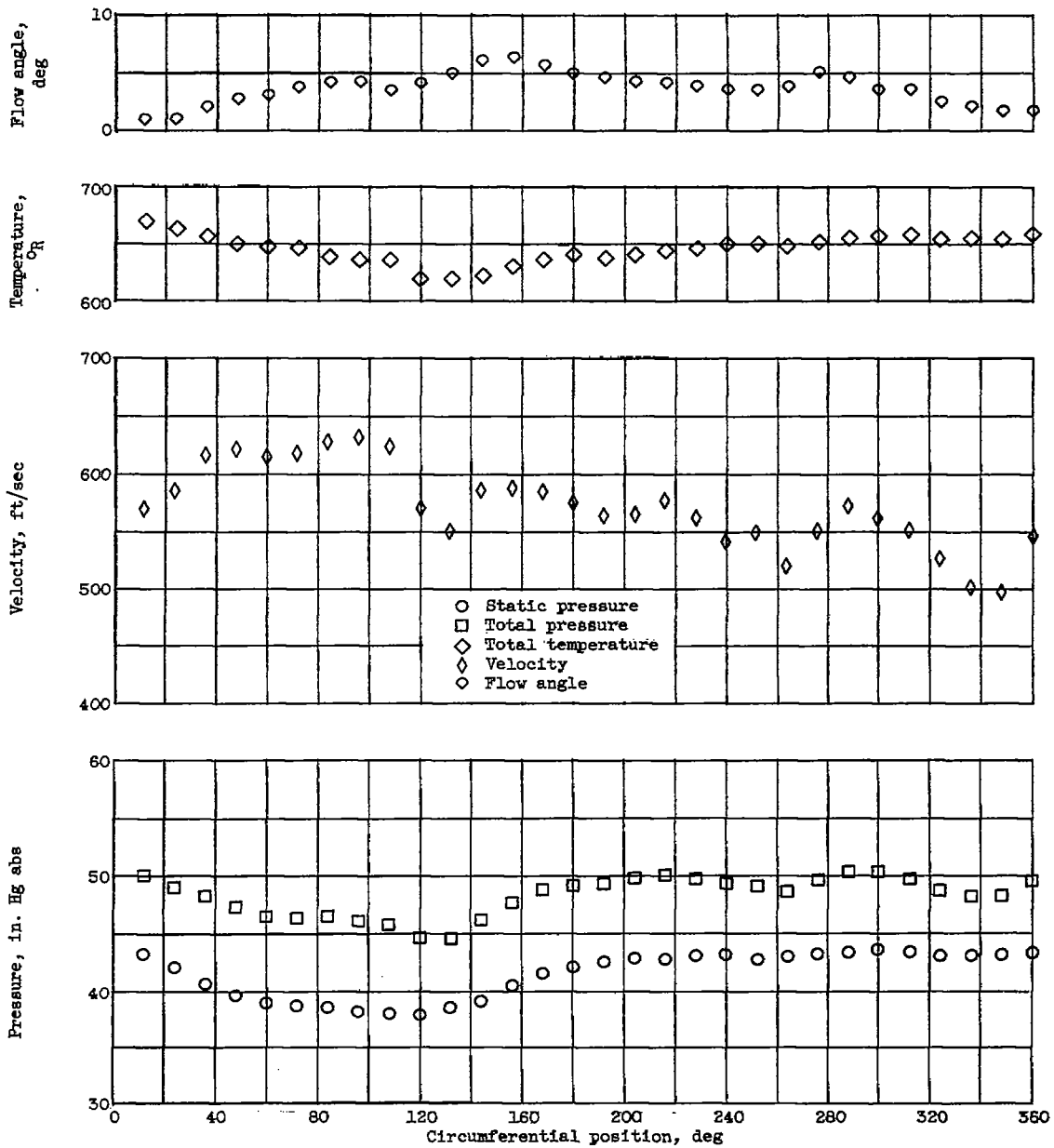
Figure 10. - Continued. Variation of distorted-flow patterns with circumferential position.
Design speed.

4710



(?) Station 5; hub.

Figure 10. - Continued. Variation of distorted-flow patterns with circumferential position. Design speed.

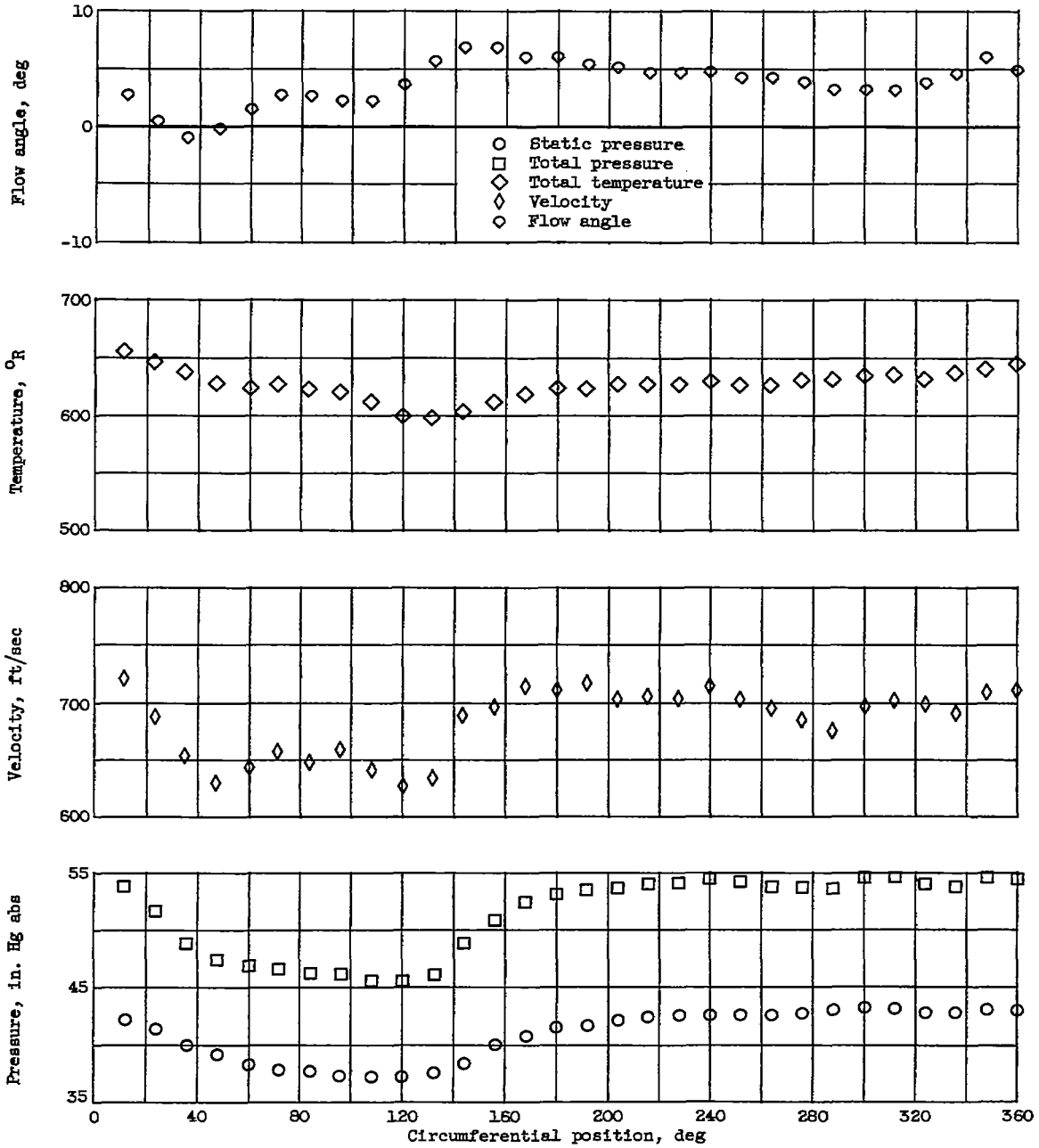


(m) Station 6; tip.

Figure 10. - Continued: Variation of distorted-flow patterns with circumferential position. Design speed.

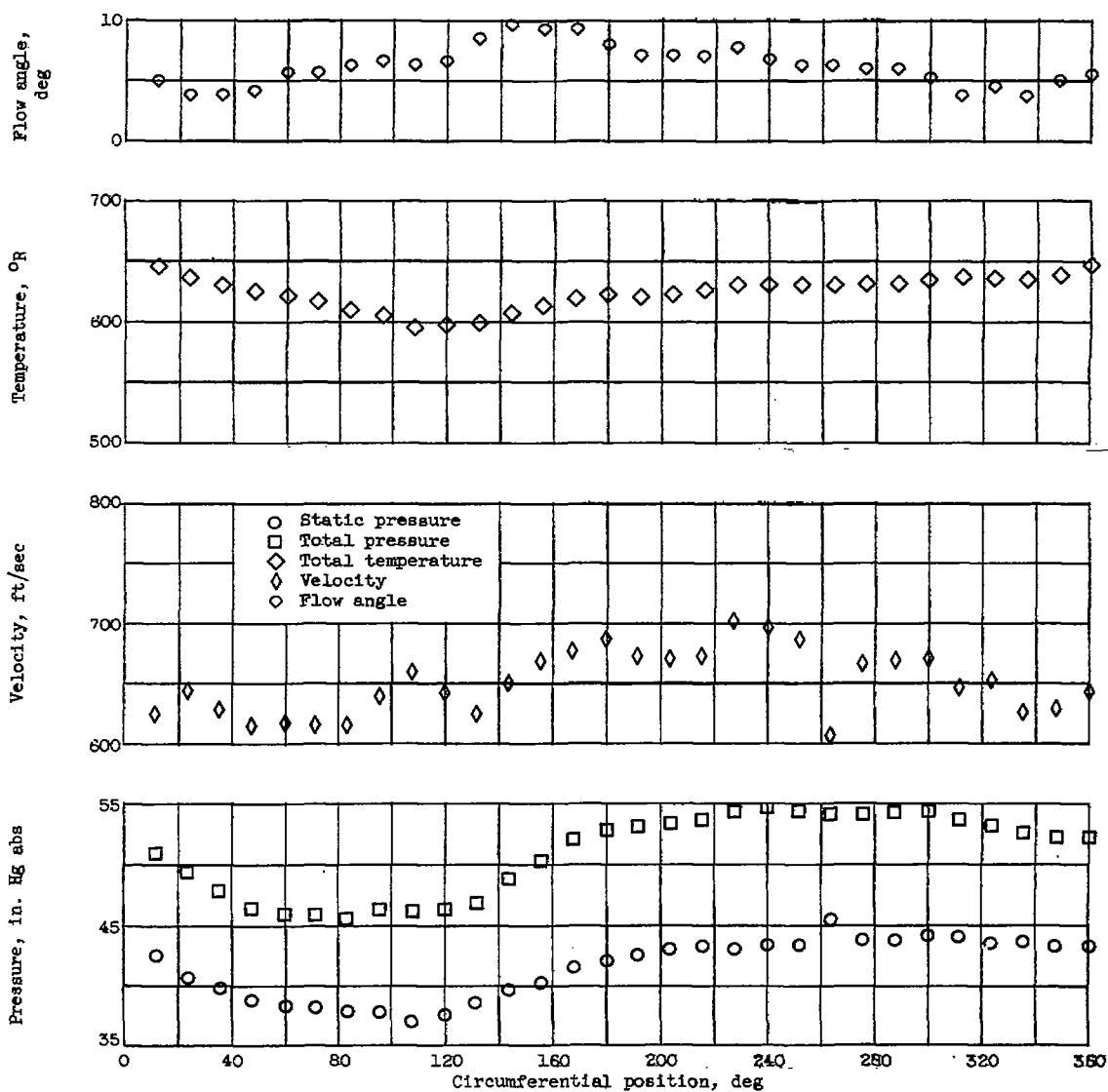
4710

CB-12



(n) Station 6; mean.

Figure 10. - Continued. Variation of distorted-flow patterns with circumferential position. Design speed.

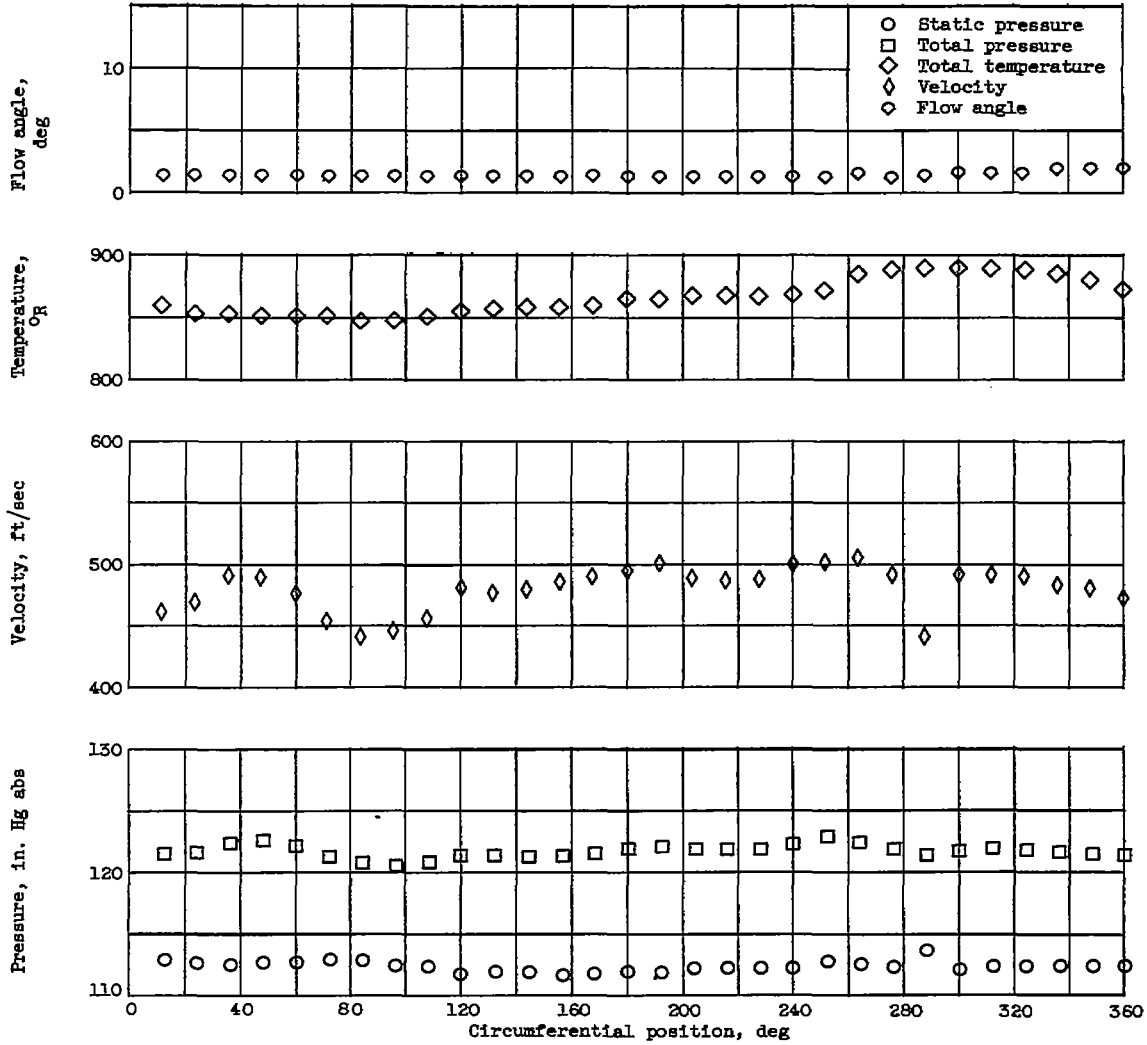


(o) Station 6; hub.

Figure 10. - Continued. Variation of distorted-flow patterns with circumferential position. Design speed.

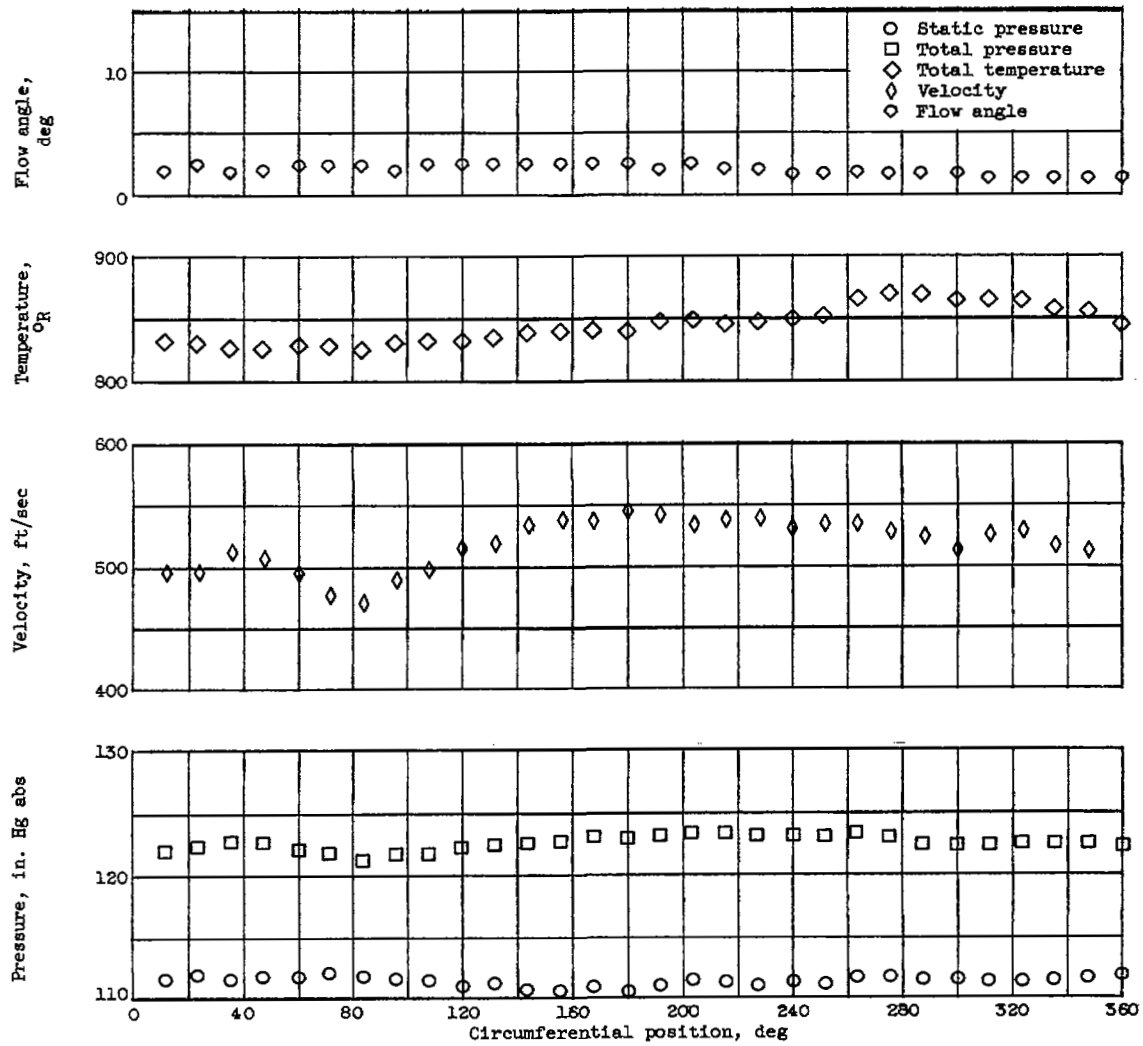
4710

CB-12 back



(p) Station 7; tip.

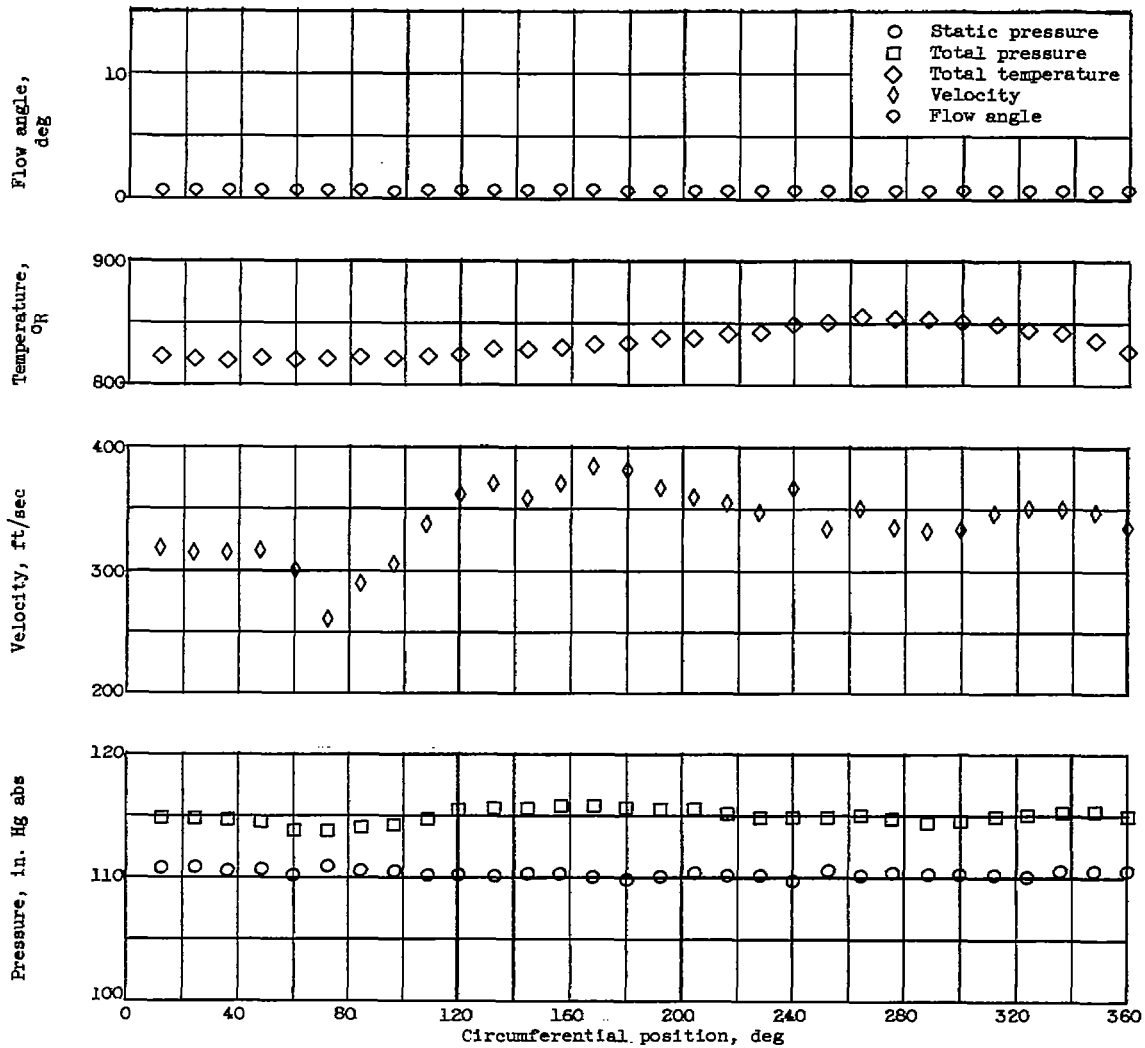
Figure 10. - Continued. Variation of distorted-flow patterns with circumferential position. Design speed.



(q) Station 7; mean.

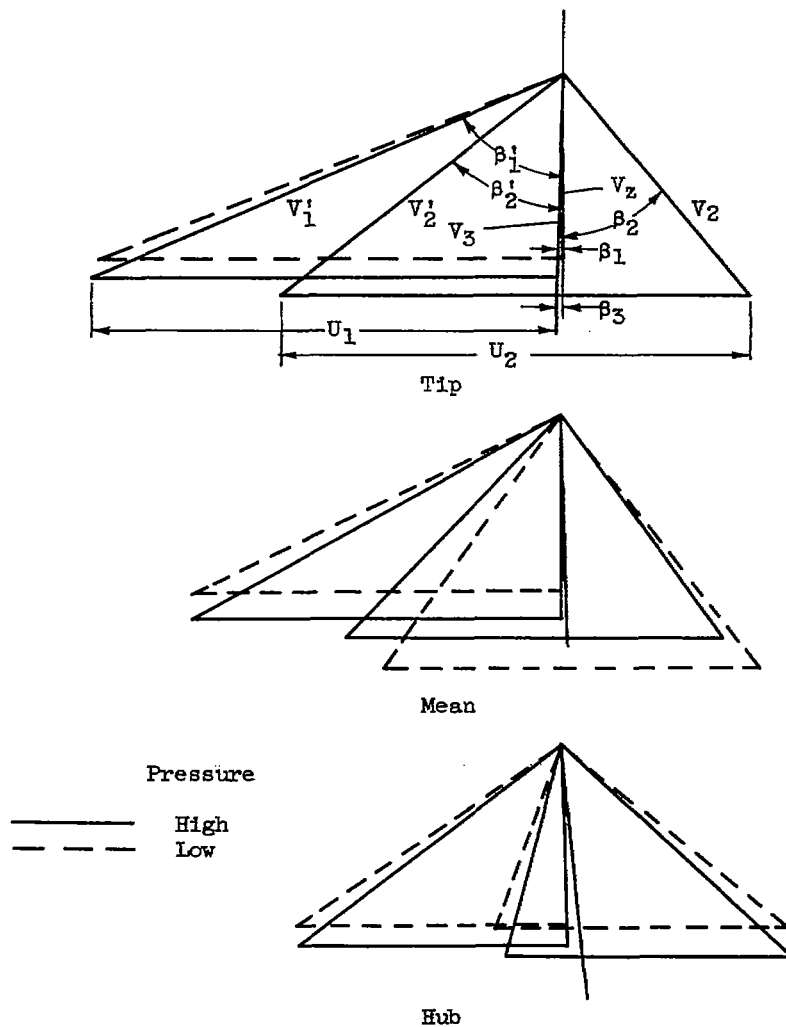
Figure 10. - Continued. Variation of distorted-flow patterns with circumferential position. Design speed.

4710



(r) Station 7; hub.

Figure 10. - Concluded. Variation of distorted-flow patterns with circumferential position. Design speed.



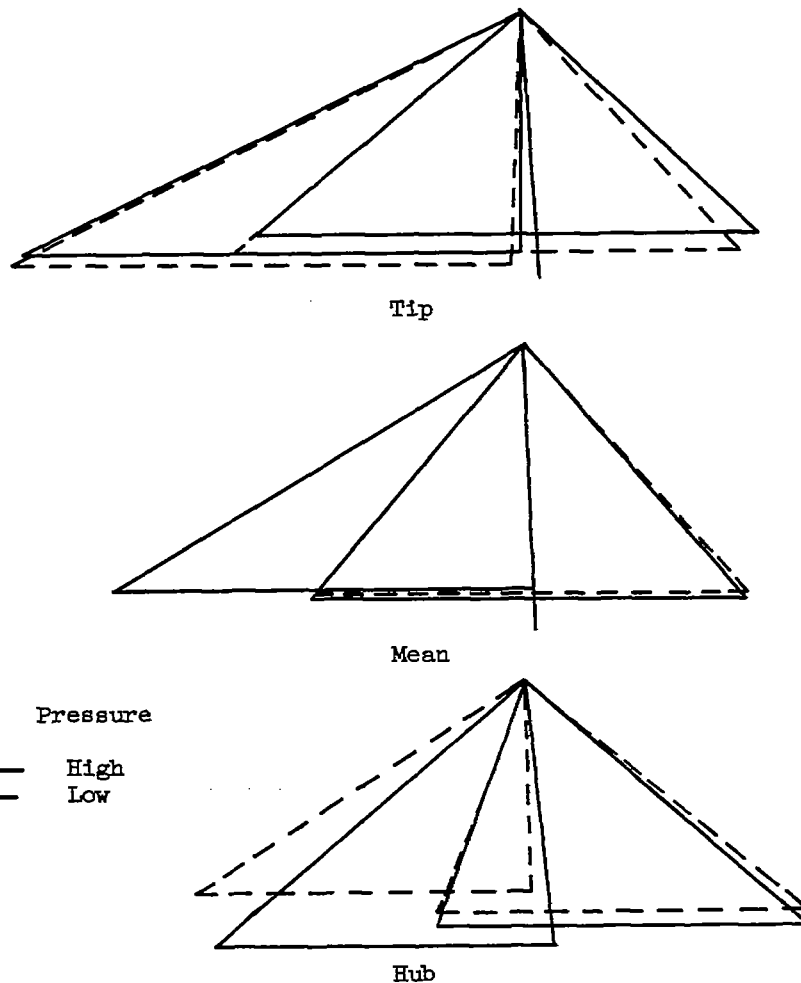
(a) Stage 1.

| Stage | Percent passage depth | Velocity diagram | | | | | | | | | | | | | | |
|-------|-----------------------|----------------------|-----------|-----------|-------|-------|-------|--------|--------|-------|-------|------------|------------|-----------|-----------|-----------|
| | | High-pressure region | | | | | | | | | | | | | | |
| | | $v_{z,1}$ | $v_{z,2}$ | $v_{z,3}$ | v_1 | v_2 | v_3 | v_1' | v_2' | U_1 | U_2 | β_1' | β_2' | β_1 | β_2 | β_3 |
| 1 | 10 | 341 | 370 | 382 | 341 | 472 | 382 | 812 | 576 | 732 | 735 | 65 | 50 | -0.9 | 38 | -0.7 |
| | 50 | 345 | 377 | 390 | 345 | 455 | 390 | 671 | 508 | 578 | 595 | 59 | 42 | .4 | 34 | 1.9 |
| | 90 | 339 | 359 | 424 | 339 | 515 | 426 | 536 | 368 | 424 | 455 | 51 | 13 | 1.4 | 46 | 5.5 |
| | | Low-pressure region | | | | | | | | | | | | | | |
| 1 | 10 | 311 | 367 | 397 | 311 | 473 | 398 | 796 | 571 | 732 | 735 | 67 | 50 | -0.2 | 39 | -2.1 |
| | 50 | 302 | 429 | 395 | 302 | 532 | 395 | 649 | 512 | 578 | 595 | 62 | 33 | .6 | 36 | 2.1 |
| | 90 | 304 | 308 | 341 | 304 | 466 | 341 | 514 | 325 | 424 | 455 | 54 | 19 | 1.6 | 49 | 1.7 |

(b) Stage 1; data summation.

Figure 11. - Velocity diagram plots. 70-Percent speed.

4710

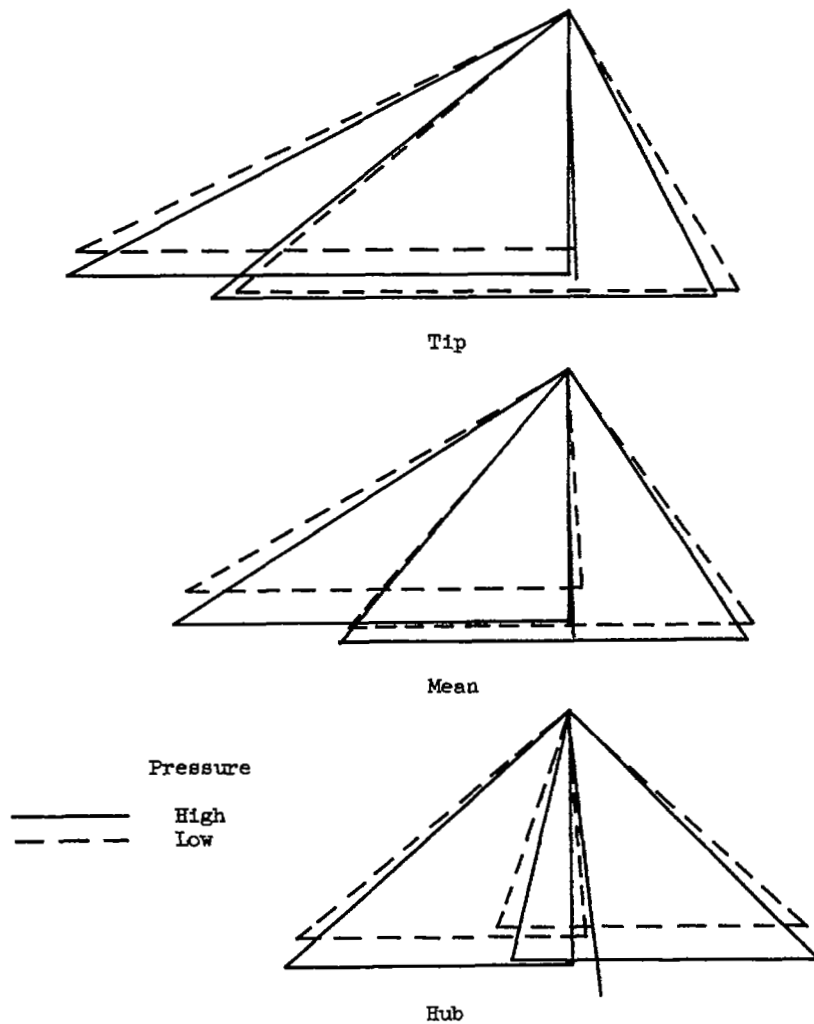


(c) Stage 2.

| Stage | Percent passage depth | Velocity diagram | | | | | | | | | | | | | | |
|-------|-----------------------|----------------------|-----------|-----------|-------|-------|-------|--------|--------|-------|-------|------------|------------|-----------|-----------|-----------|
| | | High-pressure region | | | | | | | | | | | | | | |
| | | $V_{z,1}$ | $V_{z,2}$ | $V_{z,3}$ | V_1 | V_2 | V_3 | V_1' | V_2' | U_1 | U_2 | β_1' | β_2' | β_1 | β_2 | β_3 |
| 2 | 10 | 382 | 351 | 420 | 382 | 492 | 421 | 837 | 533 | 740 | 745 | 63 | 49 | -0.7 | 44 | 3.8 |
| | 50 | 390 | 404 | 459 | 390 | 519 | 459 | 720 | 516 | 618 | 645 | 57 | 38 | 1.9 | 39 | 2.6 |
| | 90 | 424 | 395 | 438 | 426 | 571 | 440 | 623 | 416 | 497 | 546 | 47 | 19 | 5.5 | 46 | 6.0 |
| | | Low-pressure region | | | | | | | | | | | | | | |
| 2 | 10 | 397 | 376 | 412 | 398 | 491 | 413 | 852 | 570 | 740 | 745 | 62 | 49 | -2.1 | 40 | 3.4 |
| | 50 | 395 | 394 | 450 | 395 | 515 | 451 | 722 | 503 | 618 | 645 | 57 | 38 | 2.1 | 40 | 2.8 |
| | 90 | 341 | 372 | 421 | 341 | 558 | 423 | 595 | 394 | 497 | 546 | 55 | 19 | 1.7 | 48 | 5.8 |

(d) Stage 2; data summation.

Figure 11. - Concluded. Velocity diagram plots. 70-Percent speed.



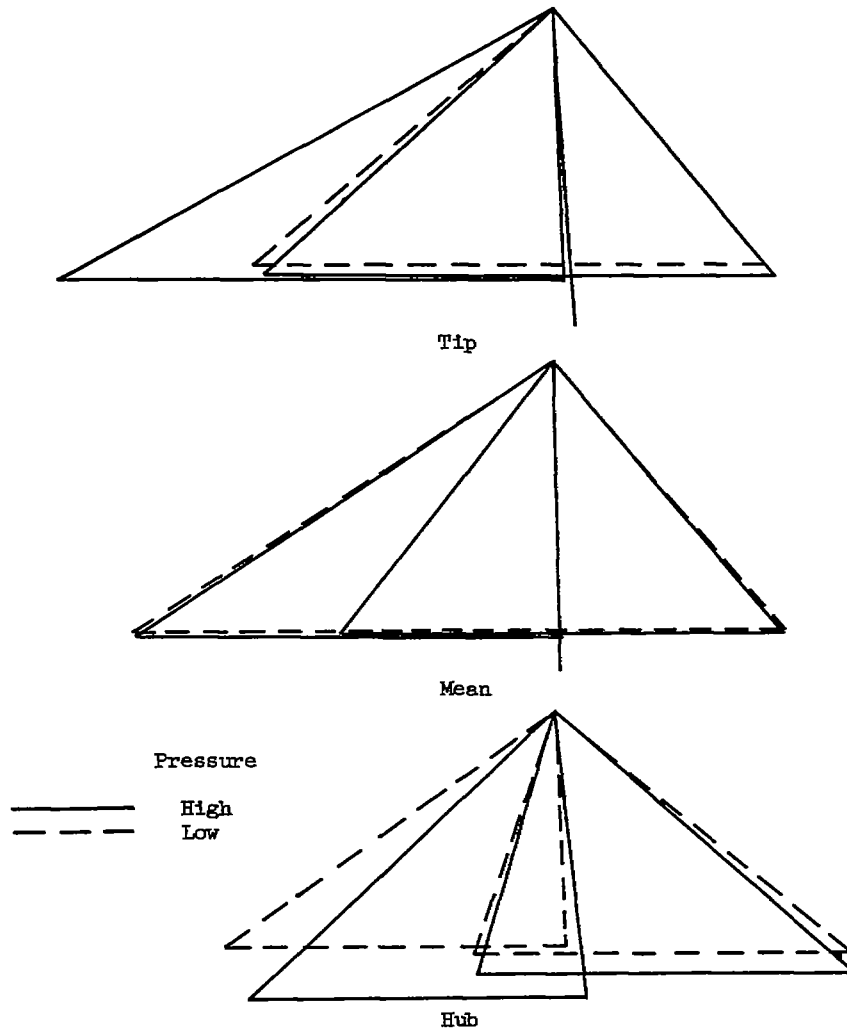
| Stage | Percent passage depth | Velocity diagram | | | | | | | | | | | | | | |
|-------|-----------------------|----------------------|-----------|-----------|-------|-------|-------|--------|--------|-------|-------|------------|------------|-----------|-----------|-----------|
| | | High-pressure region | | | | | | | | | | | | | | |
| | | $V_{z,1}$ | $V_{z,2}$ | $V_{z,3}$ | V_1 | V_2 | V_3 | V_1' | V_2' | U_1 | U_2 | β_1' | β_2' | β_1 | β_2 | β_3 |
| 1 | 10 | 468 | 509 | 482 | 468 | 570 | 482 | 959 | 774 | 836 | 840 | 61 | 49 | -0.2 | 27 | 2.1 |
| | 50 | 455 | 488 | 484 | 455 | 572 | 484 | 801 | 619 | 660 | 680 | 55 | 38 | .2 | 31 | 1.0 |
| | 90 | 455 | 447 | 512 | 456 | 617 | 515 | 657 | 467 | 484 | 520 | 46 | 12 | 1.3 | 44 | 6.0 |
| | | Low-pressure region | | | | | | | | | | | | | | |
| 1 | 10 | 426 | 500 | 480 | 427 | 574 | 480 | 925 | 750 | 836 | 840 | 63 | 48 | 2.1 | 29 | 1.3 |
| | 50 | 392 | 461 | 475 | 392 | 554 | 476 | 754 | 593 | 660 | 680 | 59 | 39 | 2.4 | 34 | 1.3 |
| | 90 | 406 | 386 | 416 | 408 | 556 | 416 | 607 | 404 | 484 | 520 | 48 | 17 | 4.6 | 46 | 2.3 |

(b) Stage 1; data summation.

Figure 12. - Velocity diagram plots. 80-Percent speed.

4710

CB-13

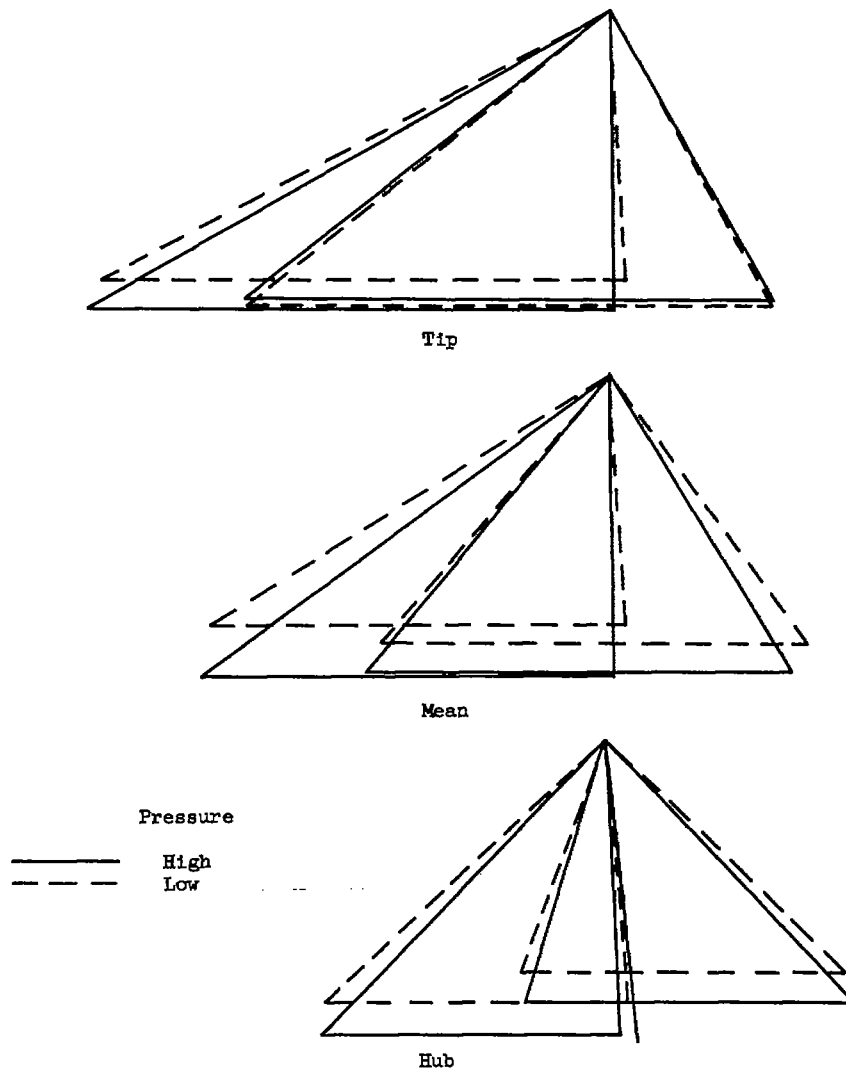


(c) Stage 2.

| Stage | Percent passage depth | Velocity diagram | | | | | | | | | | | | | | |
|-------|-----------------------|----------------------|-----------|-----------|-------|-------|-------|--------|--------|-------|-------|------------|------------|-----------|-----------|-----------|
| | | High-pressure region | | | | | | | | | | | | | | |
| | | $V_{z,1}$ | $V_{z,2}$ | $V_{z,3}$ | V_1 | V_2 | V_3 | V_1' | V_2' | U_1 | U_2 | β_1' | β_2' | β_1 | β_2 | β_3 |
| 2 | 10 | 462 | 472 | 560 | 482 | 598 | 561 | 958 | 675 | 845 | 852 | 60 | 46 | 2.1 | 38 | 4.1 |
| | 50 | 484 | 479 | 546 | 484 | 612 | 546 | 849 | 598 | 707 | 738 | 55 | 37 | 1.0 | 38 | 1.3 |
| | 90 | 512 | 466 | 518 | 515 | 676 | 520 | 726 | 484 | 563 | 624 | 45 | 16 | 6.0 | 46 | 5.0 |
| | | Low-pressure region | | | | | | | | | | | | | | |
| 2 | 10 | 480 | 455 | 541 | 480 | 574 | 542 | 963 | 676 | 845 | 852 | 60 | 48 | 1.3 | 38 | 3.6 |
| | 50 | 475 | 472 | 527 | 476 | 612 | 527 | 843 | 587 | 707 | 738 | 56 | 36 | 1.3 | 40 | 1.2 |
| | 90 | 416 | 430 | 487 | 416 | 650 | 489 | 691 | 451 | 568 | 624 | 53 | 18 | 2.3 | 49 | 5.3 |

(d) Stage 2; data summation.

Figure 12. - Concluded. Velocity diagram plots. 80-Percent speed.

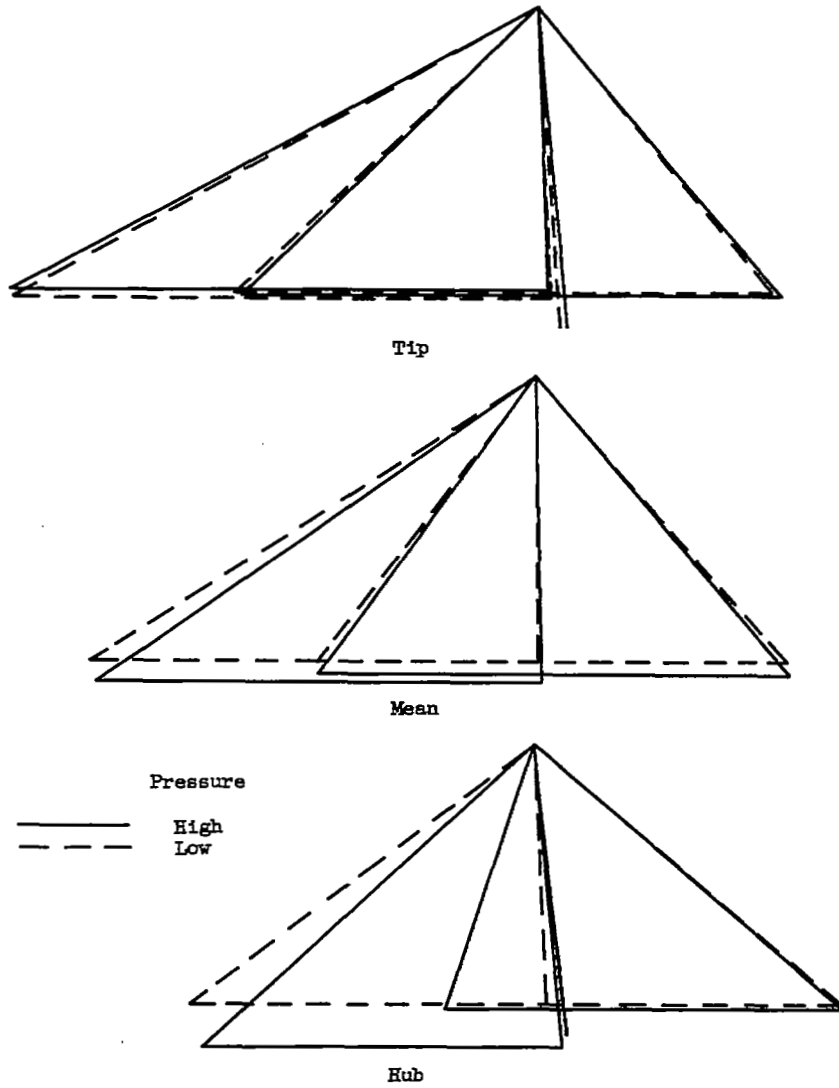


| Stage | Percent passage depth | Velocity diagram | | | | | | | | | | | | | | |
|-------|-----------------------|----------------------|-----------|-----------|-------|-------|-------|--------|--------|-------|-------|------------|------------|-----------|-----------|-----------|
| | | High-pressure region | | | | | | | | | | | | | | |
| | | $V_{z,1}$ | $V_{z,2}$ | $V_{z,3}$ | V_1 | V_2 | V_3 | V'_1 | V'_2 | U_1 | U_2 | β'_1 | β'_2 | β_1 | β_2 | β_3 |
| 1 | 10 | 569 | 551 | 538 | 569 | 621 | 539 | 1030 | 860 | 944 | 945 | 59 | 50 | 1.2 | 27 | 1.9 |
| | 50 | 577 | 568 | 580 | 577 | 657 | 580 | 932 | 716 | 743 | 765 | 52 | 37 | 1.0 | 30 | 1.1 |
| | 90 | 563 | 496 | 578 | 563 | 670 | 581 | 765 | 514 | 545 | 585 | 43 | 15 | 2.7 | 42 | 5.5 |
| | | Low-pressure region | | | | | | | | | | | | | | |
| 1 | 10 | 514 | 568 | 552 | 515 | 640 | 552 | 1044 | 863 | 941 | 945 | 60 | 49 | 3.6 | 27 | 2.3 |
| | 50 | 479 | 516 | 544 | 480 | 617 | 544 | 858 | 670 | 743 | 765 | 56 | 40 | 3.7 | 33 | .7 |
| | 90 | 501 | 440 | 494 | 503 | 615 | 495 | 709 | 466 | 545 | 585 | 45 | 19 | 4.8 | 44 | 2.5 |

(b) Stage 1; data summation.

Figure 13. - Velocity diagram plots. 90-Percent speed.

4710
CB-13 back

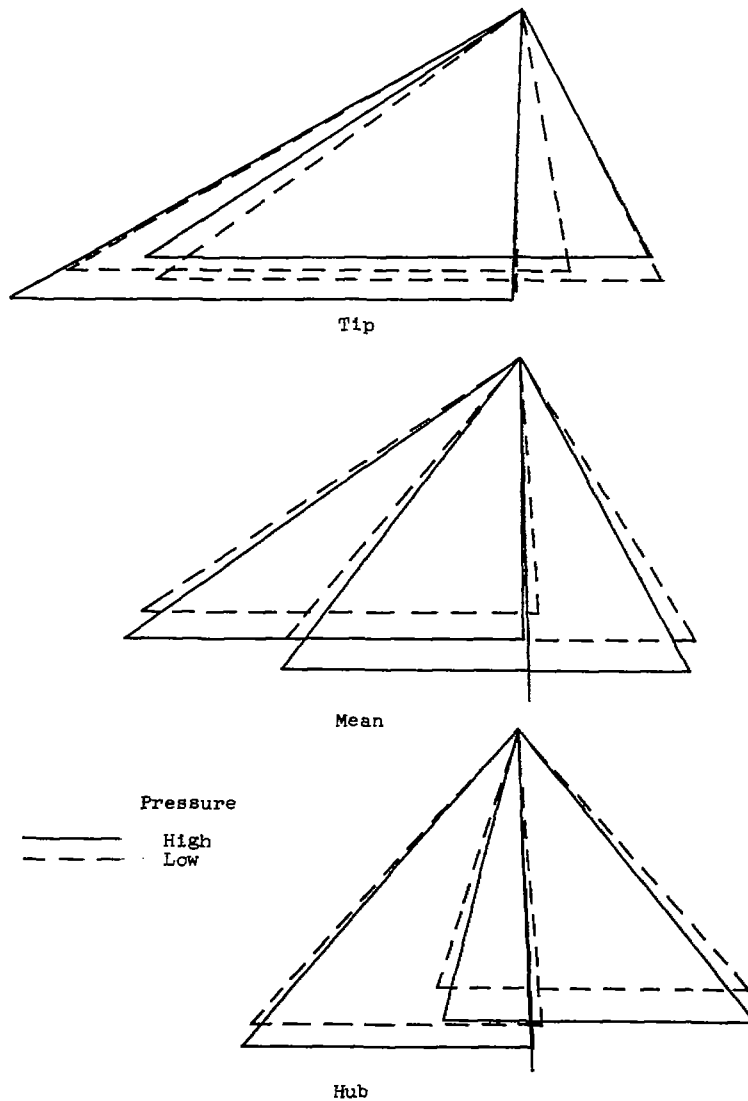


(c) Stage 2.

| Stage | Percent passage depth | Velocity diagram | | | | | | | | | | | | | | |
|-------|-----------------------|----------------------|-----------|-----------|-------|-------|-------|--------|--------|-------|-------|------------|------------|-----------|-----------|-----------|
| | | High-pressure region | | | | | | | | | | | | | | |
| | | $V_{z,1}$ | $V_{z,2}$ | $V_{z,3}$ | V_1 | V_2 | V_3 | V_1' | V_2' | U_1 | U_2 | β_1' | β_2' | β_1 | β_2 | β_3 |
| 2 | 10 | 538 | 543 | 617 | 539 | 690 | 620 | 1078 | 760 | 951 | 958 | 60 | 44 | 1.9 | 38 | 5.1 |
| | 50 | 580 | 568 | 590 | 580 | 722 | 590 | 975 | 687 | 795 | 830 | 54 | 34 | 1.1 | 38 | 1.2 |
| | 90 | 578 | 507 | 559 | 581 | 743 | 563 | 821 | 531 | 639 | 702 | 45 | 17 | 5.5 | 47 | 6.3 |
| | | Low-pressure region | | | | | | | | | | | | | | |
| 2 | 10 | 552 | 539 | 608 | 552 | 681 | 609 | 1080 | 764 | 951 | 958 | 59 | 45 | 2.3 | 38 | 3.8 |
| | 50 | 544 | 542 | 559 | 544 | 695 | 559 | 957 | 670 | 795 | 830 | 55 | 36 | .7 | 39 | 1.4 |
| | 90 | 494 | 488 | 524 | 495 | 736 | 526 | 791 | 511 | 639 | 702 | 51 | 17 | 2.5 | 48 | 5.2 |

(d) Stage 2; data summation.

Figure 13. - Concluded. Velocity diagram plots. 90-Percent speed.



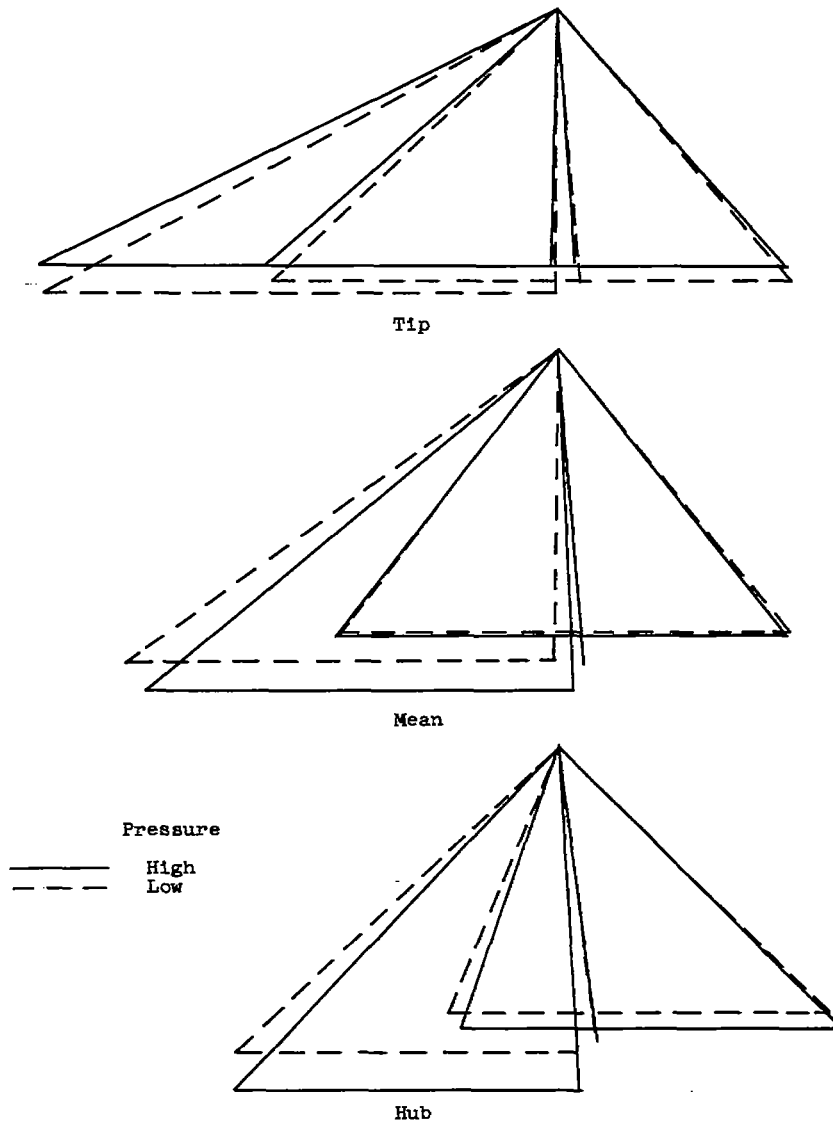
(a) Stage 1.

| Stage | Percent passage depth | Velocity diagram | | | | | | | | | | | | | | |
|-------|-----------------------|----------------------|-----------|-----------|-------|-------|-------|--------|--------|-------|-------|------------|------------|-----------|-----------|-----------|
| | | High-pressure region | | | | | | | | | | | | | | |
| | | $v_{z,1}$ | $v_{z,2}$ | $v_{z,3}$ | v_1 | v_2 | v_3 | v'_1 | v'_2 | u_1 | u_2 | β'_1 | β'_2 | β_1 | β_2 | β_3 |
| 1 | 10 | 650 | 552 | 566 | 650 | 611 | 566 | 1249 | 962 | 1045 | 1050 | 59 | 55 | -1.9 | 25 | -1.3 |
| | 50 | 627 | 694 | 759 | 627 | 581 | 760 | 1027 | 851 | 825 | 850 | 52 | 35 | 1.0 | 27 | 2.2 |
| | 90 | 706 | 648 | 761 | 707 | 820 | 762 | 903 | 665 | 605 | 650 | 39 | 13 | 3.4 | 38 | 3.2 |
| | | Low-pressure region | | | | | | | | | | | | | | |
| 1 | 10 | 589 | 609 | 625 | 598 | 671 | 625 | 1111 | 980 | 1045 | 1050 | 58 | 52 | 9.9 | 25 | -0.9 |
| | 50 | 566 | 628 | 695 | 568 | 727 | 695 | 964 | 793 | 825 | 850 | 54 | 38 | 4.5 | 30 | 1.2 |
| | 90 | 658 | 571 | 679 | 661 | 755 | 680 | 851 | 593 | 605 | 650 | 39 | 15 | 5.6 | 41 | 3.2 |

(b) Stage 1; data summation.

Figure 14. - Velocity diagram plots. Design speed.

4710



(c) Stage 2.

| Stage | Percent passage depth | Velocity diagram | | | | | | | | | | | | | | | |
|-------|-----------------------|----------------------|-----------|-----------|-------|-------|-------|--------|--------|-------|-------|-----------|------------|-----------|-----------|-----------|-----|
| | | High-pressure region | | | | | | | | | | | | | | | |
| | | $v_{z,1}$ | $v_{z,2}$ | $v_{z,3}$ | v_1 | v_2 | v_3 | v'_1 | v'_2 | u_1 | u_2 | β_1 | β'_2 | β_1 | β_2 | β_3 | |
| 2 | 10 | 566 | 567 | 561 | 566 | 727 | 562 | 1210 | 832 | 1057 | 1064 | 62 | 47 | -1.3 | 39 | 3.6 | |
| | 50 | 759 | 637 | 700 | 760 | 788 | 702 | 1143 | 784 | 884 | 922 | 48 | 36 | 2.2 | 36 | 4.3 | |
| | 90 | 761 | 622 | 659 | 762 | 849 | 663 | 1012 | 653 | 710 | 780 | 41 | 18 | 3.2 | 43 | 6.4 | |
| 2 | | Low-pressure region | | | | | | | | | | | | | | | |
| | | 10 | 629 | 599 | 602 | 629 | 760 | 604 | 1238 | 845 | 1057 | 1064 | 59 | 45 | -0.9 | 38 | 4.4 |
| | | 50 | 695 | 627 | 644 | 695 | 783 | 644 | 1112 | 774 | 884 | 922 | 51 | 36 | 1.2 | 37 | 2.5 |
| 90 | 679 | 588 | 626 | 680 | 807 | 630 | 955 | 631 | 710 | 780 | 45 | 21 | 3.2 | 43 | 6.4 | | |

(d) Stage 2; data summation.

Figure 14. - Concluded. Velocity diagram plots. Design speed.

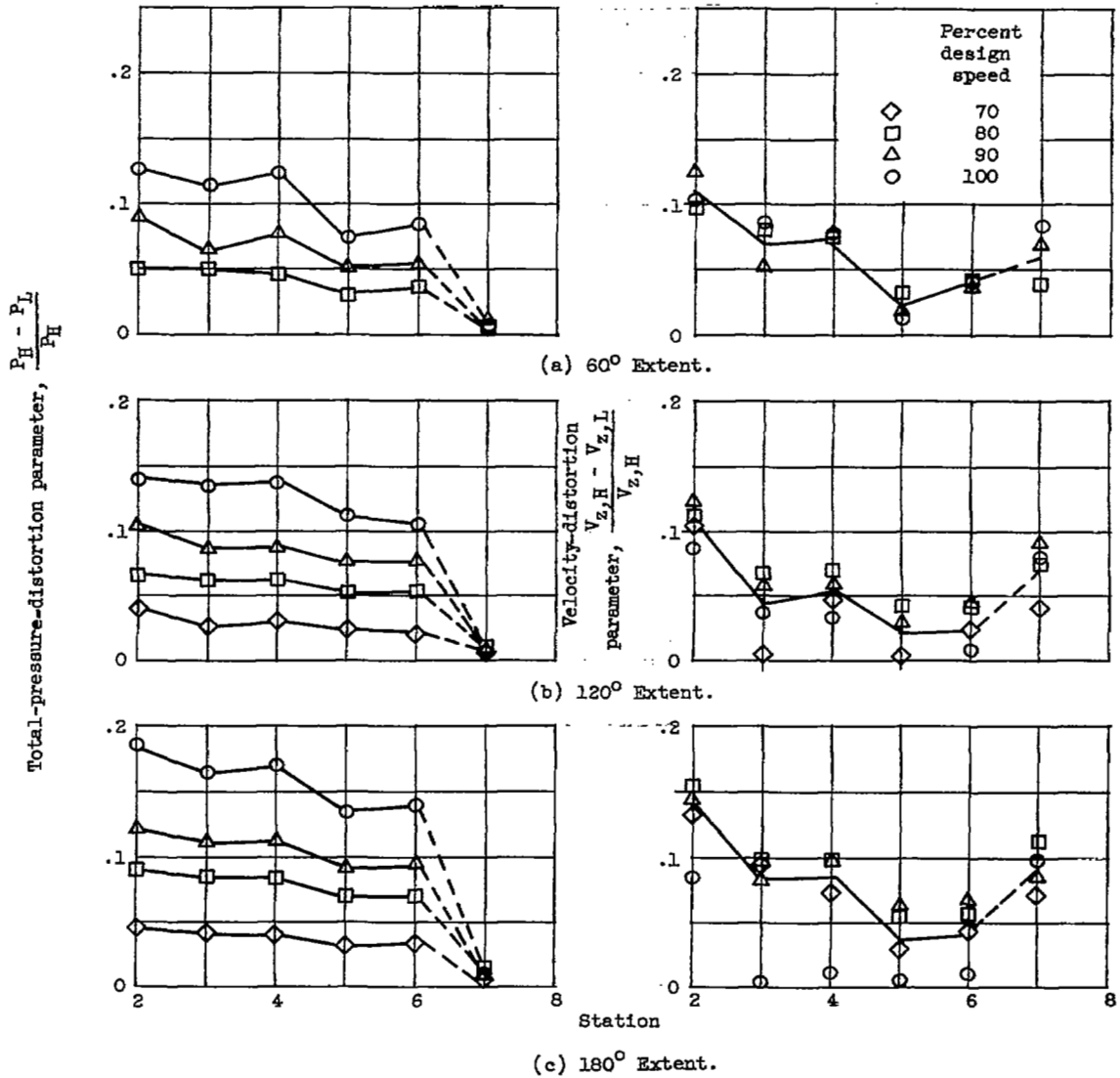


Figure 15. - Variation of total-pressure and velocity distortions through the compressor.

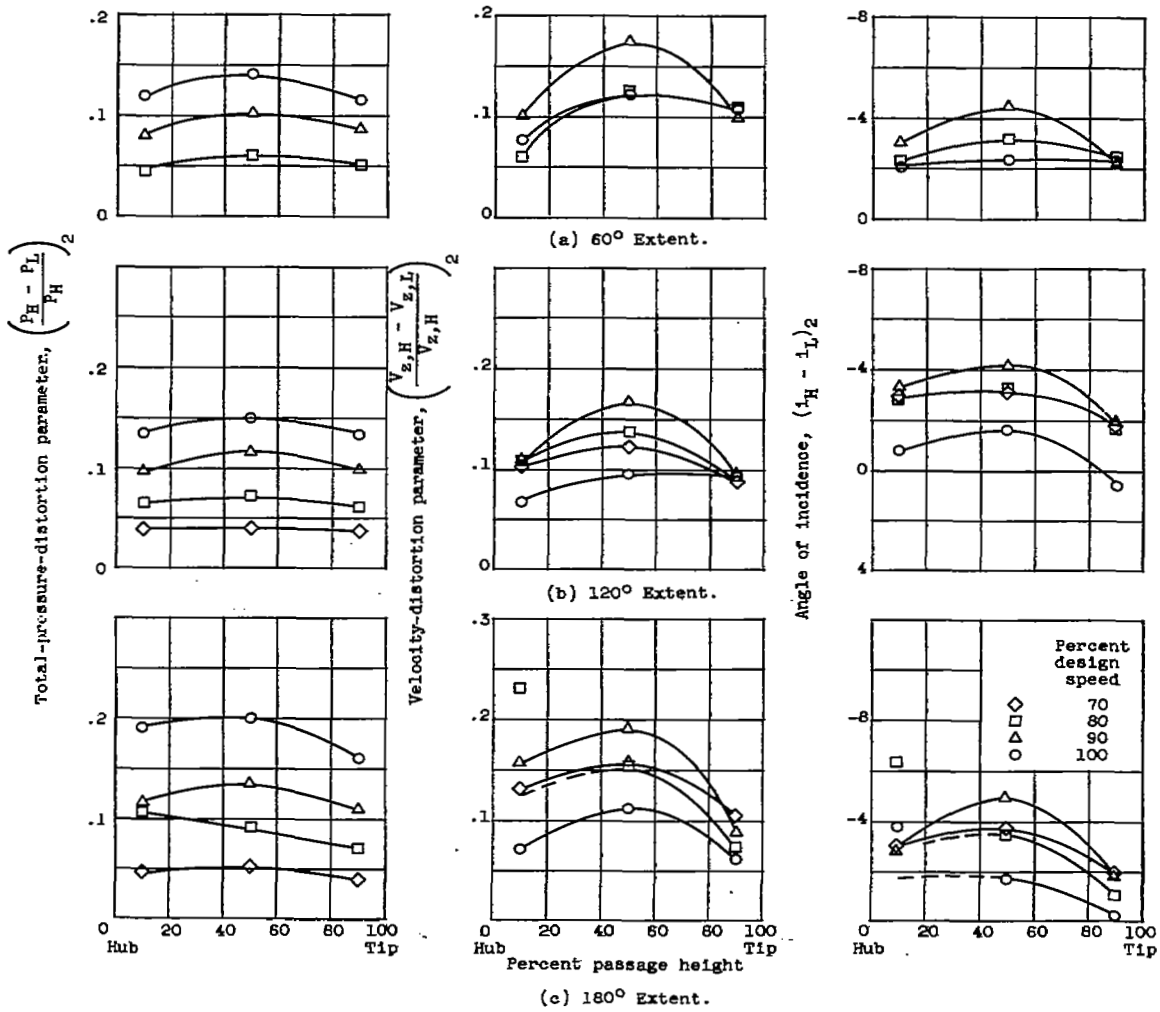


Figure 16. - Radial variation of distortion parameters over a range of compressor tip speeds at the compressor face (station 2).

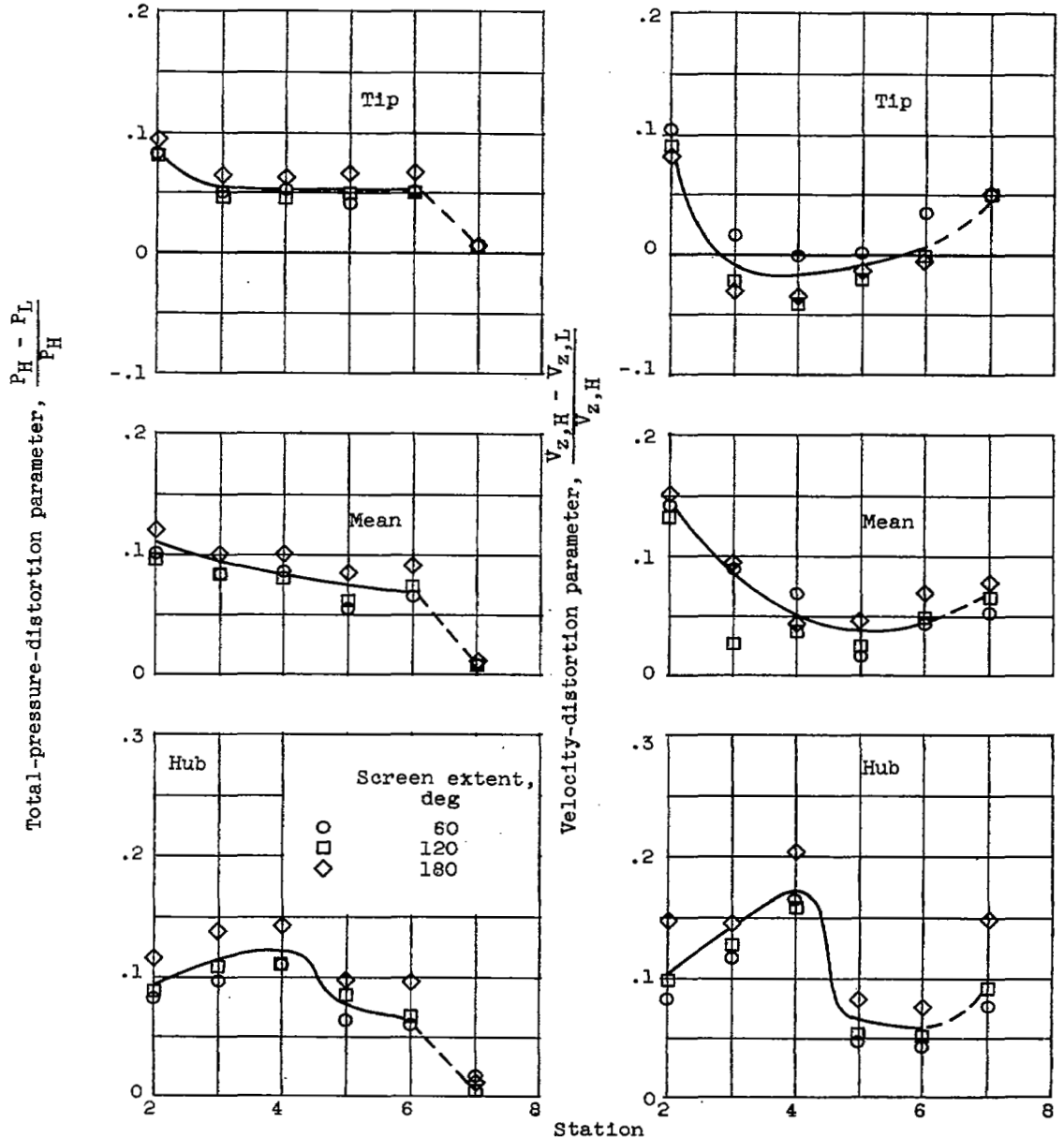
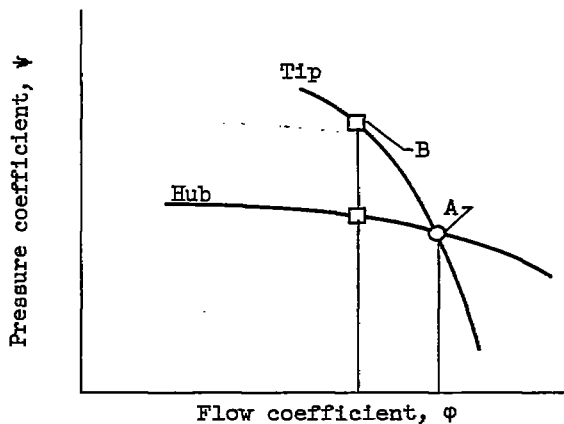
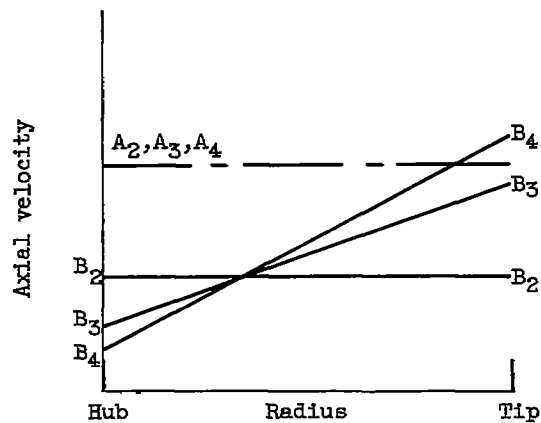


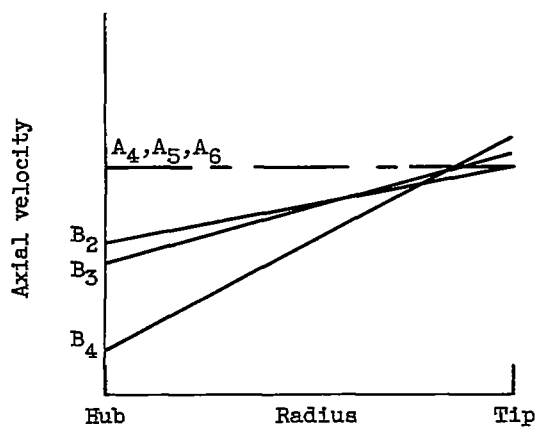
Figure 17. - Radial variation of distorted flow through compressor.



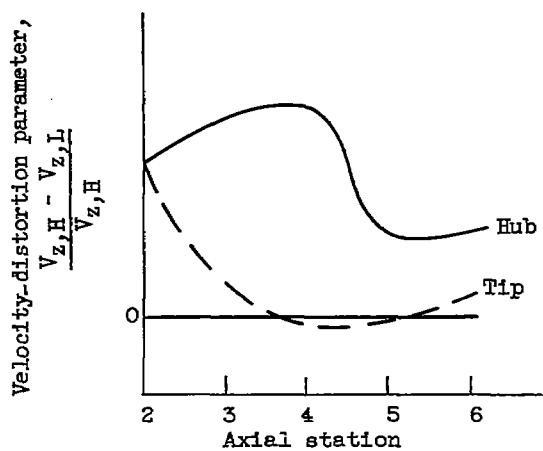
(a) Compressor characteristic.



(b) First-stage velocity variation.



(c) Second-stage velocity variation.



(d) Axial variation of velocity distortion parameter

Figure 18. - Qualitative velocity distributions through compressor with distorted inlet flow.